DESIGN, CONSTRUCTION AND PERFORMANCE EVALUATION OF A VARIABLE PITCH AXIAL FLOW FAN

A MASTER'S THESIS

in

Mechanical Engineering
Middle East Technical University

By
Cengiz ÖZEN

September 1985

Approval of the Graduate School of Natural and Applied Sciences.

Prof.Dr.Bilgin KAFTANOĞLU

Director

I certify that this thesis satisfies all the requirements as a thesis for the degree of Master of Science in Mechanical Engineering Department.

Prof.Dr. Alp ESİN

Chairman of the Department

We certify that we have read this thesis and that in our opinion it is fully adequate, in scope and quality, as a thesis for the degree of Master of Science in Mechanical Engineering Department.

Assoc.Prof.Dr. Ömer T.GÖKSEL

Supervisor

Examining Committee in Charge :

Prof.Dr.Alp ESİN .....

Assoc.Prof.Dr.Ömer T.GÖKSEL .....

Assoc.Prof.Dr.Mazhar ÜNSAL .....

Assoc.Prof.Dr.Muhammed KÖKSAL .....

Ins.Dr.Kahraman ALBAYRAK .....

ABSTRACT

DESIGN, CONSTRUCTION AND PERFORMANCE EVALUATION OF A VARIABLE PITCH AXIAL FLOW FAN

ÖZEN, Cengiz

M.S. in Mechanical Engineering

Supervisor : Assoc.Prof.Dr. Ömer T. GÖKSEL

September 1985,103 Pages

In this study a variable pitch axial flow fan was constructed for a smoke tunnel in the Fluid Mechanics Laboratory and a test set up for testing the fan were designed and constructed. The fan was tested at different speeds including the design speed and at different blade angle settings. The effect of the speed and the blade angle on the fan performance characteristics were evaluated, and the theoretical design values at the design point were compared with the experimental results.

Key Words : variable pitch axial flow fan.

ÖZET

PALA AÇISI DEĞİŞTİRİLEBİLEN EKSENEL BİR FAN TASARIMI VE İMALATININ YAPILMASI İLE PERFORMANSININ İNCELENMESİ

ÖZEN, Cengiz
M.S. in Mechanical Engineering
Supervisor : Assoc.Prof.Dr.Ömer T. GÖKSEL
September 1985,103 Pages

Bu çalışmada Akışkanlar Mekaniği Laboratuvarında mevcut bir duman tüneli için hücum açısı değiştirilebilen palalı, eksenel bir fan ve onun test edileceği bir deney düzeneği tasarlandı ve imal edildi. Fan, tasarım hızını da içeren değişik hızlarda ve değişik pala açılarında test edildi. Fan hızının ve pala açısının fan performansı üzerindeki etkileri incelendi ve tasarım noktasındaki teorik değerlerle deneysel değerler mukayese edildi.

Anahtar Kelimeler : Değişen açılı eksenel fan.

ACKNOWLEDGEMENTS

I would like to express my gratitude to Assoc.Prof.Dr. Ömer T. GÖKSEL for his kind supervison, encouragement and valuable comments.

I am also grateful to Dr. Kahraman ALBAYRAK for his kind helps during this study.

I wish to thank to the technicians of the work shop of Mechanical Engineering Department for their help in the manufacturing of the components and to Yaşar AKŞİT and Mehmet Abuş AKSOY for their continuous help during this work.

I thank to Tülây ARDIÇ for her typing and Ayşegül DALBUDAK for her kind help in technical drawings and in tracing the figures.

TABLE OF CONTENTS

LIST OF TABLES

LIST OF FIGURES

LIST OF SYMBOLS

a	diameter of wall pressure tapping.
c	cord length.
d	orifice diameter, impeller diameter.
e	expansibility factor.
f	fineness ratio.
g	gravitational acceleration.
k	constant.
k_c	compressibility coefficient.
l	length.
n	speed of rotation.
p	pressure.
p_f	fan dynamic pressure.
p_{st}	fan static pressure.
p_{tf}	fan total pressure,
q_m	mass flowrate.
r	radius.
s	blade spacing, $2\pi r/z$.
u	tangential velocity.
v	velocity.
w	blade relative velocity.
z	number of blades.
A	area.
C_d	discharge coefficient.
C_D	coefficient of drag
C_L	coefficient of lift.
D	drag force, diameter.
F	force.

H head.

H_i ideal head.

H_{st} static head.

H_{tl} total head loss.

L lift force.

M moment.

N speed of rotation.

P power.

Q volume flowrate.

T torque, absolute temperature.

V average velocity.

W angular velocity.

α angle of attack.

β blade angle.

γ isentropic coefficient, drag to lift ratio.

η_{st} static efficiency.

η_t overall efficiency.

η_h hydraulic efficiency.

θ pressure ratio.

λ power coefficient, orifice diameter/air duct diameter.

ν kinematic viscosity.

ξ constant used to define compressibility coefficient.

ρ density.

σ solidity, normal stress.

ϕ volume coefficient.

ψ pressure coefficient.

ψ_i ideal pressure coefficient.

ψ_{st} static pressure coefficient.

ϵ strain.

CHAPTER 1

INTRODUCTION

The object of the present work is to design, construct and determine its performance characteristics of an axial flow fan with variable pitch for the smoke tunnel existing in the Fluid Mechanics Laboratory.

An axial flow fan may be described as a fan in which the flow of air is parallel to the axis of the impeller. In the simplest form, air approaches the impeller in an axial direction and leaves it with a rotational component due to the work done by the impeller. More advanced designs have inlet and/or outlet guide vanes to obtain a higher static pressure difference across the impeller.

The flowrate through a fan unit is normally varied by changing the rotor speed. An alternative method for changing the flowrate is to use variable pitch rotor blades. Since variable speed fan needs a variable speed prime mover which is not available at hand and is also expensive, variable pitch rotor blades are found to be more suitable for the present fan.

The system characteristic of the smoke tunnel was obtained experimentally. The fan was designed for the conditions of a design point selected from the system characteristic. The blades were designed using isolated aerofoil method and the design procedure is outlined in Chapter 3.

Aluminium alloy was used as blade material. In order to manufacture the blades, its model was made out of plexiglass material and then the blades were cast from this model. Selection of the fan material and strength calculations are given in Chapter 4. Manufacturing of the fan blade and construction of the fan are presented in Section 5.1 and 5.2

A test set-up for testing the fan was designed and constructed. It is presented in Section 5.3 . The measurement techniques used, and the calculations related with fan performance paramaters such as power, volume flowrate and fan total pressure are presented in Chapter 6.

The fan was tested at different speeds and at different blade pitch angle settings. The effect of speed and blade pitch angle on the fan performance was studied. The performance characteristics of the fan, the discussion of the experimental results, and the conclusions reached from this study are presented in Chapter 7. Recomendations for further work are also given in Chapter 7.

CHAPTER 2

LITERATURE SURVEY

2.1. INTRODUCTION

Propeller, or axial, type fans have been in use for many decades but it was only during the last three or four decades that much attention has been paid to their technical refinement (1). For the first part of this century, centrifugal fans enjoyed popularity owing to their greater operating flexibility, efficiency and quietness. However the axial flow fans are rapidly gaining importance due to the present preference for such fans in large ventilating installations and in other systems where there is a demand for large flowrates. This is due to the experimental and theoretical studies which have ensured the attainment of very high efficiencies together with satisfactory operation of the axial fans within the desired range. Marked reductions in noise level have also been achieved.

Technology of fan engineering was given an unexpected impetus when the construction of high efficiency blowers in 1952 with 90% efficiencies become practicable (2).

2.2. GENERAL TYPES OF AXIAL FLOW FANS

In the existing literature the axial flow fans are generally placed in three main catagories.

a) Free fan : A free fan is one which rotates in a common unrestricted air space. It is so widely used that it is called as the table fan. It can move large quantities of air but is unable to produce a significant pressure increase on the air being moved. The low driving

power and the satisfaction of being able to obtain results even with a simple design caused this application to receive little scientific attention. Many firms are attempting to market technically upto date designs. An interesting design by the Samson United Corporation in Rochester, USA, is shown in figure 2.1(2). Blades, which have a twisted circular section, are made of rubber sheets thickened at the hub end. These blades are inserted into grooves of a hub in the shape of a bell. From the aerodynamic aspect, the shape is fairly satisfactory and the use of rubber eliminates danger, so that the fan can be used without a guard. Due to their higher efficiencies, these impellers can be run at low peripheral speeds. These free fans are also used as ceiling fans for circulating air in an enclosed space as shown in figure 2.2.

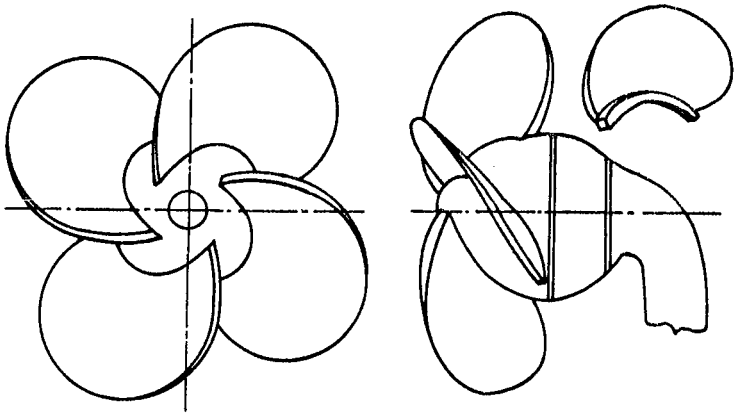

Fig.2.1 Axial Flow Fan with Rubber Blades

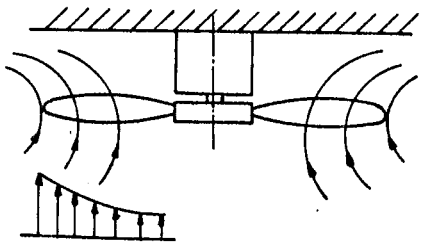

Fig.2.2 Ceiling Fan

b) Diaphragm mounted fan : This type of fan is shown in figure 2.3 . It transfers air from one relatively large space to another. A shroud ring may be attached to the blades or, alternatively, to the partitioning structure. It is a relatively long-established fan and it is probably one of the most common fan in use.

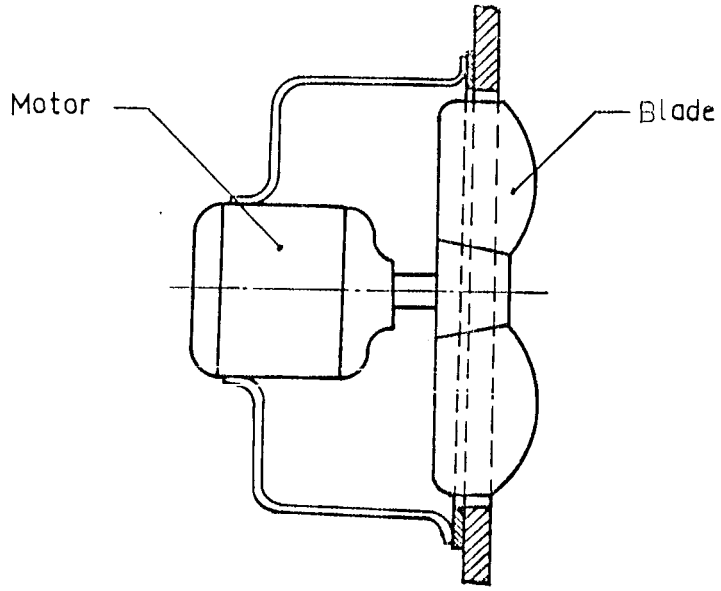

Fig.2.3 Diaphragm Mounted Exhaust Fan

One of the notable improvements of recent years has been the design of exhaust fans which operate in short and compact ducts (1). These fans are superseding the cheap but crude type of diaphragm mounted fan illustrated in figure 2.3 . Diaphragm mounted exhaust fan type represents a passing phase in the development of quite and high efficiency exhaust fans.

c) Ducted fans : This type of fan is ducted and the enclosing duct constrains the air to enter and leave the fan unit in axial direction. The various components which make up a ducted fan unit are indicated in figure 2.4 . When additional fan stages are fitted in series, the pressure rise which a single unit is capable of increases, in the extreme case a multistage unit becomes a compressor.

Stationary vanes known as stators or guide vanes, are often located upstream and/or downstream of the fan to achieve maximum amount of useful

pressure. The question is often raised whether an upstream guide vane or a downstream guide vane should be chosen.

In many cases the decision is governed by the type of installation and overall arrengements. Marcinowski.H(3) investigated this problem very throughly and reached the conclusion that the upstream quide vane is only of benefit for very low hub to impeller diameter ratios and particularly for fans having blades with small lift to drag ratios. In practice, present tendency is to design axial flow impellers with down stream guide vanes. This is justified because,a down stream guide vane removes the swirl component of velocity in the discharging flow hence increases the static pressure developed by the fan.

A third way to achieve the maximum useful static pressure is to dispense with guide vanes and to have a second impeller downstream of the first but rotating in opposite direction. This second impeller then acts in a manner similar to that upstream guide vane unit, taking its prerotated air from the discharge of the first impeller. Such an assembly is known as a contra-rotating fan.

Comparative characteristics for fans having impellers of similar proportions are shown in figure 2.5. As seen in figure 2.5 although fans with upstream guide vanes develope higher pressures than fans equipped with downstream guide vanes,they show marked stalling characteristic. The highest pressure is naturally expeoted from a contra-rotating fan.

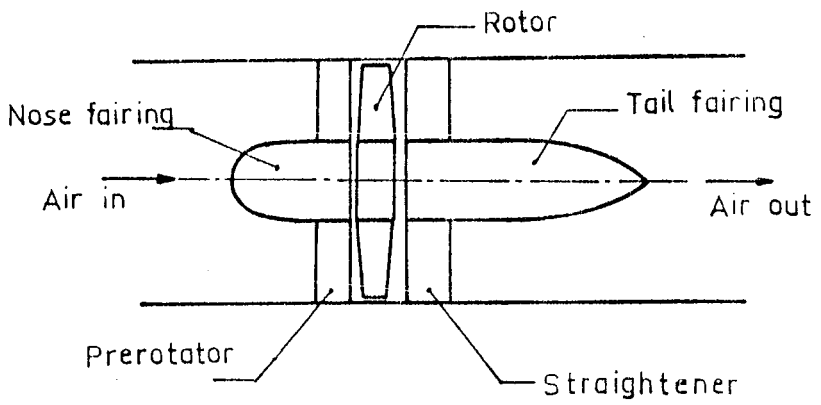

Fig.2.4 Components of a Ducted Fan Unit

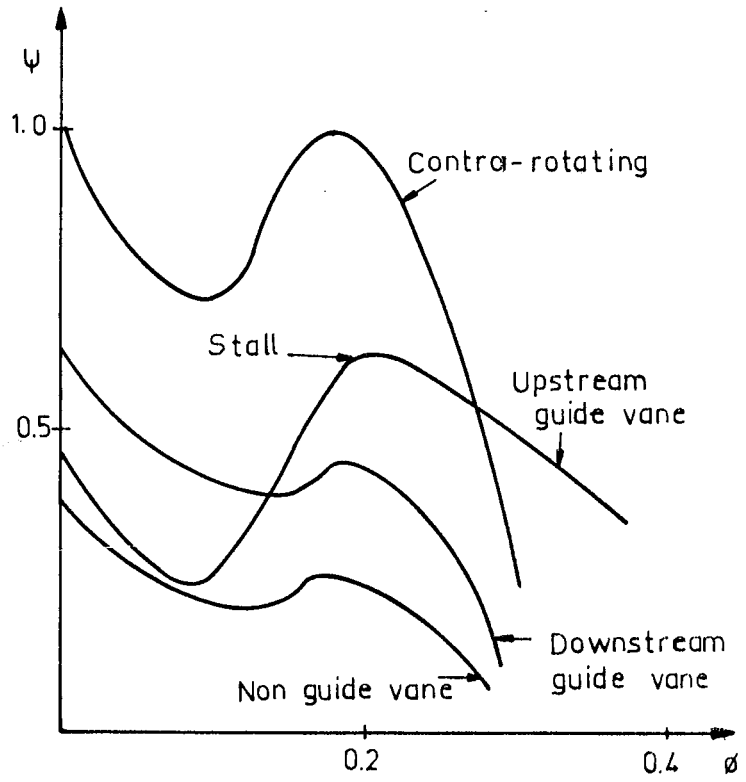

Fig.2.5 Characteristics of Axial Flow Fans

2.3. DESIGN METHODS OF A FAN BLADE

Design of ducted axial flow fans may be approached by either single aerofoil or cascade theories.

In Reference (1) it is stated that no single design method can cover the entire range of ducted axial flow fans and choice of appropriate design method depends basically on the following factors.

a) Multiplane interference

b) Blade solidity c/s

c) Whether the fan is a high pressure or a low pressure fan

Multiplane interference may be explained as follows :

When the aerofoil sections are brought closer and closer to each other, there is mutual interference between the flow patterns around the aerofoils. This leads to a change of the slope of the lift curve of the blade and hence it causes a decrease in the maximum lift.

Blade solidity is defined as the ratio of the blade cord to the spacing of blades perpendicular to fan axis. For low blade solidities, no interference is experienced and two - dimensional test data obtained for a single aerofoil can be used with confidence in design. But since the interference between the blades is high for high blade solidities, then cascade theory is used for the blade design (1). Theoretical methods of calculating cascades of aerofoils and the detailes of the flow through them are given in References (6) and (7).

Attempts have been made to extend the scope of the isolated aerofoil method by introducing an interference factor such as the ratio of the actual lift of the blade to the lift it would exert in the absence of other blades. These methods have, however, failed in general to produce consistent results.

In Reference (4) it is stated that since the solidity is high near the blade root and low at the remaining major portion of the blade, the design of a complete fan blade requires the use of cascade method in the vicinity of the blade root while over the remaining major portion of the blade span the isolated aerofoil method is the appropriate one. A solution for blending the two methods is outlined in Reference (5).

In Reference (1) it is also stated that the cascade method is used in high pressure fans and isolated aerofoil method is used for low pressure fans. In present design, since the designed fan is a low pressure fan, the isolated aerofoil method was used in the design of the blade. It is explained in Section 3.5.

CHAPTER 3

AERODYNAMIC DESIGN OF THE FAN

3.1. SELECTION OF THE FAN TYPE

The smoke tunnel existing in the Fluid Mechanics Laboratory is an open circuit tunnel and is designed to be driven by an axial flow fan. The fan is planned to be placed at the exit of the diffuser cone of the tunnel.

The axial flow fan for this tunnel may be designed without inlet and outlet guide vanes. Since the tunnel is an open circuit type and the fan is to be placed at the outlet of the tunnel, the outlet guide vanes, whose function is to convert the outlet swirl into static head, are not necessary. Furthermore, a low pressure axial flow fan may be sufficient for this purpose. Low pressure fans do not usually require inlet guide vanes. When there are no guide vanes at the inlet of the fan, air enters the fan axially and is discharged with a swirl velocity v_{u2}.

For a given duct system, the volume flowrate through the fan is normally varied by changing the rotor speed. Alternative method which has been devised for the purpose of changing the flow rate passing through the fan is the use of variable pitch rotor blades. Therefore fans may also be classified according to adjustability of rotor blades. Three types of blade configuration, in ascending order of complexity, are listed below.

a) A standard blade is designed for a rotor of given boss, and the fan diameter for a specific task. The correct number of blades is permanently fixed to the boss at the desired pitch angle. When a change in fan duty occurs the blade pitch is altered by substituting a different rotor having a different blade pitch. This method avoids necessary mechanism for adjusting the blade pitch angle and may provide a cheap

solution if the replaced rotor is used for an other duty at the same installation. The blade root setting and the number of blades used are sufficient to specify a particular variant. The sheet metal bladed fans are probably the most suitable for this particular treatment since the blades can readly be welded to the boss.

b) As an alternative to a permanent root fixing, the blade pitch can be altered manually, by remote control or otherwise, when the fan is inactive. The blade root is usually provided with a screwed attachment by which the blade is screwed to the boss.

c) In some instances it may not be practical to stop the fan in order to change the blade pitch, in which case suitable manual or automatic mechanisms must be provided to change the blade pitch while the fan is in operation.

The second type of fan unit is the most popular, since the mechanical complications are by no means excessive.

In the light of the above explanations a variable pitch fan of the second type without guide vanes was selected for the present smoke tunnel.

3.2. FAN LAWS AND PERFORMANCE COEFFICIENT

The performance of a fan in terms of pressure, volume flowrate and the power absorbed by the fan rotor depends on the following factors.

a) The design and the type of fan,

b) The volume flowrate, Q, through the fan and the pressure, p, developed by the fan at the point of operation,

c) Size of the fan,

d) Speed of rotation of the impeller,

e) Thermodynamic state of the air or gas passing through the fan.

It is usually desired to compute the performance of any fan from a minimum number of test data. The relationship between the volume flowrate and the pressure developed by the fan is not generally capable of being expressed as a simple mathematical function. However, by considering any single point on the p - Q characteristic of the fan, it is possible to derive some simple relationships generally known as the fan laws or

the similarity laws.

Using dimensional analysis, the following fan laws may be derived (8).

Volume flowrate

$$Q = k_q . d^3 . n \qquad (3.1)$$

Fan pressure

$$p = k_p . d^2 . n^2 . \rho \qquad (3.2)$$

Where k_p and k_q are numerical constants. n and d are the rotational speed and the diameter of the fan impeller respectively.

Fan power

$$P = p.Q = k_P . d^5 . n^3 . \rho \qquad (3.3)$$

Where $k_P = k_p . k_q$

The coefficients k_p, k_q and k_P are constant for a range of geometrically similar fans.

Since the fan laws are valid for any one particular point on the fan p - Q characteristic , similar laws will also be valid for other points of operation on the p - Q characteristic; however, the numerical values of the coefficients will be different for each point of operation. Thus a plot of k_p against k_q will have exactly the same form as the p - Q characteristic of each fan in the homologous series.

p - Q characteristic of a fan is usually plotted using non - dimensional parameters called the volume flowrate coefficient, ϕ, and the pressure coefficient, ψ . They are defined as follows :

$$\phi = \frac{Q}{(\pi d^2/4).u} \qquad (3.4)$$

$$\psi = \frac{p_{tf}}{\frac{1}{2}\rho . u^2} \qquad (3.5)$$

$\pi d^2/4$ in equation 3.4 is the area normal to the flow and d is the characteristic length of the fan impeller which may be equal to the impeller diameter. p_{tf} in equation 3.5 stands for total fan pressure developed by the fan.

The other dimensionless coefficients are static pressure coefficient, ψ_{st}, and power coefficient, λ. They are defined in equations 3.6 and 3.7 respectively

$$\psi_{st} = \frac{p_{st}}{\frac{1}{2}\rho . u^2} \tag{3.6}$$

$$\lambda = \frac{\phi . \psi}{\eta_t} \tag{3.7}$$

Where u is the impeller peripheral velocity, p_{st} is the static pressure developed by the fan and η_t is the total efficiency of the fan.

Fan static pressure, p_{st}, is defined to be the fan total pressure p_{tf} minus the fan velocity pressure (8). Fan velocity pressure is the velocity pressure corresponding to the average flow velocity at the fan outlet.

3.3. ENERGY TRANSFER IN AXIAL FLOW FANS

Figure 3.1 shows an axial flow fan blade section at some particular radius. The parameters in the velocity triangles shown in figure 3.1 with subscripts 1 and 2 denote the inlet and discharge conditions. In this figure, w is the relative velocity of the fluid, v_m is the axial component of the absolute fluid velocity v and v_u is the tangential component of the absolute fluid velocity.

Since there are no inlet guide vanes in the present fan, air enters the impeller axially with velocity $v_1 = v_{m_1}$ and leaves with velocity v_2. The tangential speed of the impeller at the mean blade radius is assumed to be the same at inlet and outlet of the blade, i.e. $u_1 = u_2$.

v_m is also assumed to be the same at inlet and outlet of the fan blade. Therefore :

$$v_{m_1} = v_{m_2}$$

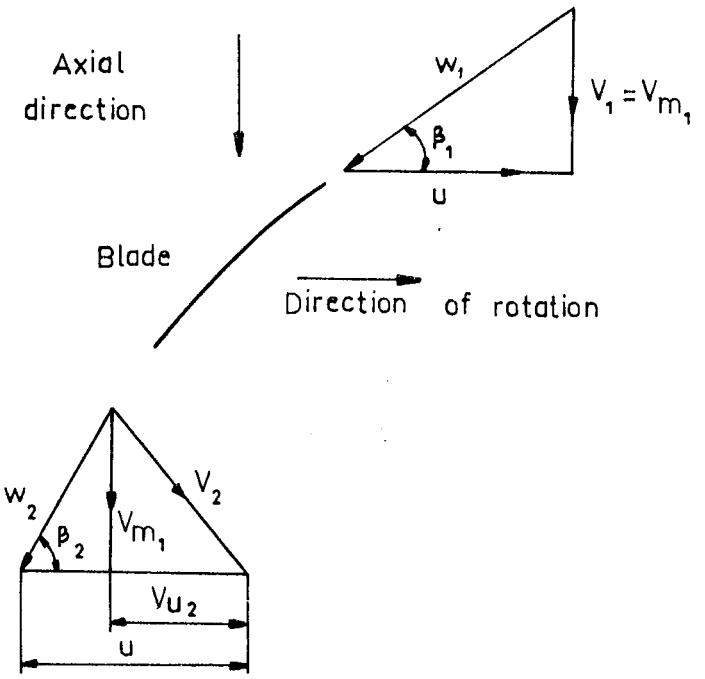

Fig.3.1 Axial Flow Fan Blade Velocity Triangles.

The ideal total head developed by the fan impeller is given by Euler Turbine Equation (8) as

$$H = \frac{u_2 \cdot v_{u_2} - u_1 \cdot v_{u_1}}{g} \qquad (3.8)$$

Since $u_1 = u_2$ and assuming axial entry $v_{u_1} = 0$

Therefore

$$H = \frac{u_2 \cdot v_{u_2}}{g} \qquad (3.9)$$

Since $H = \frac{p}{\rho \cdot g}$

Equation 3.9 may also be written as

$$p = H \cdot \rho \cdot g = \rho \cdot u \cdot v_{u_2} \qquad (3.10)$$

In order to show the components of the energy transfered by the fan impeller, equation 3.8 may be written in the following form (8).

$$H = \left(\frac{v_2^2 - v_1^2}{2g} \right) + \left(\frac{w_1^2 - w_2^2}{2g} \right) \qquad (3.11)$$

The first term in equation 3.11 represents the increase of head due to the forced vortex caused by the impeller rotation. The second term in equation 3.11 represents the regain of static head due to the reduction of relative velocity, w, of the air passing through the impeller.

Figure 3.2 shows the theoretical performance characteristic of an axial flow fan together with the actual or measured performance characteristic of an axial flow fan without guide vanes.
In this figure the maximum point on the measured performance characteristic corresponds to the stall point of the impeller blades. Fans are not operated to the left of this point because of poor fan efficiency and unstable flow conditions causing large fluctuating forces on the blades.

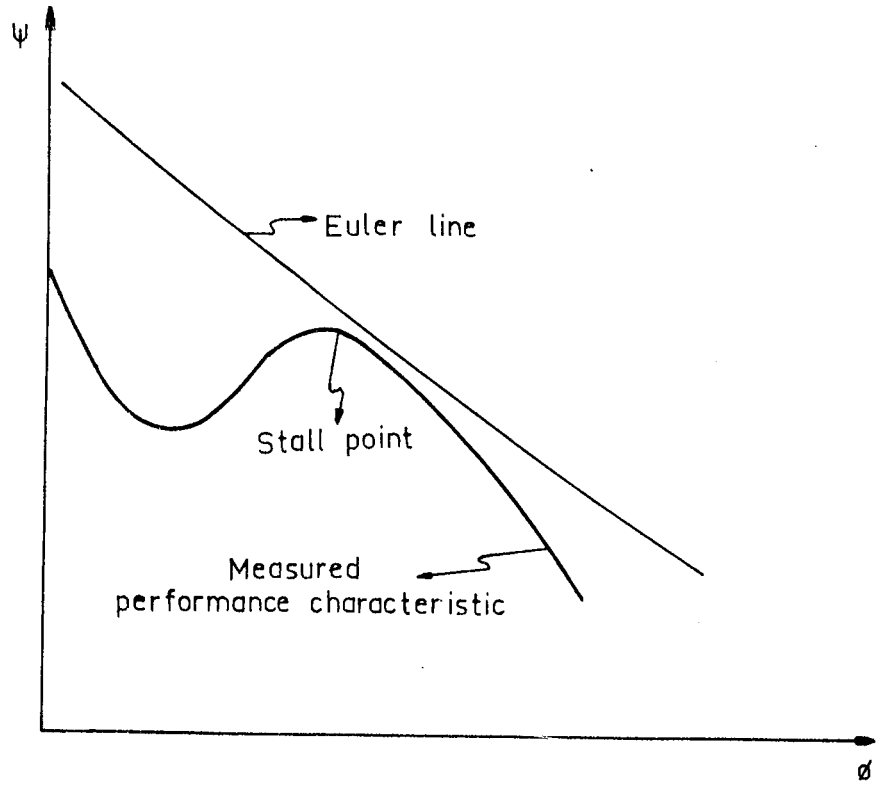

Fig. 3.2 Theoretical and Actual Performance Characteristics of an Axial Flow Fan

3.4. THE SELECTION OF THE BLADE DESIGN METHOD

In the existing literature, there are basically two types of blade design methods as was explained in section 2.3.
These were :

a) Isolated aerofoil design method

b) Cascade design method

Multiplane interference which was explained in section 2.3 prevents the use of isolated aerofoil design method for solidities above unity, while the cascade design method can not be used for solidities much less than 2/3 (1). Solidity of a blade is defined as

$$\sigma = \frac{c}{s} \tag{3.12}$$

Where c is the cord length of the blade and s is the spacing between the blades and is given in equation 3.13 .

$$s = \frac{2\pi r}{z} \tag{3.13}$$

Where z is the number of blades and r is the radius of any circle on the fan blades concentric with the fan rotational axis.

For the present design, since the fan pressure is low, i.e. it is a low pressure fan, the isolated aerofoil design method was found to be suitable. The solidity σ was kept below unity in the blade design so that no interference between blades is expected.

3.5. ISOLATED AEROFOIL DESIGN METHOD

According to this design method, the flow through the blade row produces an effect on the blades which is the same as the effect of a free stream with velocity w_∞ which is equal to the mean of inlet and outlet relative velocities on a single aerofoil (1) .

$$\vec{w}_\infty = \frac{1}{2}\left(\vec{w}_1 + \vec{w}_2\right) \tag{3.14}$$

Geometric details of the blade element for isolated aerofoil method is shown in figure 3.3 . In this figure α is called the angle of attack.

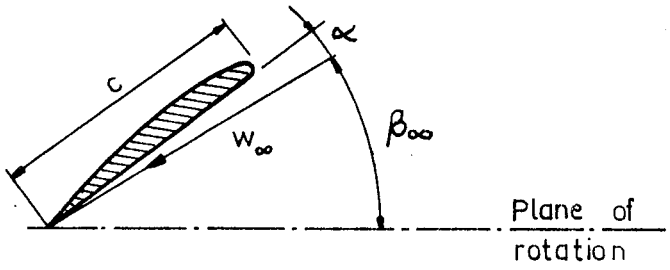

Fig.3.3 Geometric Details of a Blade Element

Figure 3.4 shows the configuration of inlet and outlet velocity triangles of the rotor blade shown in figure 3.3. In this figure

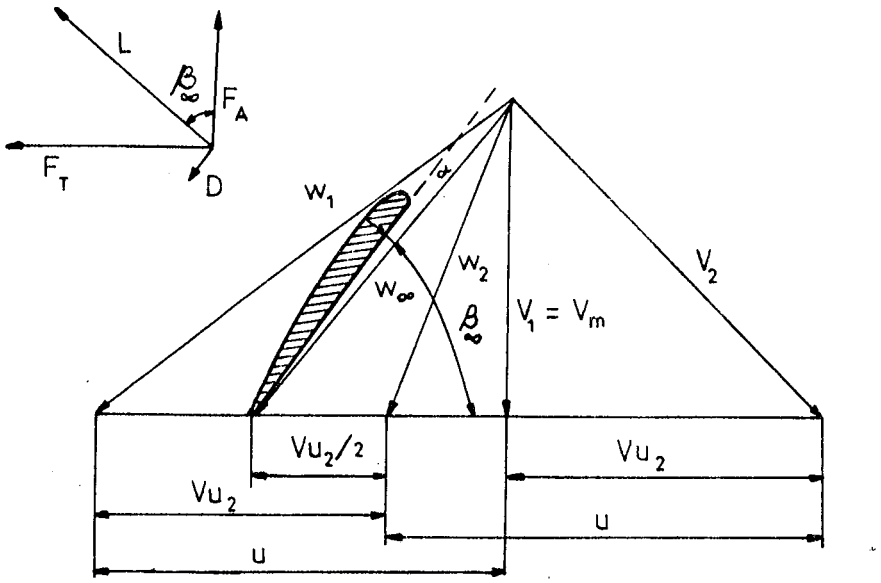

Fig.3.4 Inlet and Outlet Velocity Triangles Relative to a Rotor Blade.

the lift force, L , and the drag force, D , are perpendicular and parallel to the mean relative velocity w_∞ respectively. For two-dimensional flow, they are defined as follows (1) :

$$D/\text{unit span} = C_D \cdot \frac{1}{2} c \cdot w_\infty^2 \qquad (3.15)$$

$$L/\text{unit span} = C_L \cdot \frac{1}{2} c \cdot W_\infty^2 \qquad (3.16)$$

Where C_D and C_L are known as the drag and lift coefficients respectively. For a given aerofoil shape C_L and C_D are functions of the angle of attack α and Reynolds number.

The Reynolds number is defined as

$$Re = \frac{W_\infty c}{\nu} \qquad (3.17)$$

Where ν is the kinematic viscosity of air and c is the cord length of the aerofoil section.

The flow coefficent ϕ and the static pressure coefficient ψ_{st} in equations 3.4 and 3.6 can be written as shown below.

$$\phi = \frac{v_a}{u} \qquad (3.18)$$

$$\psi_{st} = \frac{g \cdot H_{st}}{u^2} \qquad (3.19)$$

If the static head, H_{st}, axial velocity of flow, v_a, at any radius r and the impeller angular velocity W, in rad/sec, are known, the flow coefficient ϕ and the static pressure coefficient ψ_{st} can be calculated by equations 3.18 and 3.19 .

Using the above coefficient together with the inlet and outlet velocity triangles given in figure 3.5, the following equations were derived for an axial flow fan with no guide vanes. The derivations of these design equations written below are given in Appendix 1.

$$\psi_i = \frac{\psi_{st}}{\eta_{st}} \qquad (3.20)$$

$$\beta_\infty = \frac{2\phi}{2 - \psi_i} \qquad (3.21)$$

$$\eta_h = 1 - \phi \cdot \gamma \cdot \frac{\text{Cosec}^2 \beta_\infty}{(1 + \gamma \cdot \cot \beta_\infty)} \qquad (3.22)$$

$$\eta_{st} = \eta_h - \frac{\phi^2}{2\psi_i} \qquad (3.23)$$

$$\sigma = \frac{2\psi_i \cdot \mathrm{Sin}\beta_\infty}{C_L \cdot \phi \cdot (1 + \gamma \cdot \mathrm{Cot}\beta_\infty)} \qquad (3.24)$$

and

$$c = \frac{2\pi r}{z} \cdot \sigma \qquad (3.25)$$

Where γ is the ratio of drag coefficient to lift coefficient C_D/C_L, η_{st} is the static pressure efficiency of the fan, η_h is the hydraulic efficiency which accounts for the blade drag. ψ_i is the ideal pressure coefficient.

If a blade profile is selected, the values of C_L and γ are taken from the two - dimensional test data for the selected aerofoil profile. Then, equations from 3.20 to 3.23 are solved iteratively by assuming a value for η_{st} given in equation 3.20 until the assumed value of η_{st} converges to the value of η_{st} evaluated by equation 3.23. After the determination of relevant parameters by means of prementioned iterative solution, equations 3.24 and 3.25 are used to calculate the solidity σ and the cord length c at desired blade sections.

3.6. DESIGN RESTRICTIONS

There are some restrictions in designing the blade. First of these is the effect of compressibility of the fluid on fan performance. The compressibility of the fluid becomes significant when the relative fluid velocity at the impeller tip exceeds 150 - 165 m/sec, or the tip speed is greater than half of the local speed of sound (1). Fan noise also increases with increased impeller tip speed.

The second restriction is the solidity σ. For solidities approaching unity or greater than unity there is an aerodynamic interference between the adjacent blades which usually results in a marked reduction in lift for a given blade incidence (1). Selection of the lift coefficient effects the performance of the fan. Mair (9) suggests that the fan blade lift coefficients should not exceed 0.9 or 1 at the root and 0.7 at the tip in order to avoid stalling due to boundary layer interference at the root.

The number of blades is arbitrary. The product of the number of blades and the cord of the blade represent total blade area which must be in accordance with the trust requirements. To avoid excessive flow pulsations, a minimum number of 4 blades is used in wind tunnel fans. The maximum blade number is limited by the strength of the fan material used.

In well designed units, the rotor boss dimater will normally be within the range of 40 - 70 % of rotor diameter. The larger boss diameter is usually associated with fans designed for high pressure requirements (1) and very large boss requires a large and a long nascelle for proper streamlining, which involves costly and difficult construction.

3.7. DESIGN OF THE FAN ROTOR BLADE

In the excepted design method,it is appropriate to consider each blade element as an isolated two dimensional aerofoil. Production con - siderations often influence the choice of the blade section. The RAF 6E and the clark Y series of aerfoils are very popular as both have flat undersurfaces and are capable of high efficiency operation (1). Aerofoil sections with flat undersurfaces are usually preferred because, they can be manufactured and set easily. Aerofoil sections suitable for fan design are shown in figure 3.5.

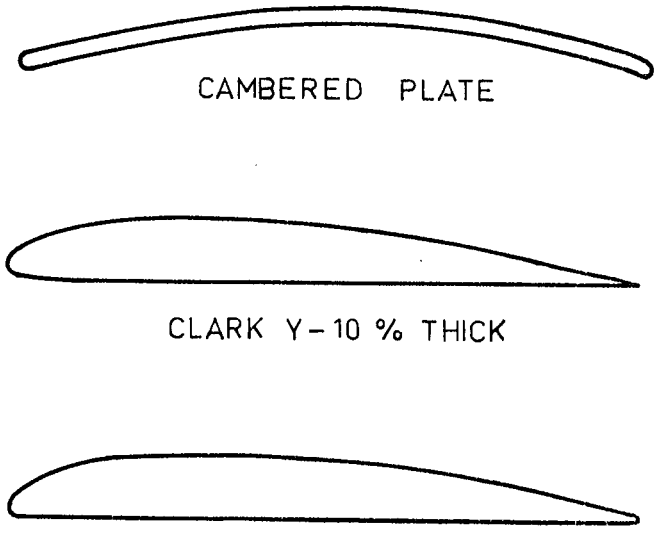

Fig. 3.5 Aerofoil Sections Suitable for Fan Design

RAF 6E aerofoil with flat undersurface is selected for the present design. The section coordinates of RAF 6E aerofoil are given in table 3.1. The experimental aerodynamic characteristics of the selected aerofoil plotted against the angle of attack α at Reynolds number $Re = 3.12 \times 10^5$ are given in figure 3.6(1).

It is common to design a blade to give the same axial velocity v_a and the pressure p at any given radius of the fan (8).
In which case ;

$$p = \rho . u . v_u = \text{Constant} \tag{3.26}$$

or

$$r . v_u = \text{Constant} \tag{3.27}$$

This is seen to be the condition for a free vortex. In this case, it necessary to have increased blade angles at the hub sections to achieve higher values of v_u at smaller radii.

In the present work the design of the blade was made for the desired maximum flowrate through the smoke tunnel. If the maximum flowrate, Q, and the corresponding static head, H_{st}, are known, the blade dimensions can be calculated by using equations 3.20 and 3.25.

Table 3.1 RAF 6E Section Characteristics (16)

For solid RAF 6E profile

A^{*} : 0.7380 c.h

I_{min} : 0.0472 $c.h^3$ (about the horizontal centrodial axis)

I_{max} : 0.0446 $c^3.h$ (about the vertical centrodial axis)

y_g : 0.4210 h (location of center of gravity above cord line)

x_g : 0.4405 c (location of center of gravity from leading edge)

h^{**} is approximately equal to 0.10 c

Distance from leading edge (% c)	Distance from Cord line (% c)	Lower Surface
0.00	1.15	Flat
1.25	3.19	
2.50	4.42	
5.00	6.10	
7.50	7.24	
10.00	8.09	
15.00	9.28	
20.00	9.90	
30.00	10.30	
40.00	10.22	
50.00	9.80	
60.00	8.98	
70.00	7.70	
80.00	5.91	
90.00	3.79	
95.00	2.58	
100.00	0.76	

Leading edge radius : 1.15 (% c)

Trailing edge radius : 0.76 (% c)

Distances are given in percentage of cord length

* A is the area of the cross section of blade normal to the line joining the centroids of the blade profile at the root and at the tip of the selected blade.

** h is the thickness of the blade profile at the centroid.

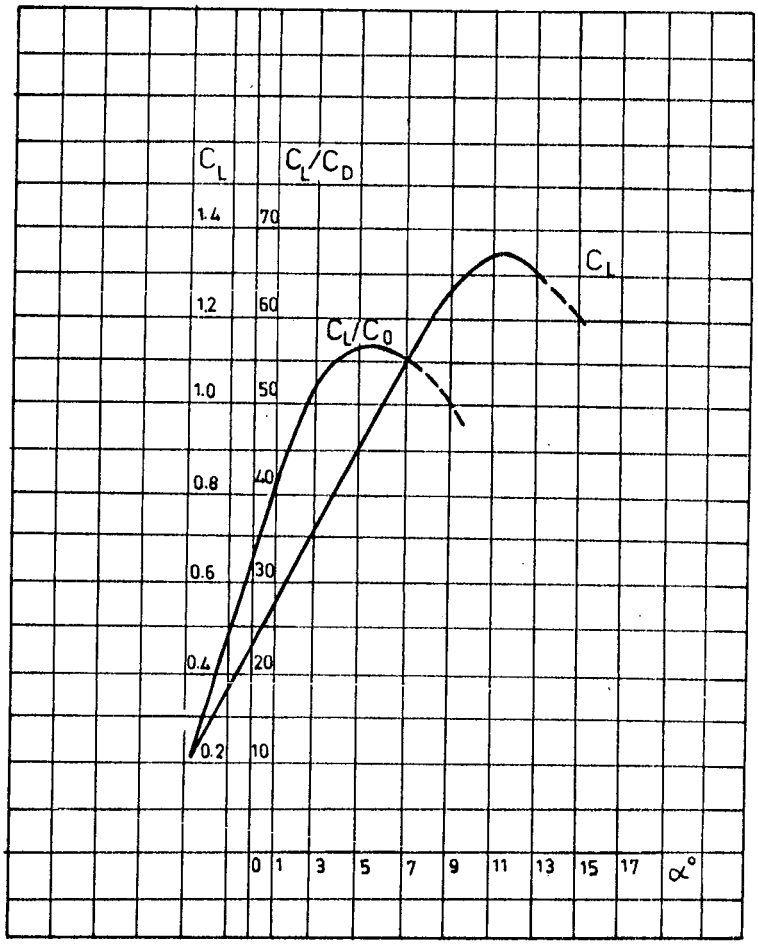

Fig.3.6 Lift - Drag Characteristic of RAF 6E Profile at Re = $3.12 \cdot 10^5$ (16)

3.8. DETERMINATION OF THE FAN STATIC HEAD AND THE FAN INLET VELOCITY

The maximum desired velocity at the smoke tunnel test section was assumed to be 45 m/sec. Then, maximum flowrate can be written as

$$Q_{max} = V_t \cdot A_t \qquad (3.28)$$

Where A_t is the test section area of the smoke tunnel and V_t is the maximum average velocity at the test section.

Substituting the known values of A_t and V_t into equation 3.28, the maximum flowrate is calculated as

$$Q_{max} = 0.988 \ m^3/sec$$

The necessary fan total head, H_{tf}, and static head, H_{st}, corresponding to this maximum flowrate, Q_{max}, are calculated as follows :

In general, the estimation of losses can not be accomplished with anywhere near the degree of accuracy associated with the design of the ducted axial flow fan. It will be appreciated therefore that the greatest care hould be exercised in assesing the losses. The most accurate way to estimate the losses is to determine it experimentally. To do this, an axial flow fan with the diameter of the tunnel outlet was fitted to the tunnel as shown in figure 3.7. By using a pitot tube, the velocity profile across the tunnel test section was determined. Then, the average velocity at the test section, consequently the flowrate, was calculated from this velocity profile.

The fan total head, H_{tf}, may be expressed as

$$H_{tf} = H_L + V^2/2g \qquad (3.29)$$

Where H_L is the loss through the tunnel and V is the discharge velocity at the tunnel outlet.

The loss H_L through the tunnel, neglecting the losses downstream of the section 2 shown in figure 3.7, is calculated using equation 3.30 which is Bernoulli equation written between section 1 and section 2 shown in figure 3.7 .

$$H_L = \frac{p_a}{\rho \cdot g} - \left(\frac{p_{s2}}{\rho \cdot g} + \frac{V_2^2}{2g} + H_E \right) \qquad (3.30)$$

Where p_a is the atmospheric pressure,

p_{s2} is the static pressure at section 2,

V_2 is the average velocity at section 2,

H_E is the elevation head.

Since the fan total pressure H_{ft} at each flowrate passing through the tunnel corresponds to a point an the tunnel loss characteristic, it is then written that

$$H_{ft} = H_{tl} \qquad (3.31)$$

Where H_{tl} is a point on the tunnel loss characteristic and called total tunnel loss.

Then substituting equation 3.30 to 3.29, an expression for H_{tl} may be written as

$$H_{tl} = \frac{p_a}{\rho \cdot g} - \left(\frac{p_{s2}}{\rho \cdot g} + \frac{V_2^2}{2g} + H_E \right) + V^2/2g \qquad (3.32)$$

Using equation 3.32, tunnel losses, H_{tl} , at five different flowrates were determined experimentally and were given in table 3.2. Different flowrates were obtained by blocking the tunnel outlet uniformly and the static pressure p_{s2} was measured from static pressure holes at section 2. Since the flowrate may be found from the measurements at the test section of the smoke tunnel as mention before, the velocities V_2 and V were found using the continuity equation.

Since the loss through a duct system is proportional to the square of the flowrate, the loss characteristic of the tunnel is parabolic. It may be given in the following form.

$$H_{tl} = k \cdot Q^2 \qquad (3.33)$$

Where k is the constant of proportionality.

Table 3.2 Experimental Results for the Hydraulic Losses of the Smoke Tunnel.

$Q(m^3/sec)$	V_t(m/sec)	H_{t1}(m-air)	$k = H_{t1}/Q^2$
0.133	6.06	0.35	19.7
0.247	11.25	1.25	18.8
0.334	15.24	1.69	15.2
0.354	16.26	2.79	21.8
0.407	18.57	4.47	27.0

The value of k in equation 3.33 may be estimated by taking the average of the experimental values of k given in table 3.2 and it is found to be as

$$k_{AV} = 20.5$$

Then, the smoke tunnel loss characteristic is given by equation 3.34 and is plotted in figure 3.8 .

$$H_{t1} = 20.5\ Q^2 \qquad (3.34)$$

Models with different sizes are going to be tested in the test section of smoke tunnel. These models will cause blockage losses. According to reference 17, this blockage loss may be taken between 10% and 15% of the total tunnel loss. In the present case because of small tunnel size the total tunnel loss was increased by 15% at each flowrate and the corrected tunnel loss characteristic was determined. It wasplotted in figure 3.8 and may be expressed as

$$H_{t1} = 23.6\ Q^2 \qquad (3.35)$$

For designing of the fan blade, the static head H_{st} and the inlet velocity v_a at the design flowrate are needed. The static head H_{st} is defined as the fan total head minus the fan velocity head, $V_{out}^2/2g$, which is the head corresponding to the average velocity V_{out} at the fan outlet. (The outlet velocity V_{out} is found by dividing the flowrate by the gross area at the outlet section of the fan without deducting the area occupied by the motors, the fairings and the other obstructions (12)).Therefore the static head H_{st} may be written as

$$H_{st} = H_{tf} - V_{out}^2/2g \qquad (3.36)$$

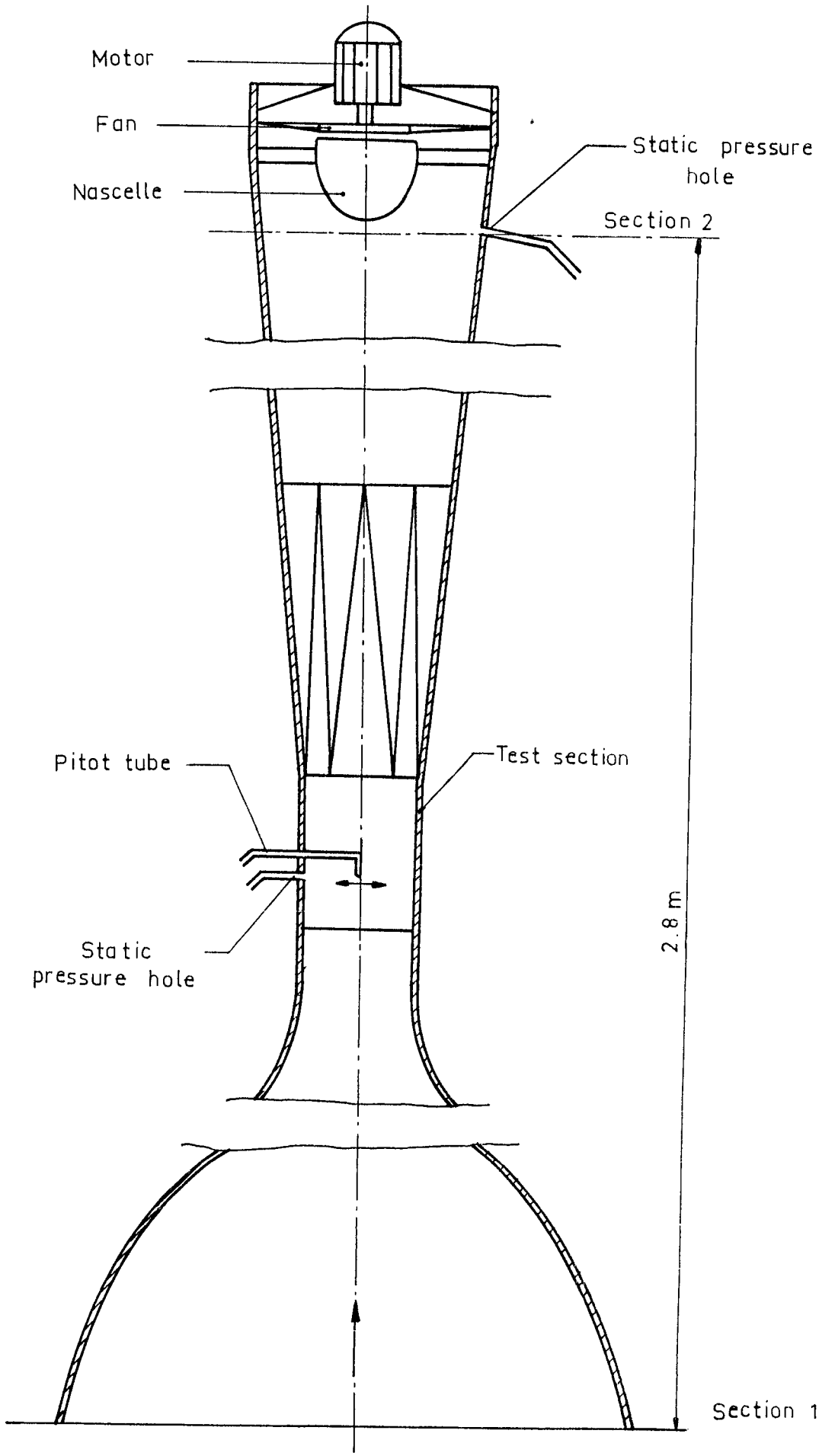

Fig.3.7 Section View of the Smoke Tunnel

Since $H_{ft} = H_{tl} = 23.6\ Q^2$

Then equation 3.36 may be expressed as

$$H_{st} = 23.6\ Q^2 - V_{out}^2/2g \qquad (3.37)$$

Since the design flowrate and the fan outlet area are known, the static head, H_{st}, at the design point is determined from equation 3.37 as

$$H_{st} = 20.2 \text{ m - air column.}$$

The axial velocity, v_a, at the design point is also calculated as

$$v_a = 11.80 \text{ m/sec}$$

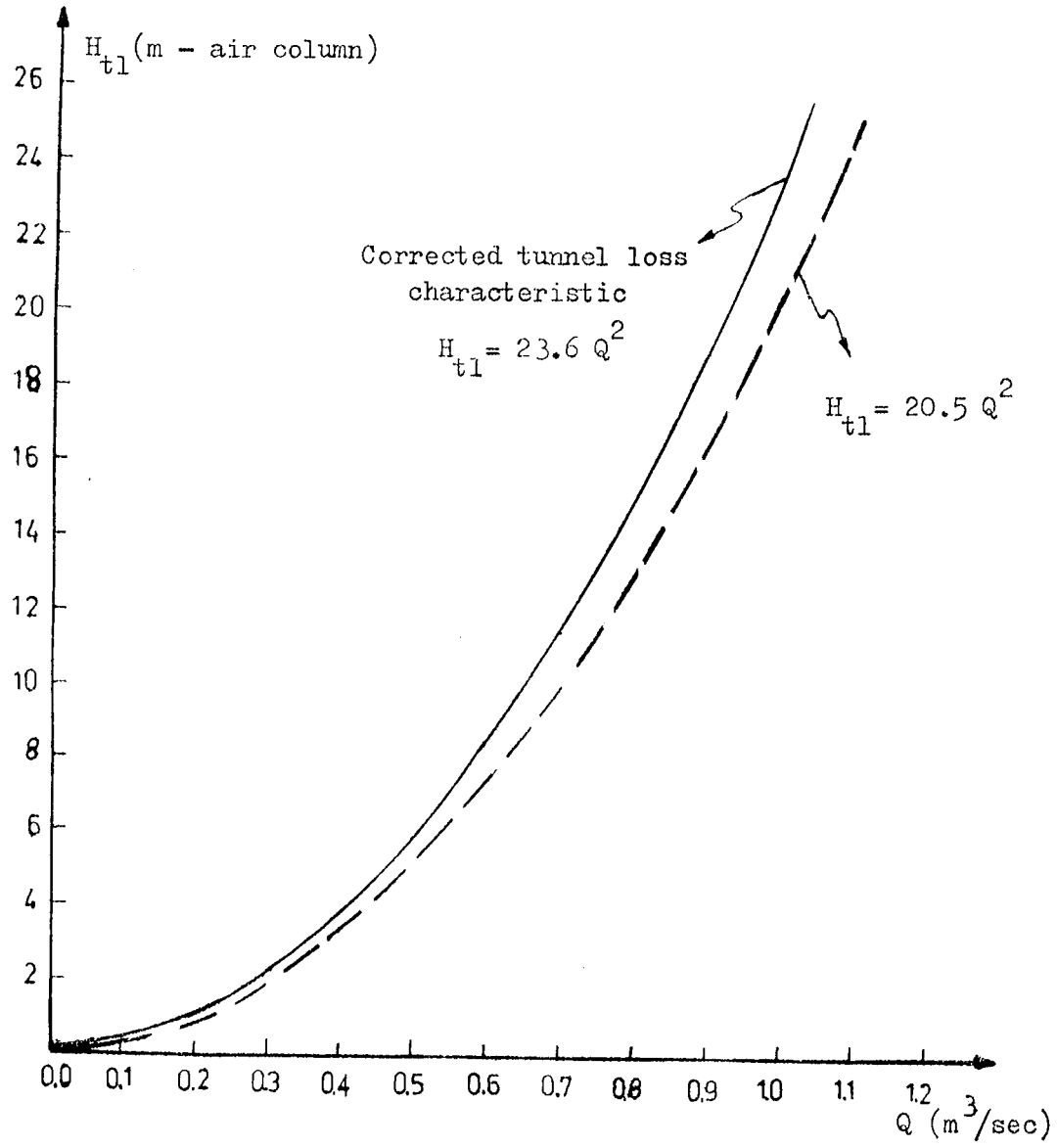

Fig.3.8 Tunnel Loss Characteristic

3.9. CALCULATION OF THE BLADE DIMENSIONS AND SELECTION OF THE FAN SPEED

After the fan static static pressure, H_{st}, and the axial velocity, v_a, at the design point were determined, the design of the fan impeller blades was made by using equations 3.18 to 3.25. In the blade design calculations, the rotor speed was determined as follows :

The rotor speed was assumed to change from 2000 to 3400 rpm by 200 rpm increments, and also the ratio of boss to rotor diameter was taken as 0.6. Considering the blockage effect of the rotor blades and the nascelle spokes, the axial velocity, v_a, was increased approximately by 10%. The following blade characteristics taken from figure 3.6 at $Re = 3.12 \times 10^5$ were used for each case

$$40 \leq C_L/C_D \leq 51$$

$$0.57 \leq C_L \leq 0.665$$

$$1^\circ \leq \alpha^\circ \leq 2.5$$

The change of C_L/C_D, C_L and α° along the span was assumed to be linear and is given in table 3.3.

A computer program was prepared for blade design calculations. The average Reynolds number R_{av} ($Re_{av} = (Re_{root} + Re_{tip})/2$), the root solidity σ, the average hydraulic efficiency η_h, and the average static efficiency η_{st}, were calculated at each speed and the calculated values were plotted against the speed and are given in figures 3.10 and 3.11.

In selecting the fan speed, the first restriction is the Reynolds number. Since all blade data for the selected blade profile is given for $Re = 3.12 \times 10^5$. The design speed is the one where the average Reynolds number across the blade span is equal to 3.12×10^5. From figure 3.10 it is seen that the fan speed corresponding to the above mentioned value of Reynolds number is found to be 2800 rpm. At this speed, the limitations imposed on such as the root solidity and the compressibility, mentioned in section 3.6, are also satisfied. So this speed was selected as the design speed. At the selected design speed, all blade parameters such as the blade cord c, the angle β_∞, the blade angle β, which

is equal to $\beta_\infty + \alpha$, the static efficiency η_{st}, and the hydraulic efficiency η_h were calculated and the results of calculations are tabulated in table 3.4. The orientations of the blade sections at some calculated radii are shown in figure 3.11.

Table 3.3 Variation of Blade Characteristics along the Span of RAF 6E Blade Profile at Re = 3.12×10^5

r(mm)	C_L/C_D	C_L	α°
123	51.00	0.665	2.50
126	50.58	0.661	2.44
129	50.18	0.657	2.38
132	49.77	0.654	2.33
135	49.36	0.650	2.27
138	48.95	0.647	2.22
141	48.55	0.643	2.16
144	48.14	0.640	2.11
147	47.87	0.636	2.05
150	47.48	0.633	2.00
153	46.98	0.629	1.94
156	46.55	0.626	1.88
159	46.10	0.622	1.83
162	45.70	0.619	1.77
165	45.29	0.615	1.72
168	44.88	0.612	1.66
171	44.47	0.608	1.61
174	44.07	0.605	1.55
177	43.66	0.601	1.50
180	43.25	0.598	1.44
183	42.80	0.594	1.38
186	42.44	0.591	1.33
189	42.00	0.587	1.27
192	41.60	0.584	1.22
195	41.21	0.580	1.16
198	40.27	0.577	1.11
201	40.40	0.573	1.05
204	40.00	0.570	1.00

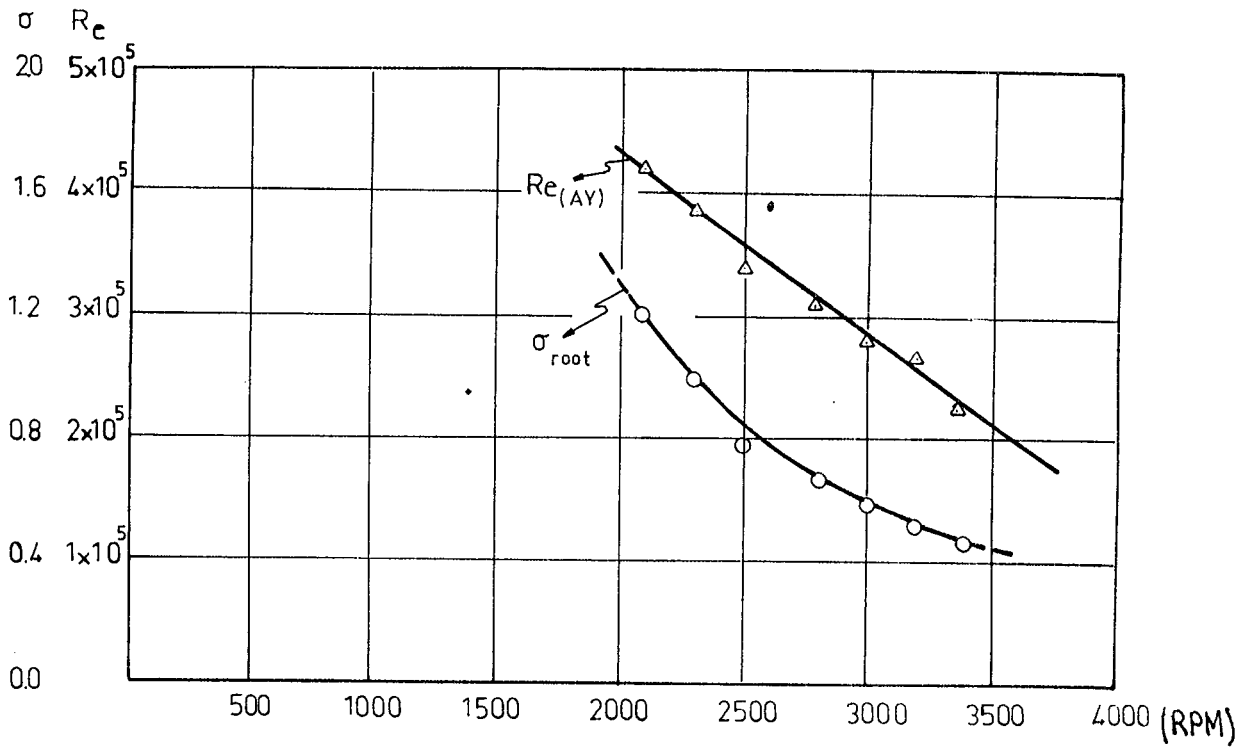

Fig.3.9 Change of Re and σ_{root} with the Fan Speed

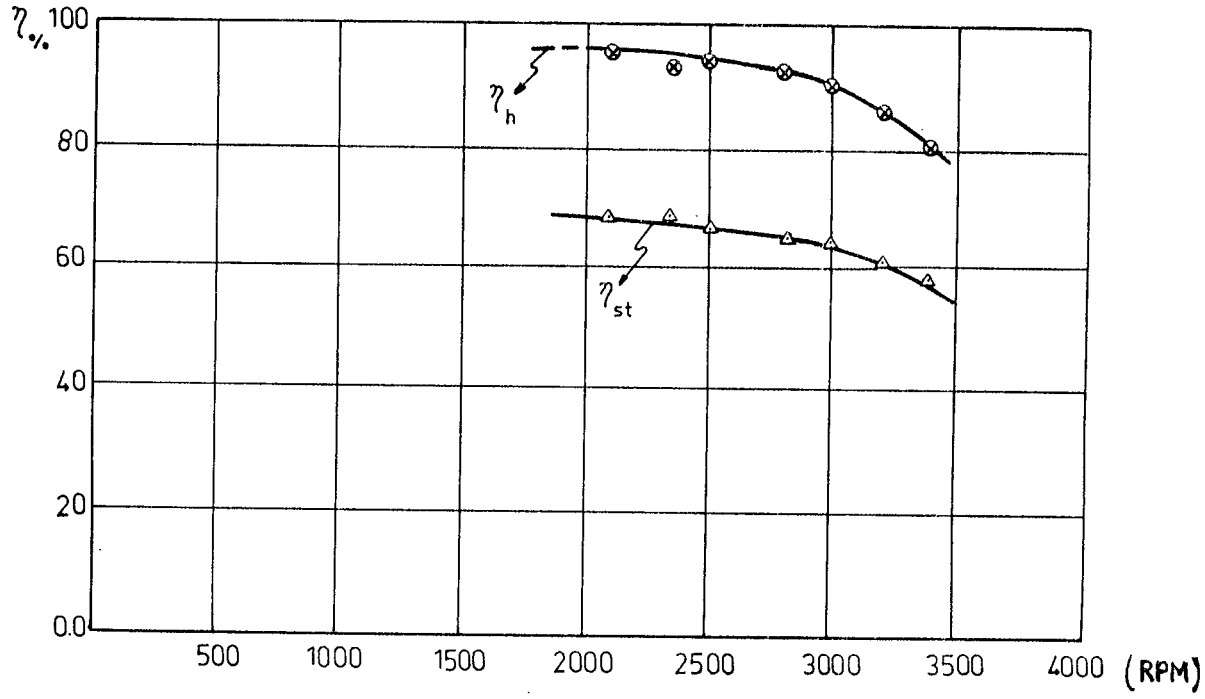

Fig.3.10 Change of η_h and η_{st} with the Fan Speed

Table 3.4 Calculated Blade Parameters.

r(mm)	η_{st}	η_h	β_∞°	β°	c(mm)
123	0.669	0.954	22.14	24.64	132.0
126	0.666	0.952	21.54	23.98	129.6
129	0.667	0.950	20.98	23.32	127.3
132	0.665	0.948	20.45	22.78	124.6
135	0.664	0.947	19.95	22.22	122.2
138	0.662	0.945	19.47	21.69	120.2
141	0.661	0.943	19.01	21.17	118.1
144	0.660	0.941	18.58	20.69	116.0
147	0.659	0.940	18.16	20.21	114.1
150	0.657	0.937	17.77	19.77	112.2
153	0.655	0.935	17.39	19.33	110.8
156	0.654	0.933	17.03	18.91	109.2
159	0.653	0.931	16.68	18.51	107.5
162	0.652	0.929	16.35	18.12	106.0
165	0.650	0.927	16.03	17.75	104.5
168	0.649	0.925	15.72	17.38	103.2
171	0.648	0.923	15.43	17.04	101.8
174	0.646	0.921	15.14	16.69	100.5
177	0.645	0.919	14.87	16.37	99.6
180	0.643	0.917	14.01	16.05	98.1
183	0.642	0.915	14.35	15.73	97.2
186	0.640	0.913	14.11	15.44	96.2
189	0.639	0.911	13.87	15.14	95.1
192	0.637	0.909	13.64	14.86	94.0
195	0.636	0.906	13.42	14.58	93.2
198	0.634	0.904	13.21	14.32	92.2
201	0.633	0.902	13.00	14.05	91.4
204	0.633	0.900	12.90	13.90	90.8

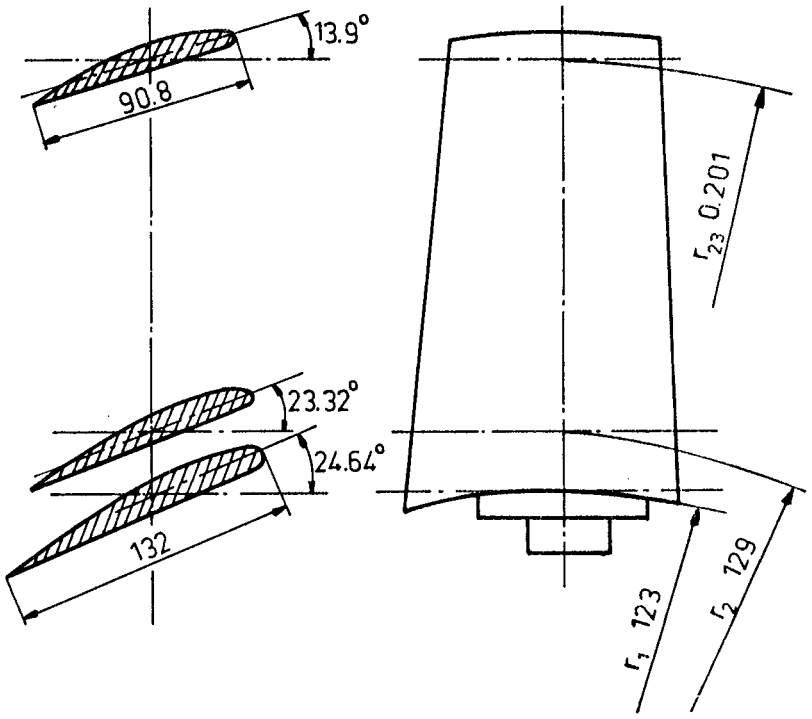

Fig.3.11 Orientation of Blade Profiles at Some Calculated Radii

3.10. DESIGN OF THE NASCELLE

For the nascelle shape, any efficient streamlined body of revolution may be used (1). One such shape is illustrated in figure 3.13 and its coordinates are given in Appendix 2.

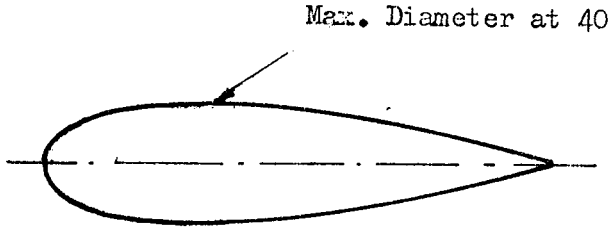

Fig.3.12 Streamlined Body of Revolution.

Since the fan discharges the air into atmosphere, only the aft portion of the streamlined body of revolution was used. The diameter of the streamlined body illustrated in gigure 3.12 reaches a maximum at 40% of cord length position. When designing the nose and tailfairing, the forward and rearward portions of the body can be considered seperately. If the flow seperation is to be avoided, the nose fairing should be kept relatively short while the tailfairing may have to be long.

In the design of the streamlined body of revolution, the term fineness ratio, f, is defined and is given in equation 3.34 (1).

$$f = \frac{l}{2\, r_b} \qquad (3.38)$$

Where l is the length of streamlined body, and r_b is the radius of the boss. A suitable fineness ratio for nose fairing is given as 1.2 at which it provides a good entry to the fan. This ratio, however, can be reduced without any noticable penalties (1).

In the present design, this ratio, f, was taken as 0.6. As is shown in figure 3.12, the aft portion of the body upto to the position where its diameter becomes maximum was used as the nascelle shape.

CHAPTER 4

MATERIAL SELECTION AND STRENGTH CALCULATIONS

4.1. FAN BLADE MATERIAL

For the selection of fan material, there are some alternatives. Mostly used fan materials are wood, aluminium alloy, steel and impregnated wood. Before choosing the fan material, its properties should be determined. The fan material should have high resistance to corrosion and abrasion in order to maintain its shape and strength under varying load conditions. Furtheremore, since the aerofoil type fan rotor blades are subjected to high inertia (mainly centrifugal forces) and bending (due to lift and drag) forces it is then highly desirable to select a blade material which has high strength -to- weight ratio when the service conditions are demanding.

The mostly used wooden material for fan blades are oak, birch and wallnut. Fan blades made out of wood have usually fixed pitch i.e. the correct number of blades are permanently fixed to the boss at the desired pitch angle. In some cases, the adjustable pitch fans are also manufactured out of wood. The fans made out of wood have some advantages over the fan made out of the other materials. If highly skilled - carving work is available, it is rather easy to manufacture the fan blades out of wood in comparison to the fan blades made out of other materials. Also its production cost is low and it has high internal damping, and high fatigue strength to weight ratio. However, it also has some disadvantages. It is easily effected by moisture, and it splits easily along the grains under longitidunal shear.

In axial fan technology, most of the aerofoil shaped axial fan blades are made of high strength cast aluminium. Advantages of aluminium are its relative ease of manufacture and its lightness compared with steel blades, It is easily machined and finished by grinding and buffing.

Though steel is occasionally used for aerofoil type fan blades, because of production diffuculties and its low strength to weight ratio, stell is not prefered material. However hollow steel blades are used for certain applications.

Impregnated wood is also used for fan blade material. Wood laminates are impregnated with a phenolformaldehyde resin, compressed and formed at elevated temperatures. After carving, it is covered with cellulose acetate. Sometimes Glass Reinforced Plastics (GRP) are used as blade material.

In the present work, since high skilled-carving work is not available in our department and keeping in mind the difficulties in manufacturing steel blades, it was decided to make the fan blade out of cast aluminium. Therefore, a model of the fan blade was made and it was ordered to a private foundry for casting. But, some difficulties arised during casting due to the low density of the aluminium. For instance, large pours existed on the surface of the blades and also the tips of the blades weren't cast faithfully. To overcome this problem, a low melting die casting alloy was substituted. This alloy, though, was a higher density and lower strength, turned out to be highly satisfactory. The fan boss was cast from aluminium succesfully and then it was machined.

4.2. STRENGTH ANALYSIS

4.2.1 Blade stress analysis

The fan blade is considered as a rotary cantilever beam when it is in operation. The blade is subjected to various loads. The following steady loads are the principal loads in determining the blade strength (8).

a) Bending forces acting on the blade,

b) Centrifugal force due to rotation

4.2.2 Bending stresses

The forces causing bending moment on the blade are drag and lift forces. The drag force may be neglected because, the drag coefficient is very small in comparison to the lift coefficient for the selected aerofoil.

The lift force on a blade may be expressed as shown in equation 4.1 (8).

$$L = \int (p_s' \, 2\pi r).dr \; / \; z. \, Cos \tag{4.1}$$

Where p_s' is the static pressure difference across the impeller which is given in equation 4.2 and its derivation is given in Appendix 1.

$$p_s' = \rho. \, u.v_{u_2} - \frac{1}{2} \rho. \, v_{u_2}^2 \tag{4.2}$$

Since the most critical section is the circular root section shown in figure 4.1, the bending moment due to the lift force at this section may be written as follows :

$$M = \int_{r_1}^{r_2} p_s' \, 2\pi r.(r-r_1) \, dr \; / \; z \, Cos\beta_\infty \tag{4.3}$$

Where r_1 and r_2 are the radii of the blade root and blade tip respectively. The integration of equation 4.3 causes some difficulties since p_s' and $cos\beta_\infty$ are both functions of radius. But, the order of the magnitude of the force may be estimated by using the fan static pressure p_{st} for p_s' and using the value of angle β_∞ which will cause maximum bending moment. This angle corresponds to the value of β_∞ at the blade root. Therefore, equation 4.3 may be written in the following form (8).

$$M = \frac{2\pi.p_{st}}{z.Cos\beta_\infty} \int_{r_1}^{r_2} r.(r-r_1).dr \tag{4.4}$$

Substituting the already determined values of r_1= 0.123 m, r_2= 0.204 m, z = 4, p_{st}= 218 pa, and β_∞= 22.14° into equation 4.4, the value of M at the root section is found to be

$$M = 0.2146 \quad N\text{-}m.$$

Bending stress, σ_B, is defined in equation 4.5 as

$$\sigma_B = \frac{M.y}{I} \tag{4.5}$$

Where M is the bending moment at the root section. y is the distance from the centroidal axis of the blade to the blade surface at the tension side.

I is the moment of area of the cross hatched about the centroidal axis shown in figure 4.1 .

Substituting the calculated values of M = 0.2146 N-m, y = 0.0055 m and $I = 8.24 \cdot 10^{-9}\ m^4$ into equation 4.5, the bending stress at the root is determined as

$$\sigma_B = 1.43 \cdot 10^5\ Pa$$

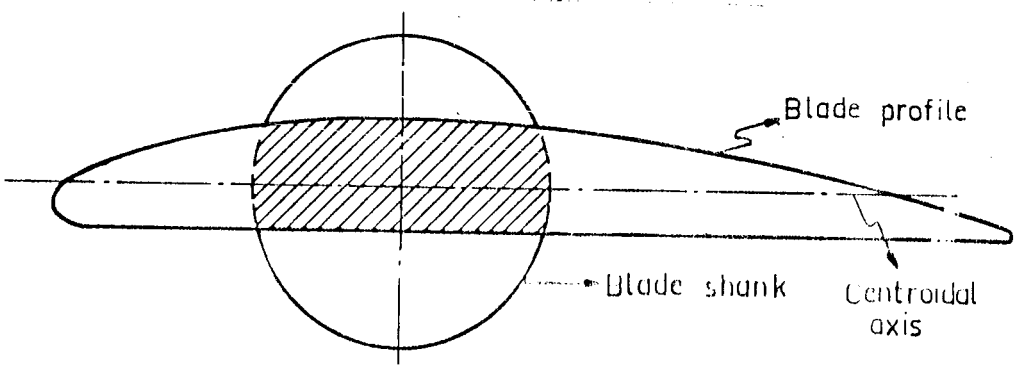

Fig. 4.1 Blade Shank Portion

4.2.3 Centrifugal stresses

The centrifugal force acting on a blade element at a distance r from the axis of rotation shown in figure 4.2 can be expressed as

$$dF_{cf} = W^2 \cdot r \cdot dm \qquad (4.6)$$

Where W is the angular speed and dm is the differential mass of the element shown in figure 4.2 .

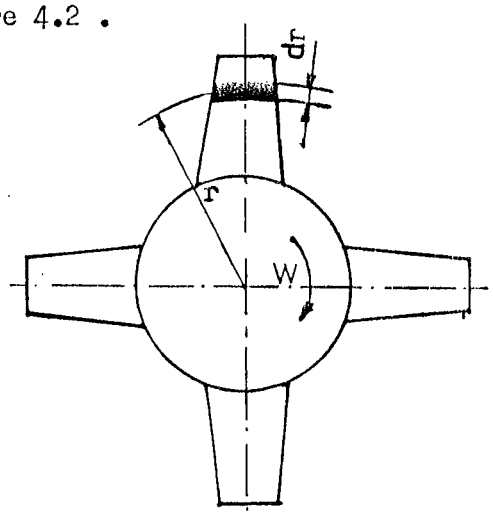

Fig. 4.2 Position of a Blade Element on the Fan Blade

If equation 4.6 is integrated over the span of the blade, the following equation is obtained.

$$F_{cf} = \rho \cdot W^2 \int_{r_1}^{r_2} A(r).r.dr \qquad (4.7)$$

Where A is the area of cross section of the blade normal to the line joining the centroids of the blade profiles at the root and at the tip of the selected blade and ρ is the density of the blade material.

The area A in equation 4.7 changes from root to tip and the expression for this area is given in table 3.1 as

$$A = 0.0738\ c^2 \qquad (4.8)$$

Where c is the cord length of the aerofoil at the desired blade cross section for which the area is calculated.

Substituting equation 4.8 into equation 4.7, the following equation may be obtained

$$F_{cf} = 0.0738\,\rho.W^2 \int_{r_1}^{r_2} c^2.r.dr \qquad (4.9)$$

Since the blades were designed such that the profile centroids lie on a radial line and the blades have approximately a straight taper, the cord c can be written as a function of r and is given in equation 4.10.

$$c = c_1 - \frac{(r - r_1)}{(r_2 - r_1)} \quad (c_1 - c_2) \qquad (4.10)$$

Where c_1 and c_2 are the cord lengths at the root and at the tip of the blade respectively.

Substituting the values of r_1, r_2, c_1 and c_2 into equation 4.10, it simplifies to the form shown below.

$$c = 0.1945 - 0.5086\ r \qquad (4.11)$$

Therefore, the centrifugal force F_{cf} can be expressed only as a function of r and is given in equation 4.12 .

$$F_{cf} = 0.0738 \rho . W^2 \int_{r_1}^{r_2} r.(0.0378 - 0.1978r + 0.258r^2).dr \qquad (4.12)$$

Since the most critical section is at the root of the blade, equation 4.12 is integrated from the root, $r_1 = 0.123$ m, to the tip, $r_2 = 0.204$ m, for N = 2800 rpm and $\rho = 7000$ kg/m^3. From this integration, the centrifugal force at the root of the blade is calculated as

$$F_{cf} = 7366.11 \text{ N}$$

The normal stress at the root of the blade due to this centrifugal force is calculated by dividing the centrifugal force, F_{cf}, at the cross hatched area shown in figure 4.1 and the result is given below.

$$\sigma_{cf} = 141.58 \cdot 10^5 \text{ Pa}$$

The combined normal stress, σ_c, due to the bending moment and centrifugal effect is equal to the summation of these two stresses and is equal to

$$\sigma_c = 143.05 \cdot 10^5 \text{ Pa}$$

When the stress is compared with the strength of the blade material which is equal to approximately $800 \cdot 10^5$ Pa , it would be seen that the design is safe. The strength of the blade material was determined experimentally by using the standard test specimens made out of blade material.

In the above calculations the stress concentration at the root of the blade was neglected because no specific data was available for this purpose. However this was taken care of by the generous allowance for the factor of safety.

The strenght calculations were based on the assumption of maximum possible static loading though it may be argued that the blades are subjected to dynamic loads, the usual design practice for low pressure fans is to employ the static load.

4.2.4 Hub stresses

In calculating the hub stresses the hub was considered as a rotating disc with a central hole and having an inner radius of r_{h_1} and an outer radius of r_{h_2}. The hub material has a density of ρ_h and poisson ratio of μ_h.

When the disc rotates with an angular velocity W about its axis, there will be stresses tending to strain the disc in a radial and tangential directions. These stresses are called radial and hoop stresses respectively. The maximum values of radial stress σ_r and hoop stress σ_h are given in equations 4.13 and 4.14 (8).

$$\sigma_{r_{max}} = \rho_h \cdot \frac{W^2}{8} (\mu_h + 3) (r_{h_2} - r_{h_1})^2 \qquad (4.13)$$

$$\sigma_{h_{max}} = \rho_h \cdot \frac{W^2}{4} ((\mu_h + 3) r_{h_2}^2 + (1 - \mu) r_{h_1}^2) \qquad (4.14)$$

Since the hub also carries the fan blades which will increase the radial and hoop stresses, their effect should be included. In reference 8 the effect of the mass of the blades is approximated by using the following equation.

$$\rho_h' = \left(\frac{\text{Disc mass + blade mass}}{\text{Disc mass}} \right) \cdot \rho_h \qquad (4.15)$$

and ρ_h' is used in place of ρ_h in equations 4.13 and 4.14 .

For the designed fan :

mass of the disc = 3.0 kg

mass of the blades = 2.2 kg

Substituting the above values into equation 4.15, the value of ρ_h' is calculated as

$$\rho_h' = 1.73 \rho_h$$

Then equations 4.13 and 4.14 reduce to

$$\sigma_{r_{max}} = 1.73\ \rho_h \cdot \frac{W^2}{8} (\mu_h + 3)(r_{h_2} - r_{h_1})^2 \qquad (4.16)$$

$$\sigma_{h_{max}} = 1.73\ \rho_h \cdot \frac{W^2}{4} ((\mu_h + 3) r_{h_2}^2 + (1 - \mu_h) r_{h_1}^2) \qquad (4.17)$$

In the design of the hub, the inner radius r_{h_1} is selected as 0.098 m . Substituting the values of $r_{h_2} = 0.123$ m, $\mu_h = 0.33$, $\rho_h = 2700\ kg/m^3$ and N = 2800 rpm into equation 4.16 and 4.17, the following values are calculated for $\sigma_{r_{max}}$ and $\sigma_{h_{max}}$.

$$\sigma_{r_{max}} = 2.08 \times 10^5\ Pa$$

$$\sigma_{h_{max}} = 56.98 \times 10^5\ Pa$$

When these stresses are compared with the strength of the hub material which is equal to approximately 12.5×10^7Pa, it would be seen that the design is safe. A large thickness is selected for hub because space is needed for shank portion of the blade. The strength of the hub material was determined experimentally by using the standard test specimen made out of hub material.

CHAPTER 5

MANUFACTURING AND CONSTRUCTION OF THE FAN AND THE TEST SET-UP

5.1. MANUFACTURING OF THE FAN BLADE

For manufacturing the blade, first its model was made. In making the model, the following procedure was carried out.

The cord length c and the blade angle β, which have been calculated at each radius r with 3 mm-increments from the root to the tip of the fan blade, are sufficient to determine the complete blade dimensions. Using the previously calculated values of c and the values listed in table 3.1, the following blade dimensions were calculated.

a) The co-ordinates of the aerofoil sections at each calculated radius.

b) The centroids of the aerofoil sections.

c) The leading and trailing edge radii of the aerofoil sections.

The blade section profiles at each radius, starting from root to tip, were drawn on a cardboard and the centroids of each section was marke on it. Because of the small dimensions of the trailing and the leading edge radii of blade section profiles, the original dimensions of the blade were magnified ten-times before it was drawn on the cardboard. Plexiglass with 3 mm-thickness was used as the model material. The blades section profiles drawn on the cardboard were copied on the plexiglass to their original dimensions by using the pantograph machine in the machine shop.

Since the blade was designed such that the centroid of each section lies on a radial line, each blade section was drilled through its centroid. As shown in figure 5.1, a straight wire was placed through the holes drilled at the centroids of each blade section profiles.

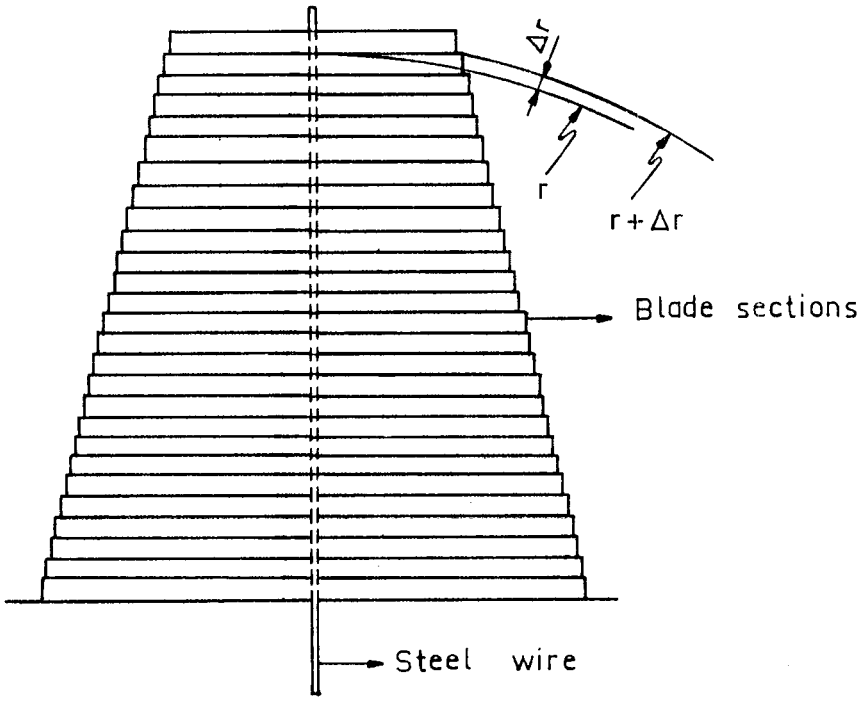

Fig.5.1. Construction of the Blade Sections

In examining figure 5.1, it will be seen that although the centroids of the blade section profiles lie on a distance of r from the axis of rotation, the leading and trailing edges of the blade sections lie on a distance of $r + \Delta r$. Since each blade section profile was designed on the assumption that each point on section profile lies on a distance r from the axis of rotation, this assumption was satisfied by bending the each blade section onto its own radius. This was accomplished by placing the plexiglass blade section on a properly curved wooden surface and the blade section was heated until it assumed the form of the wooden surface. A clamp shown in figure 5.2 was made to assemble the blade sections after each blade section was heated to its required radius.

As shown in figure 5.3 each blade section makes an angle β with respect to horizontal plane. Therefore, in the assembly clamp, first blade sections were oriented so that each blade section had the correct angle relative to horizontal plane and then they were compressed between the jaws of clamp.

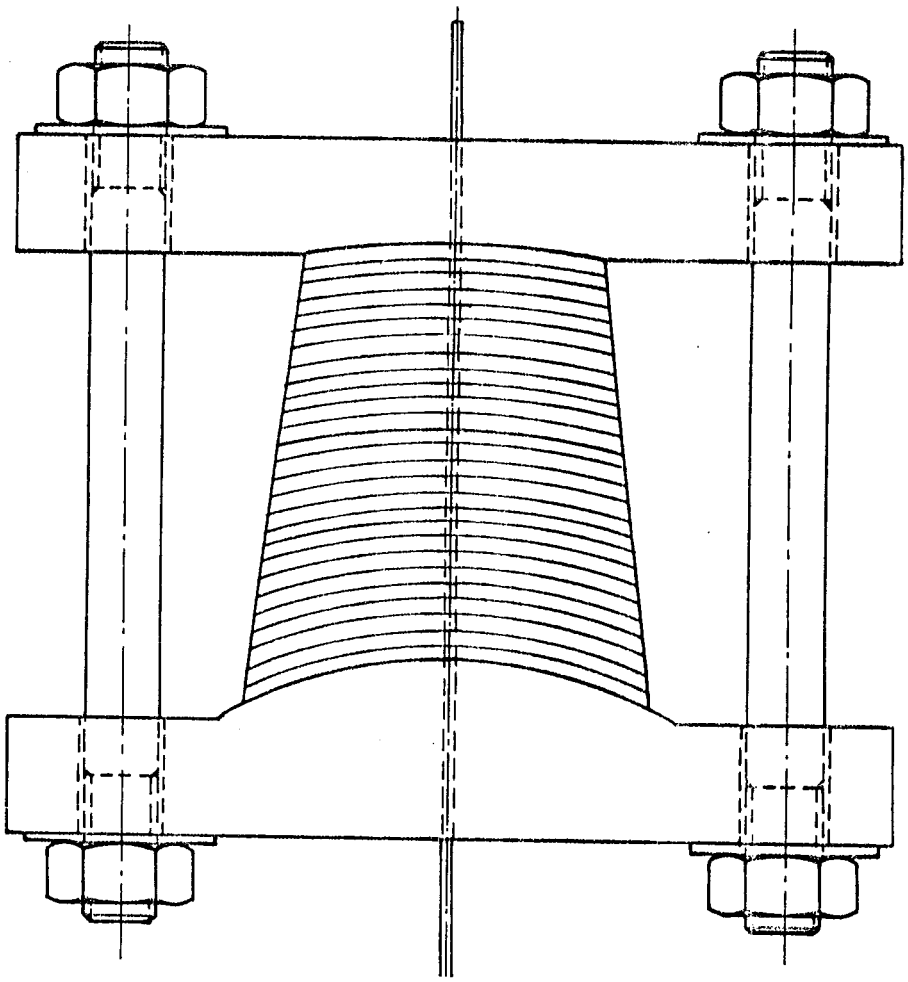

Fig.5.2 Device for Clamping the Blade Sections

Cloroform was employed as an adhesive to cement the blade sections together in layers. Then the surface of the model was finished to the required dimensions. The shank portion made out of the same material as the blade sections was glued to the root of the blade. The model of the blade where two different views of it are shown in figure 5.4a and 5.4b was made ready for casting.

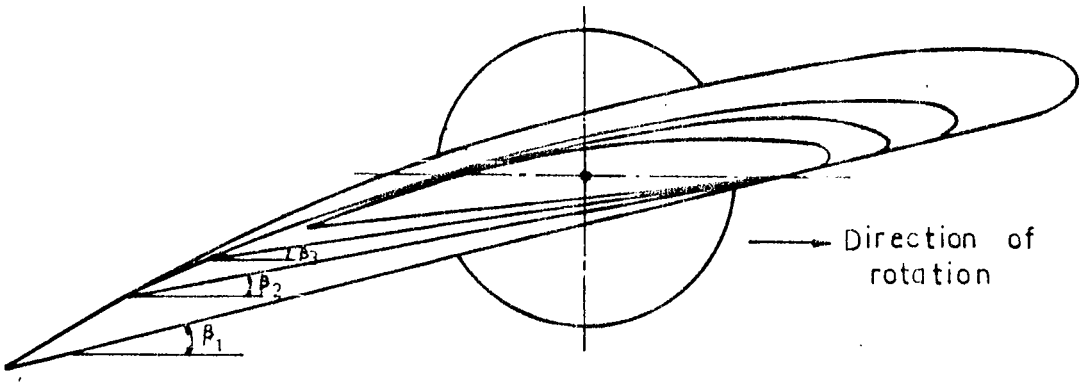

Fig.5.3 Blade Section Orientation

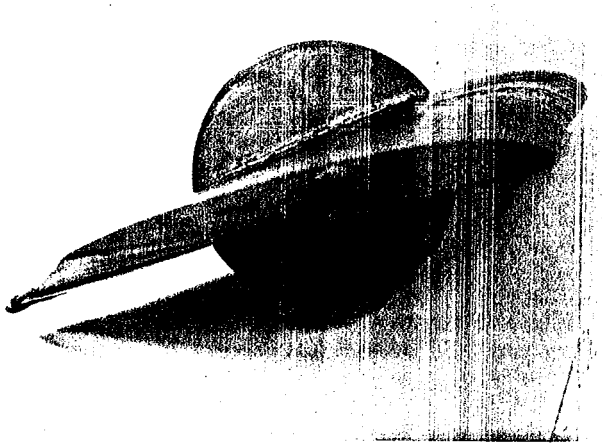

Fig.5.4a. Model of the Blade

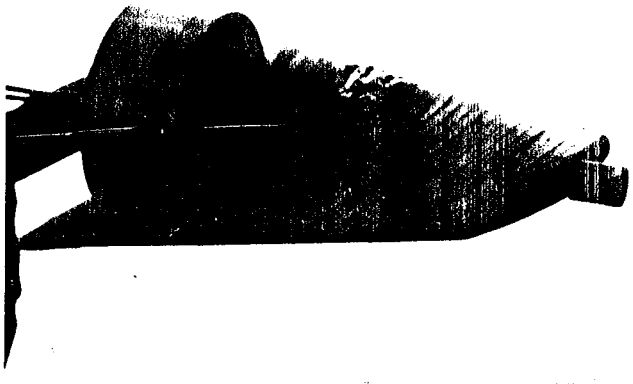

Fig.5.4b. Model of the Blade

5.2 CONSTRUCTION OF THE FAN AND THE DRIVE UNIT

The complete fan unit is basically composed of three parts namely, the fan hub, the blades and the fan shaft. Detailes of hub and blade assembly is shown in figure 5.5 . Blades are joined to the fan hub by two socket head bolts. The bolts are tightened at the outset such that although the blades can be intentionally turned by hand, they do not inadvertantly turn in actual operation. When the rotor is in rotational operation, the friction between the blade and the hub is increased by centrifugal force which prevents any change in the blade setting.
The O - Ring shown in figoru 5.5 is made of resillient material. It reduces the transmission of vibration between the blades and fan hub. Since vibration is the chief cause of material fatigue, it increases the service life of the fan.

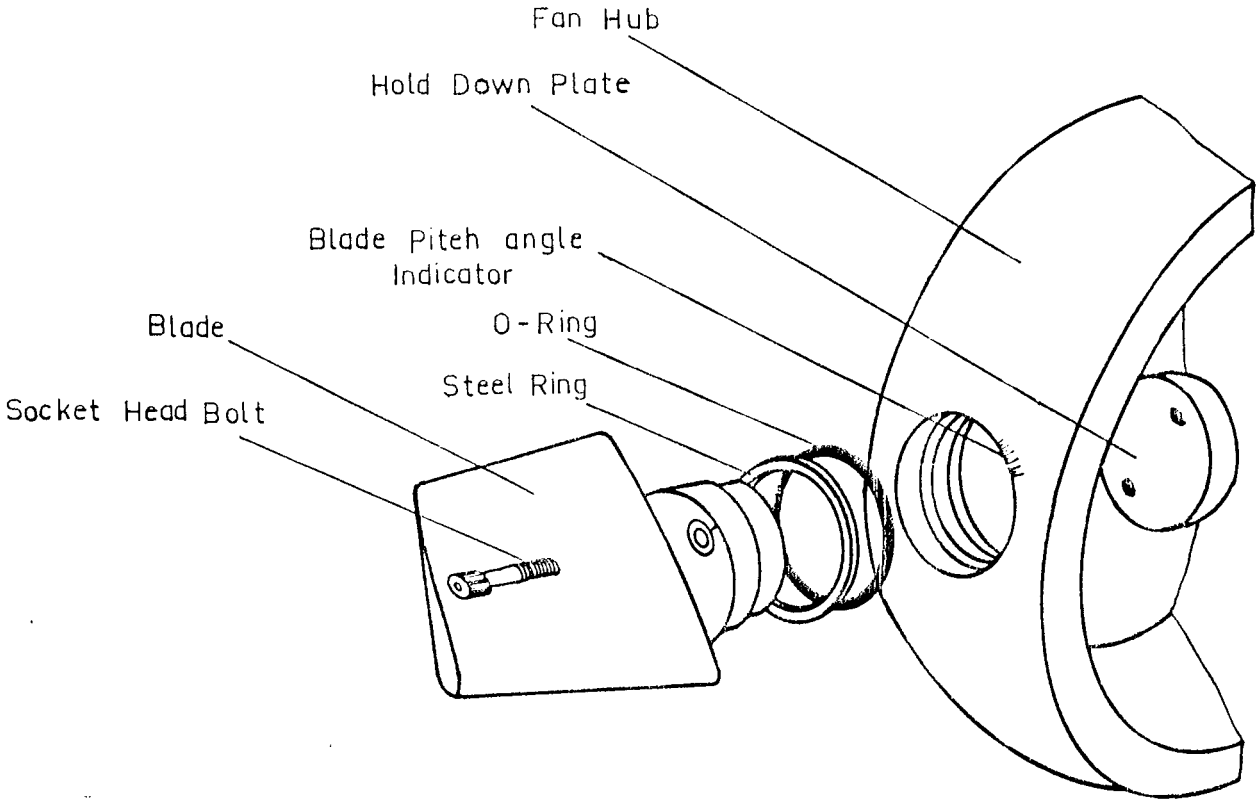

Fig.5.5 Details of Hub and Blade Assembly

Fan shaft was attached to the impeller hub by four socket head bolts and nuts and it was supported by two ball bearings. The fan and its drive unit are shown in figure 5.6 and 5.7 . In order to obtain different operational speeds, a pair of multi-stepped V-belt pulley was used. The pulley has five steps corresponding to rotational speeds of 750, 1070, 1610, 2060 and 2800 rpm.

A 4 KW A.C electric motor with a speed of 3100 rpm was used as the prime mover of the fan.

The fan was dynamically balanced together with its shaft and bearings before it was coupled to the drive unit.

Technical drawings of the fan unit are given at the end of the thesis.

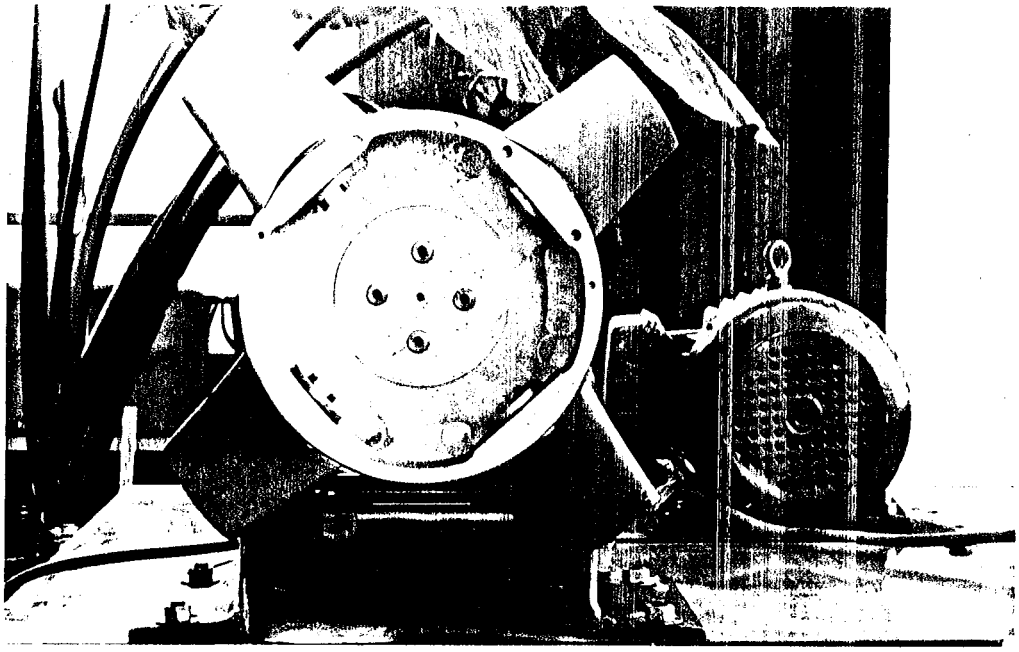

Fig.5.6 Left Side View of the Fan and its Drive Unit

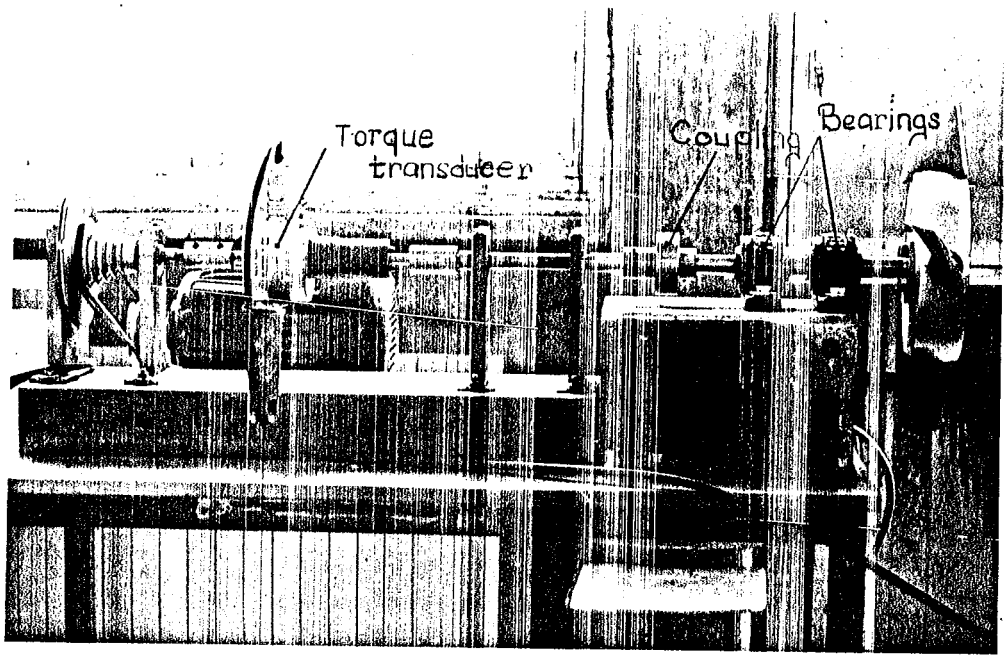

Fig.5.7 Front View of the Fan and its Drive Unit

5.3 CONSTRUCTION OF THE FAN TESTING SET-UP

The present fan was tested according to British standard BS 848. Fan testing methods are classified in this standard according to fan installation types. The four installation types used in this standard are as follows :

a) type A : Free inlet, free outlet;
b) type B : Free inlet, ducted outlet;
c) type C : Ducted inlet, free outlet;
d) type D : Ducted inlet, ducted outlet.

Although type C is more close to our application, type A was adapted to the type C as given in the standard and was used for testing of the fan because of difficulties in manufacturing the test set-up for type C. Free inlet condition was satisfied using the standardized inlet side test chamber. For the selected testing method, there are four methods of measuring the flowrate. These four methods are as follows :

a) Venturi nozzle or conical inlet

b) Inlet orifice

c) In-duct orifice with D and D/2 taps.

d) In-duct venturi nozzle.

In-duct orifice with D and D/? taps was selected as the flowrate measuring method. This type of orifice plates are easy to manufacture and the flowrate can be measured by this method as accurate as the other methods.

The selected fan testing set-up is shown in figure 5.8 . It is composed of six main parts namely :

a) Fan casing

b) Standardized inlet side test chamber

c) Diffuser

d) Orifice

e) Airduct

f) Auxiliary fan

Fan casing was made out of sheet metal having a thickness of 1.5 mm. In order that the air enters the fan with a minimum loss, a conical entry with an angle of 60^{o} was fitted to the inlet side of the fan casing as shown in figure 5.8 . A nascelle equipped with flow straighteners was placed in front of the fan, in order to enable a uniform axial entry to the fan. Furthermore, flow straighteners prevent the occurence of swirl in the inlet test chamber so that the static pressure measurement at the chamber wall is not effected by any swirling flow in that chamber. The clearance between the fan and its casing was taken to be approximately 2 mm. Inlet side test chamber was also made out of sheet metal having a thickness of 1.5 mm. It was constructed out of four pieces and was assembled to each other with the flanges.

In accordance with BS 848, some restrictions on the dimensions of the inletside test chamber are imposed. The test chamber cross section may be circular, with diameter D_3, square $D_3 x\ D_3$, or rectangular with D_3

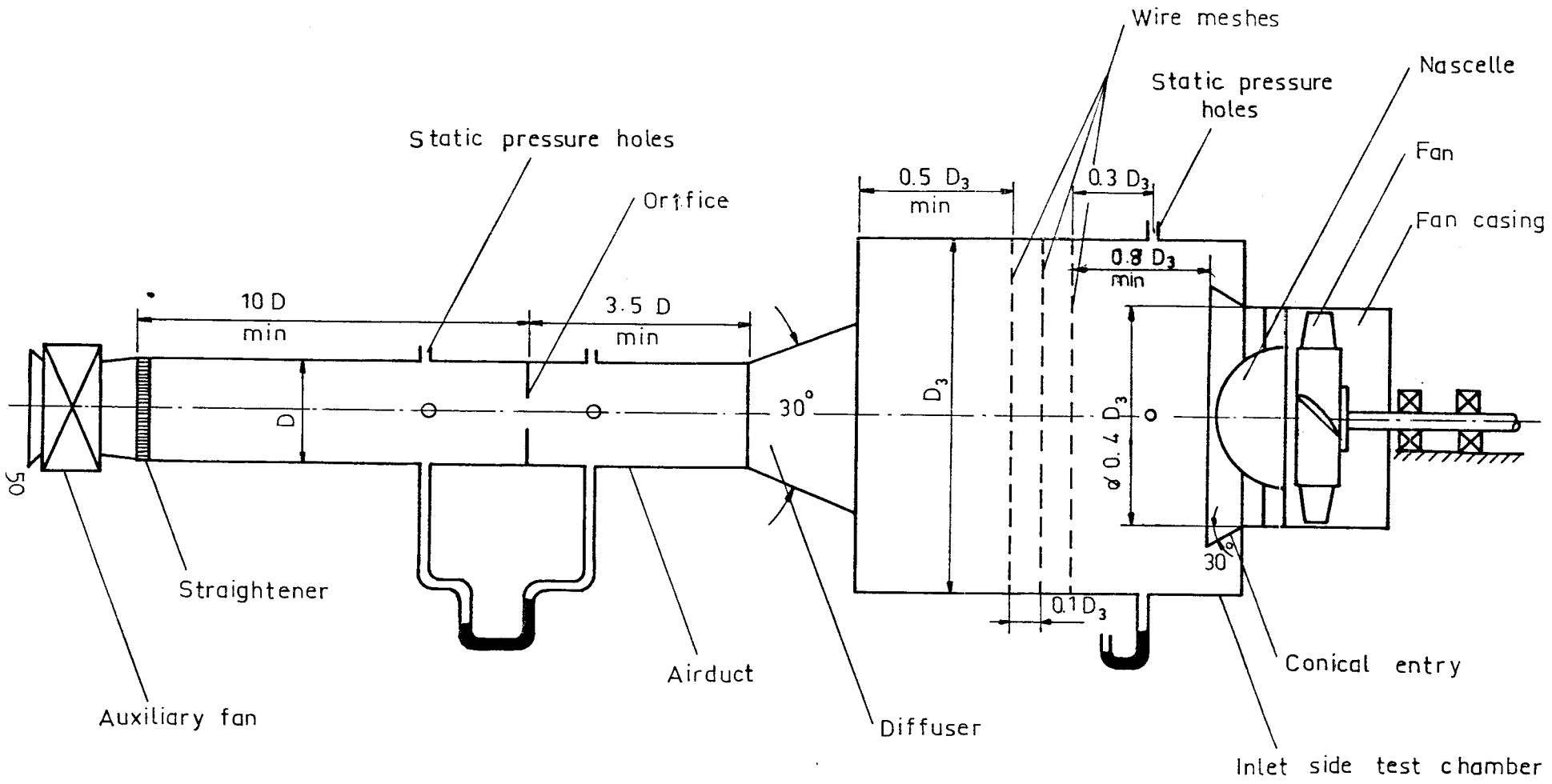

Fig.5.8 Schematic View of the Fan Test Set-up

the shorter side. The minimum dimensions of the inlet chamber are given in figure 5.8 . The inlet cross sectional area of the fan under test should not be greater than $D_3^2 / 8$. The inlet cone must be coaxial with the inlet chamber. In designing the chamber, precautions have been taken to secure reasonably uniform flow approaching the fan. The flow uniformity condition is considered to be met, if maximum air velocity at the pressure measuring section in the inlet chamber nowhere exceeds 1.25 times the average velocity at the same plane or 2.5 m/sec, whichever is greater (12). If three uniform wire screens having 60 %, 50 %, and 45 % open area are placed in the inlet chamber with $0.3D_3$ apart normal to the flow direction, and they are adequately supported and sealed at the inlet chamber wall,it is possible to have a flow at the fan inlet meeting the above mentioned conditions (12). In the present set-up, screens with 47 %, 50 % and 62 % free area were used because, screens with 45 % and 60 % free area were not available in the market. The air chamber cross section was selected square with a side length of 1060 mm which satisfies the limitations imposed on it. The air enteres the chamber through a diffuser with an included angle of 30°.

An anti-swirl device called "flow straightener" at the entrance of the air duct as shown in figure 5.9 was used to prevent the growth of swirl in the flow. This device with length l consists of a nest of equal cells of sequare cross section with a side of length t as shown in figure 5.9 .

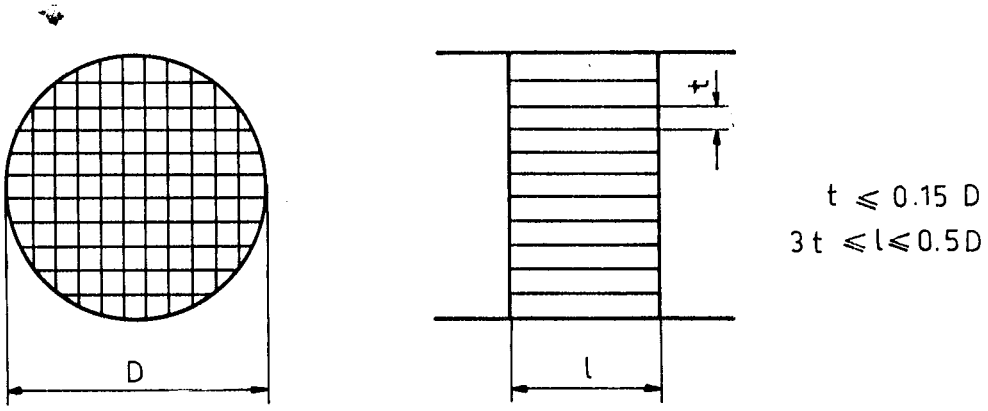

Fig.5.9 Flow Straigntener (12)

In-duct orifice with D and D/2 tappings was used to measure the flowrate through the fan. The orifice plate and the associated pressure tappings conform to the dimensions shown in figures 5.10a and 5.10b. This orifice was made out of an aluminum plate. The upstream face of the orifice was finished by a very fine radial cut from its centeroutwards so that the upstream edge of the orifice be sharp. The ratio of the orifice diameter to the duct diameter, λ, was taken to be 0.62 . The wall static pressure tappings are four in number. The axis of each tap intersects the duct axis at right angles. Dimensions of the wall tapping holes conform to the dimensions shown in figure 5.11 . Tapping connections to obtain average static pressure at the measuring station are shown in figure 5.12 .

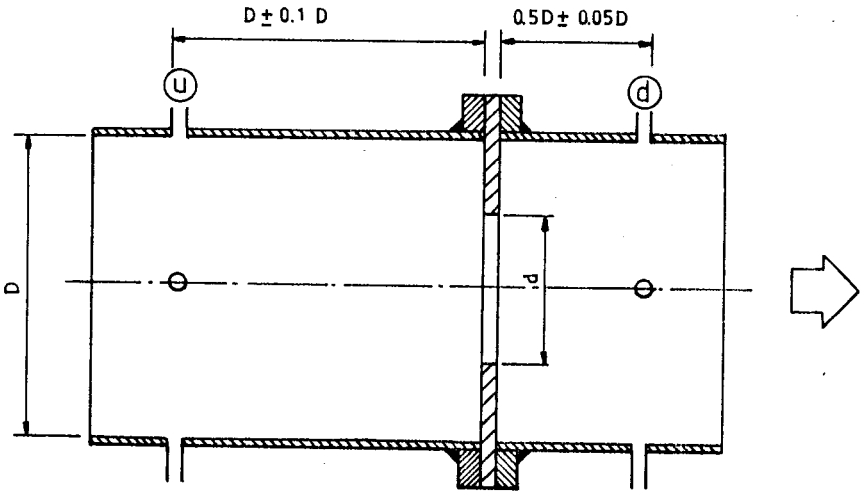

Fig.5.10a In-duct Orifice with D and D/2 Tappings (12)

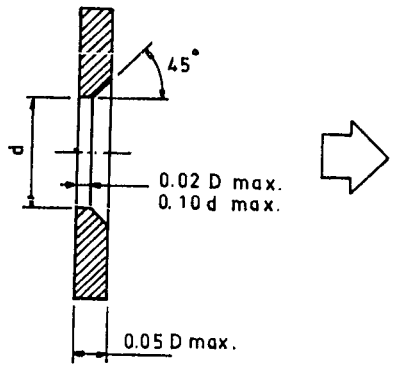

Fig.5.10b Details of the Orifice Plate (12)

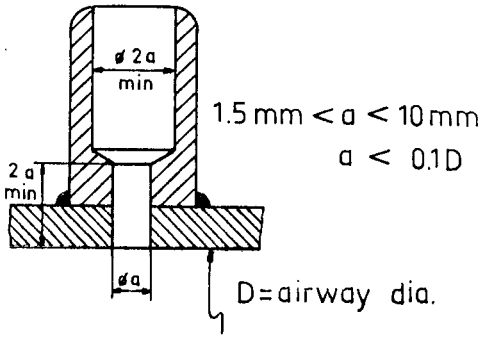

Fig.5.11 Construction of Wall Pressure Tappings (12)

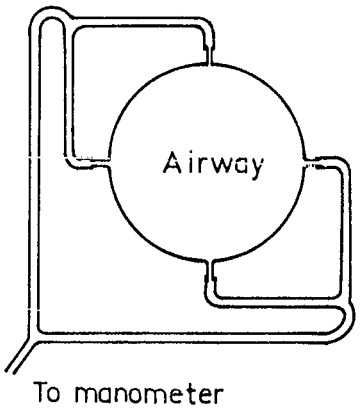

Fig.5.12 Pressure Tapping Connections to Obtain Average Static Pressure (12).

The air duct was manufactured in the work shop. It was made out of sheet metal with a thickness of 1.5 mm. The length of the duct conforms to the dimensions shown in figure 5.8 . As shown in figure 5.14, the complete air duct was constructed out of four pieces. When connecting these parts together, care was taken so that parts were in alignment with each other and the joints were free from internal protrusions. The air ducts were joined to each other as shown in figure 5.13 . According to the British standard BS 848, there are some restrictions on the diameter of the air duct and the orifice. According to this standard ;

$$D_{duct} > 50 \text{ mm}$$

$$d_{orifice} > 25 \text{ mm}$$

The upper limits of the value of the above diameters are determined by the Reynolds number of the flow through the orifice. For in-duct orifice with D and D/2 tappings, the range of the Reynolds number at the orifice is shown in figure 6.2 , and is also given below.

$$1.10^4 \leqslant Re_d \leqslant 1.10^6$$

According to BS 848, orifice plate measures the correct flowrate when operated within aforementioned range of Re_d .

In accordance with the above restrictions, the orifice diameter was selected as 186 mm.

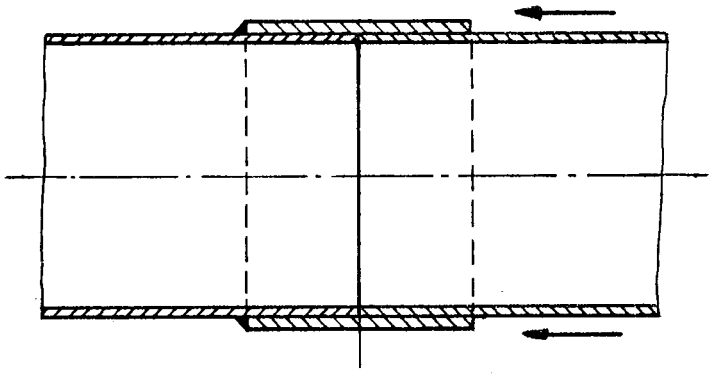

Fig.5.13 Air Duct Connection

Because of high system resistance of the fan testing set-up, an auxiliary centrifugal fan, which has backward curved blades, running at 2150 rpm was used to obtain the full range of p_{tf}- Q characteristic of the tested fan.

The flow through the air duct was throttled by a throttling plate mounted at the inlet of the auxiliary fan. When the auxiliary fan was connected to the fan testing set-up, the flowrate through the auxiliary fan inlet was found to be approximately 0.9 m^3/sec .

The whole system was assembled in the Fluid Mechanics Labaratory after manufacturing of each component of the test set-up.

Air leakage test was done on the test set-up by using soap foam.

A general view of the fan test set-up is shown in figure 5.14 .

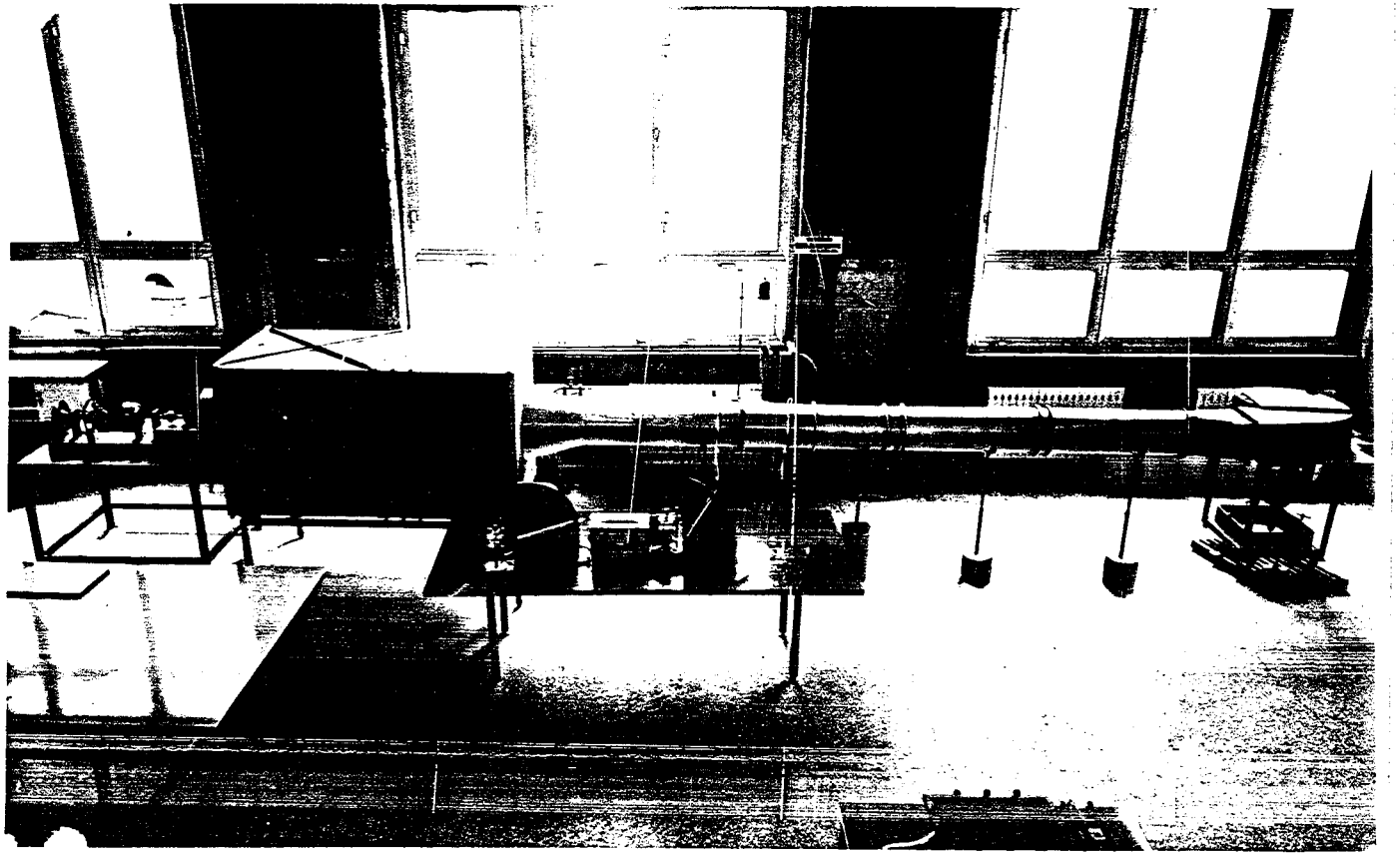

Fig.5.14. General View of the Fan and the Test Set-up

CHAPTER 6

MEASUREMENTS AND CALCULATIONS

6.1. DETERMINATION OF THE POWER INPUT TO THE FAN

The performance of a fan is determined by the power input to the fan (impeller power P_R), volume flowrate Q and the fan total pressure p_{tf} or the fan static pressure p_{st}.

In determining the power input to the fan, torque at the fan shaft was measured by a torque transducer shown in figure 5.7. A strain indicator was used as the readout instrument of the torque transducer. The specifications of the torque transducer and the strain indicator are given in Appendix 3. Calibration of the torque transducer was done with a 60 kΩ test resistor as follows :

Strain indicator was brought to zero balance where there was no torque on the transducer shaft, then the test resistor of the torque transducer which simulates 80 % of the full scale of the capacity of the torque transducer was connected to the input terminals of the strain indicator. Strain indicator reading difference of the loaded and unloaded conditions corresponds to the torque of 80 % of full load capacity of torque transducer. The reading difference was found to be 2560 μin/in. This strain corresponds to a torque of 80 in-lb (9.04 N-m). Since the strain changes linearly with the applied torque T, the relation between the applied torque and the strain is determined and is given in equation 6.1 .

$$T = 0.00353 \in \quad (N\text{-}m) \qquad (6.1)$$

Where $\in$ is strain in μin/in

The fan impeller is not mounted directly on the drive motor. Therefore, in determining the net power input to the fan impeller, it is necessary to deduct from the shaft power an alowance for bearing losses, for losses in the pulley and in the flexible coupling. These losses were determined as follows :

The impeller was replaced by a disc of equal weight having negligible aerodynamic resistance. This provided the same bearing loads, and it was run at the same speeds as the planned testing speeds of the experimental fan. The friction torque and the windage losses due to bearings and the flexible coupling were measured and are given in table 6.1 . Net torque on the fan impeller for any testing point was calculated by using equation 6.1 and 6.2 after the total strain ϵ_t on the fan shaft was measured. The strain due to the net impeller torque is calculated as

$$\epsilon = \epsilon_t - \epsilon_o - \epsilon_f \qquad (\mu in/in) \qquad (6.2)$$

Where ϵ_t : Total strain on the fan shaft read by the strain indicator at any test point

ϵ_o : Initial strain reading on the strain indicator when the fan was not running

ϵ_f : Strain caused by friction torque which is given in table 6.1

Table 6.1. Strain Caused by Friction Torque at the Test Speeds

N rpm	750	1070	1610	2060	2800
ϵ_f μin/in	80	85	90	105	130

The net power input to the impeller was calculated by using equation 6.3 .

$$P_R = \frac{T \cdot \pi N}{30} \qquad (Watt) \qquad (6.3)$$

Where N is the speed of the fan impeller in rpm.

6.2. DETERMINATION OF THE FLOWRATE

As explained in section 5.3, the flowrate through the fan was measured by the orifice with D and D/2 tappings. The mass flowrate through this orifice is given by equation 6.4 (12).

$$q_m = C_d . e . \frac{\pi d^2}{4} \sqrt{2 \rho_u . \Delta p} \qquad (kg/sec) \qquad (6.4)$$

Where d : orifice diameter, m

Δp : pressure difference across the orifice, Pa

ρ_u : air density at the upstream tapping, kg/m^3

e : expansibility factor

C_d : flow coefficient

The expansibility factor , e , is given by equation 6.5 (12) .

$$e = 1 - 0.4617 \frac{\Delta p}{\gamma p_u} \qquad \text{at} \quad \lambda = 0.62 \qquad (6.5)$$

Where P_u : absolute pressure at the upstream of the orifice, Pa

λ : ratio of the orifice diameter to the air duct diameter

γ : isentropic exponent

The value of the isantropic exponent is given as (12)

$\gamma = 1.4$ for $\Delta p > 1000$ Pa

$\gamma = 1.0$ for $\Delta p < 1000$ Pa

The expansibility factor, e,for atmospheric air is plotted as a function of λ and $\Delta p/p_u$ and is given in figure 6.1 .

The flow coefficient, C_d, is a function of Re_d and λ, and may be expressed as (12) .

$$C_d = (1-\lambda)^{-0.5}(0.5899+0.05\lambda^2-0.08\lambda^6+(0.0037\lambda^{1.25}+0.011\lambda^8).(\frac{10^6}{Re_d})^{0.5}) \qquad (6.6)$$

and it is plotted ina figure 6.2 .

In the design of the orifice, since λ has chosen as 0.62, in examining figure 6.2, it is seen that

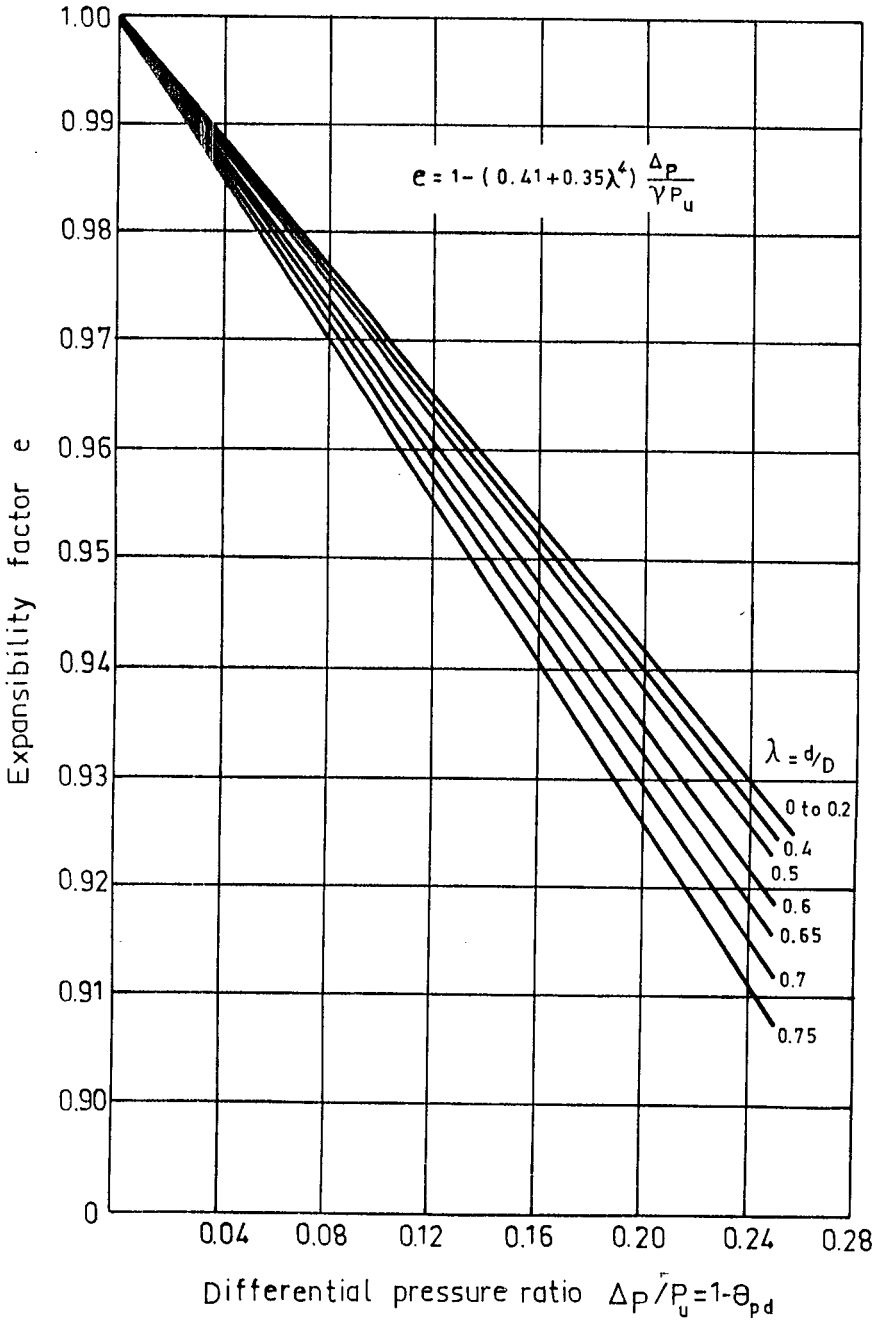

Fig.6.1 Expansibility Factor, e, for Orifice Plates for Atmospheric Air (12)

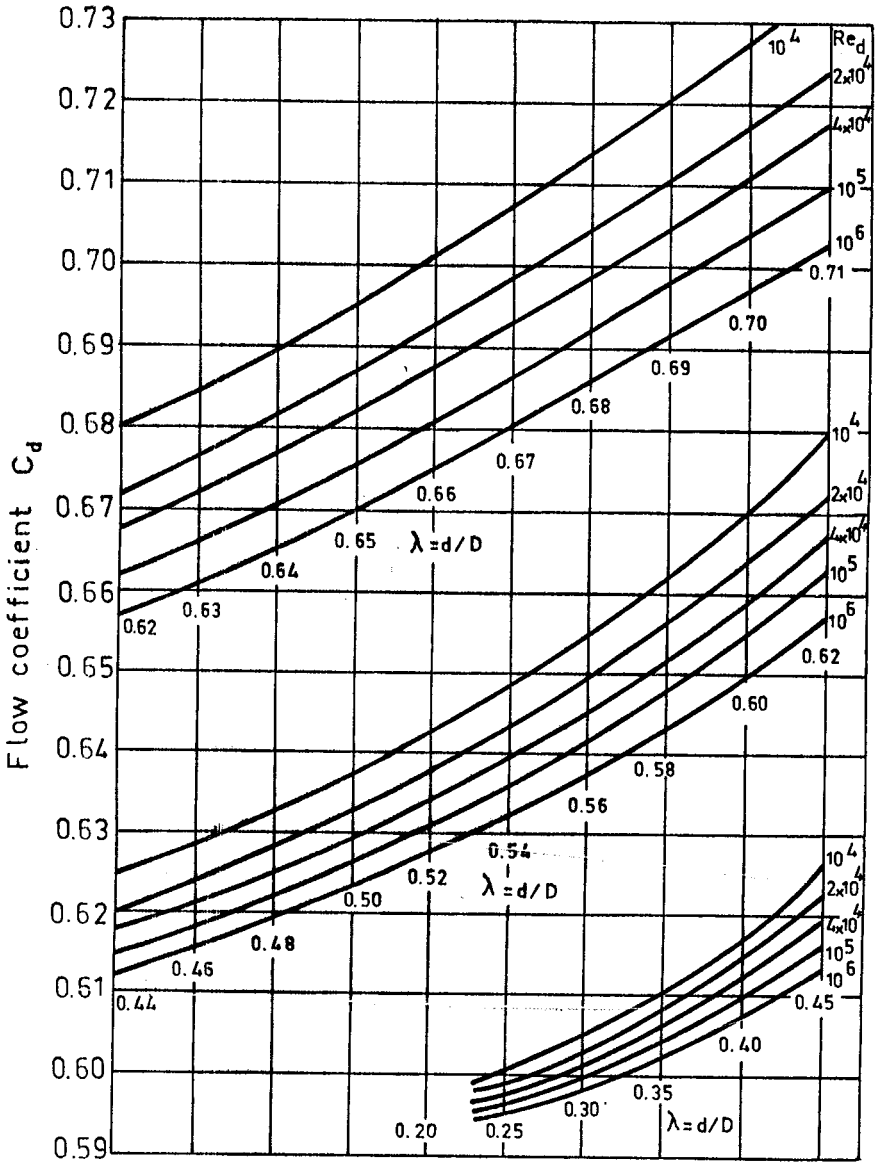

Fig.6.2 Flow Coefficients of In-Duct Orifices with D and D/2 Taps (12)

at $\lambda = 0.62$ $\qquad 0.657 \leqslant C_d \leqslant 0.68$

Since C_d and Re_d are not known in advance, a trial and error method should be used to determine the exact value C_d at each test point. On the other hand, it may be considered sufficient to calculate the mass flow-rate by taking the aritmetic mean of the flow coefficient, C_d, which produces an error in the calculated mass flowrate of about 1.7 % (12) . If the mass flowrate is determined, the volume flowrate is calculated by the following equation (12) .

$$Q = \frac{q_m}{\rho_3} \tag{6.7}$$

Where ρ_3 is the density of air in the inlet chamber and is given in equation 6.10 .

Static pressure measurements were made by using two inclined tube alcohol manometers.

6.3. FAN PERFORMANCE CALCULATIONS

In calculating the fan performance, the following relations were used (12) .

$$\text{Fan static pressure } p_{st} = - p_{t1} \tag{6.8}$$

Where $p_{t1} = p_{s_3} + p_{d_3}$

p_{s_3} is the static pressure in the inlet chamber shown in figure 5.8 .

p_{d_3} is the dynamic pressure in the same chamber.

The dynamic pressure p_{d_3} is defined as

$$p_{d_3} = \frac{q_m^2}{2\rho_3 . A_3} \tag{6.9}$$

Where ρ_3 is the density of air in the inlet chamber and A_3 is the area of the inlet chamber normal to the flow.

The density ρ_3 is defined as

$$\rho_3 = \rho_a \cdot \left(\frac{p_a + p_{s_3}}{p_a}\right) \tag{6.10}$$

Where p_a is the atmospheric pressure and ρ_a is the density of air at atmospheric pressure.

$$\text{Fan dynamic pressure } p_{df} = \frac{q_m^2}{2\rho_a \cdot A_2} \tag{6.11}$$

Where A_2 is the total discharge area of the fan.

$$\text{Fan total pressure } p_{tf} = p_{st} + p_{df} \tag{6.12}$$

$$\text{Fan static pressure } \eta_{st} = k_c \cdot \left(\frac{q_v \cdot p_{st}}{P_R}\right) \tag{6.13}$$

Where k_c is the compressibility coefficient .

The value of the compressibility coefficient, k_c, is determined as follows (12) :

If $(- p_{t1})$ is less than 2500 Pa, it is taken as $k_c = 1.0$

If $(- p_{t1})$ is greater than 2500 Pa, k_c must be determined by using equation 6.14 .

$$k_c = \frac{\varsigma \log_{10} \theta}{\log_{10}(1 + \varsigma(\theta - 1))} \tag{6.14}$$

Where ς and θ are defined below.

$$\varsigma = \frac{(\gamma - 1).\rho_3.P_R}{\gamma.q_m.(- p_{t1})} \tag{6.15}$$

$$\theta = \frac{p_a}{p_a + p_{t1}} \tag{6.16}$$

After determining the fan static efficiency η_{st}, the fan total efficiency η_t is calculated by using equation 6.17

$$\text{Fan total efficiency } \eta_t = \eta_{st} + \frac{q_m \cdot p_{df}}{\rho_a \cdot P_R} \tag{6.17}$$

A computer program was prepared to calculate the performance parameter . This program and a sample output of it are given in Appendix 4.

CHAPTER 7

EXPERIMENTAL RESULTS AND CONCLUSION

7.1. INTRODUCTION

The fan was tested at five different speeds . At each speed, the blade root angles were set to the desired angle by hand. The following quantities were measured at each test point.

Δp : Static pressure difference across the orifice, mm alcohol

p_{s_3} : Static pressure in the chamber, mm alcohol

p_u : Static pressure at the upstream of the orifice , mm alcohol

ϵ : Strain caused due to the torque at the fan shaft, μin/in

All the above quantities at each test point together with the impeller speed N, atmospheric pressure p_a, and ambient temperature T_a were used in the computer program given in Appendix 4 and the following paramaters were calculated.

P_R : Power input to impeller, Watts

Q : Volume flowrate through the fan, m^3/sec

p_{tf} : Fan total pressure, p_a

p_{st} : Fan static pressure, p_a

η_t : Fan total efficiency

η_{st} : Fan static efficiency

Re_d : Reynolds number at the orifice

Re_D : Reynolds number at the air duct

V : Flow velocity through the air duct, m/sec

Using the calculated values of the above parameters at each test point, the fan p_{tf}- Q, P_R- Q and η_t- Q characteristics were plotted for each test speed at the corresponding blade angle. These plots are shown

in figures 7.1 to 7.15 .

The fan was tested at the blade root angles of 25°, 32.5°, 40° and 47.5° for each test speed except the design speed. The auxiliary fan capacity was not sufficient to test the fan at angles greater than 25° at the design speed. Therefore, at the design speed, the fan was tested at the blade root angles of 5°, 10°, 15°, 20°, and 25° to obtain the operating points as shown in figure 7.2 . The operating point of the fan is defined as the state at which the fan characteristic intersects the system characteristic.

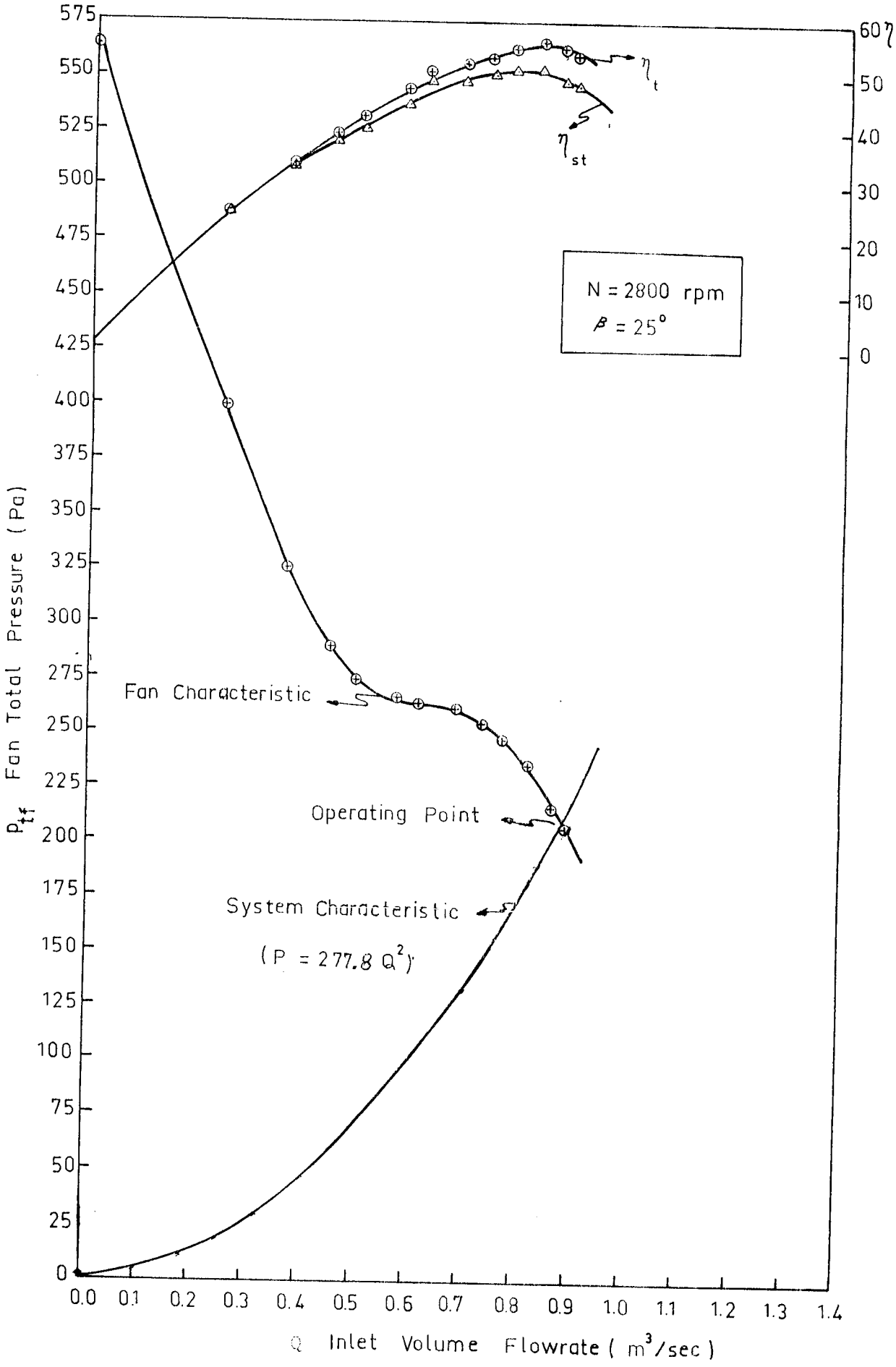

Fig.7.1 Fan Performance at the Design Speed together with the Smoke Tunnel System Resistance Line

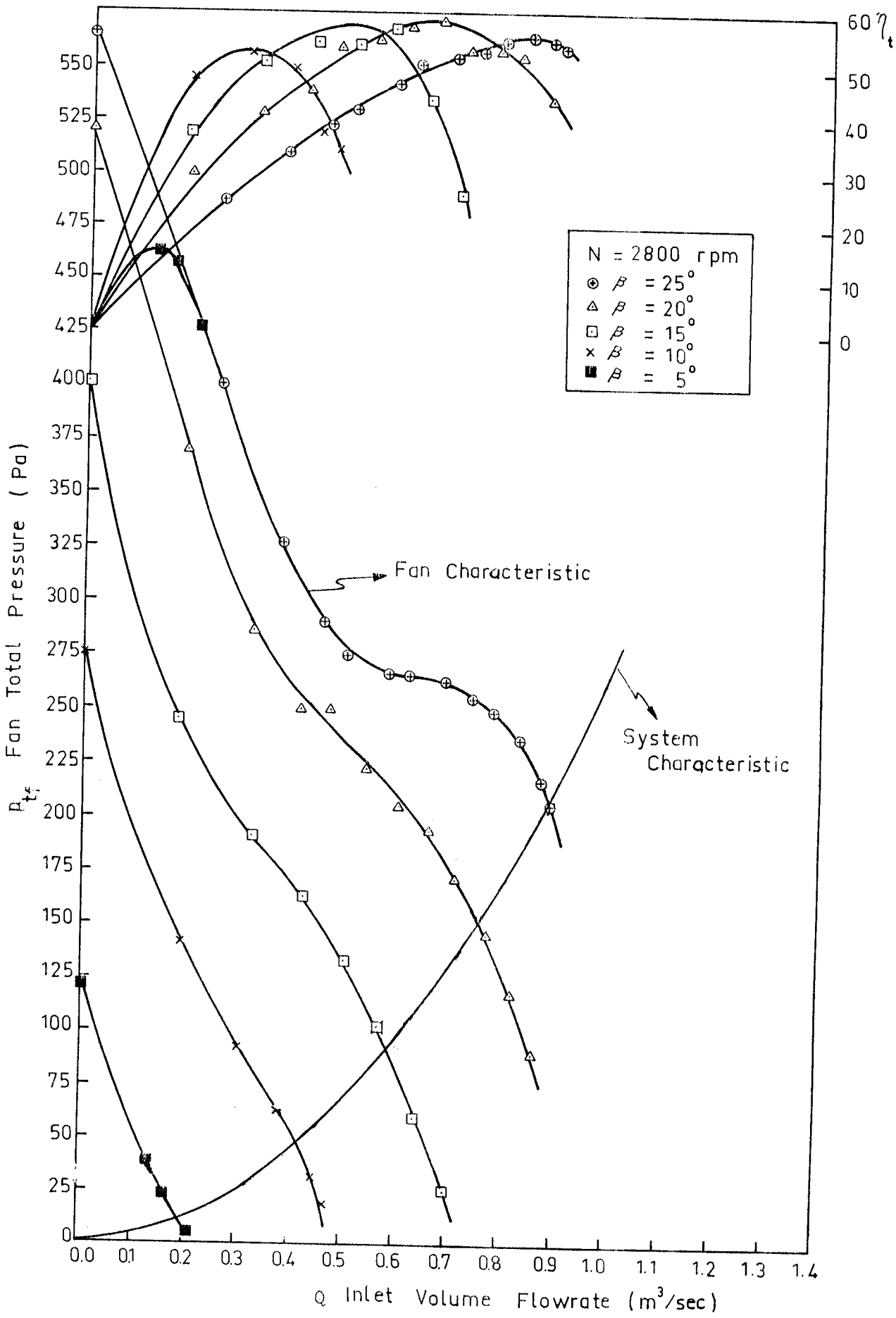

Fig.7.2 Fan Performance at the Design Speed and Different Blade Root Angles

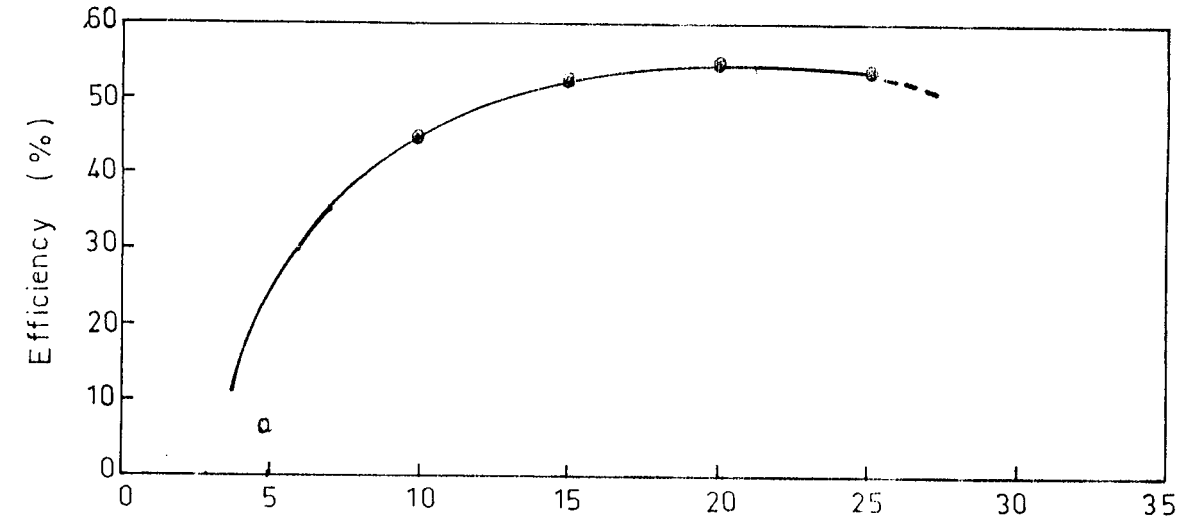

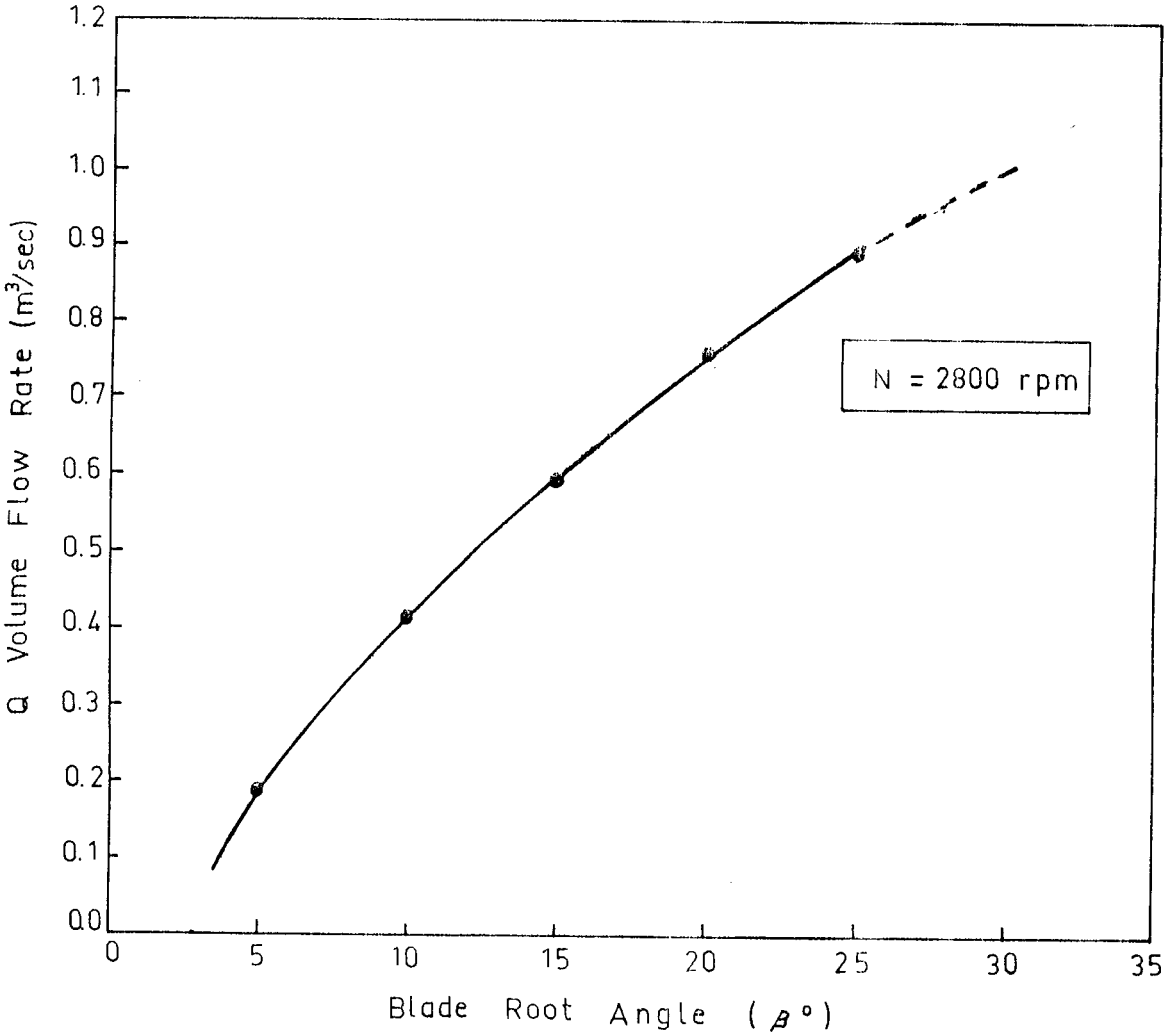

Fig.7.3 Effect of Blade Root Angle on the Volume Flowrate and Overall Efficiency at the Design Speed.

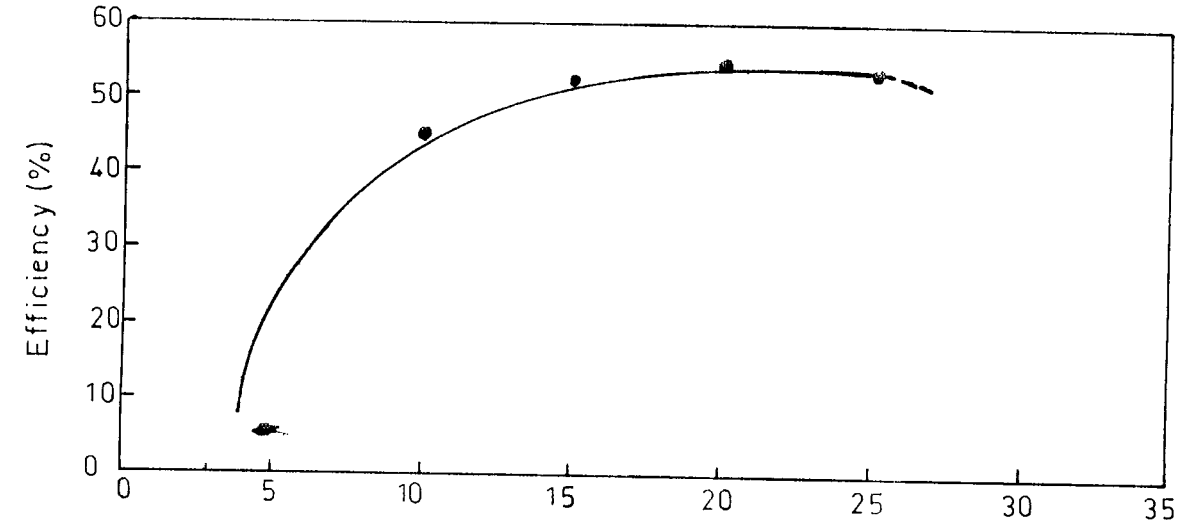

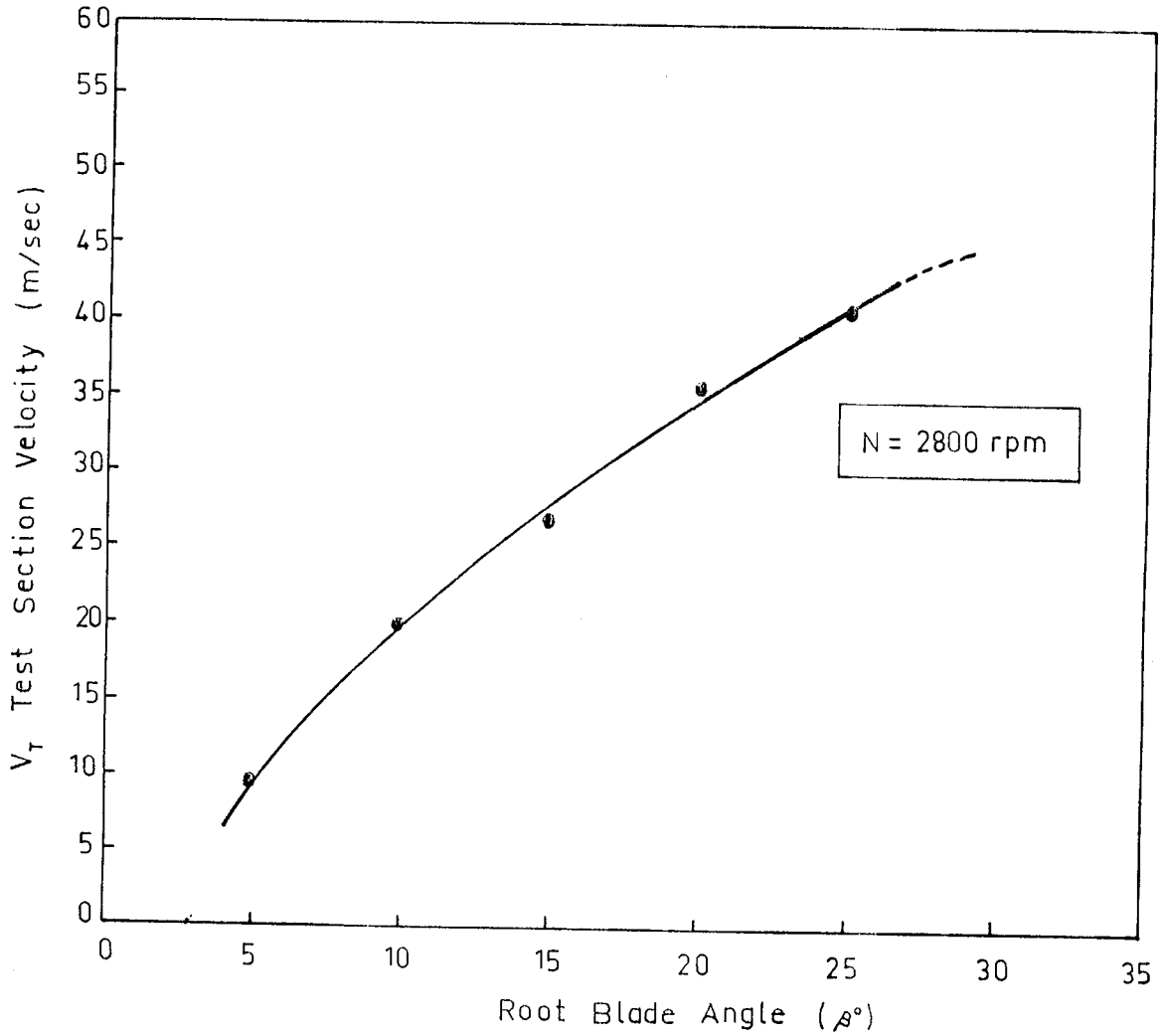

Fig.7.4 Change of Flow Velocity through the Test Section of the Smoke Tunnel with Blade Root Angle of the Fan

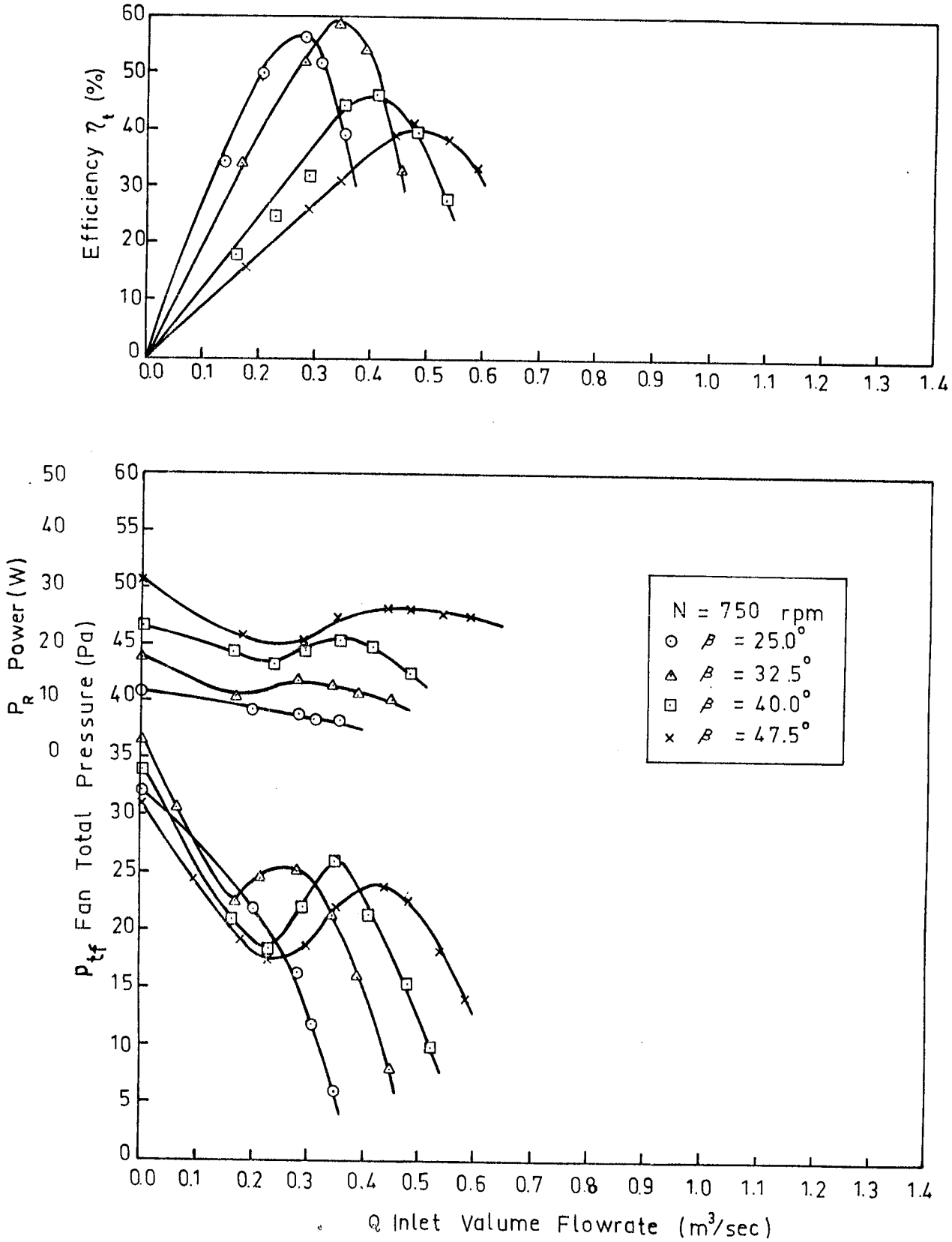

Fig.7.5 Fan Performance at 750 rpm at Different Blade Root Angles

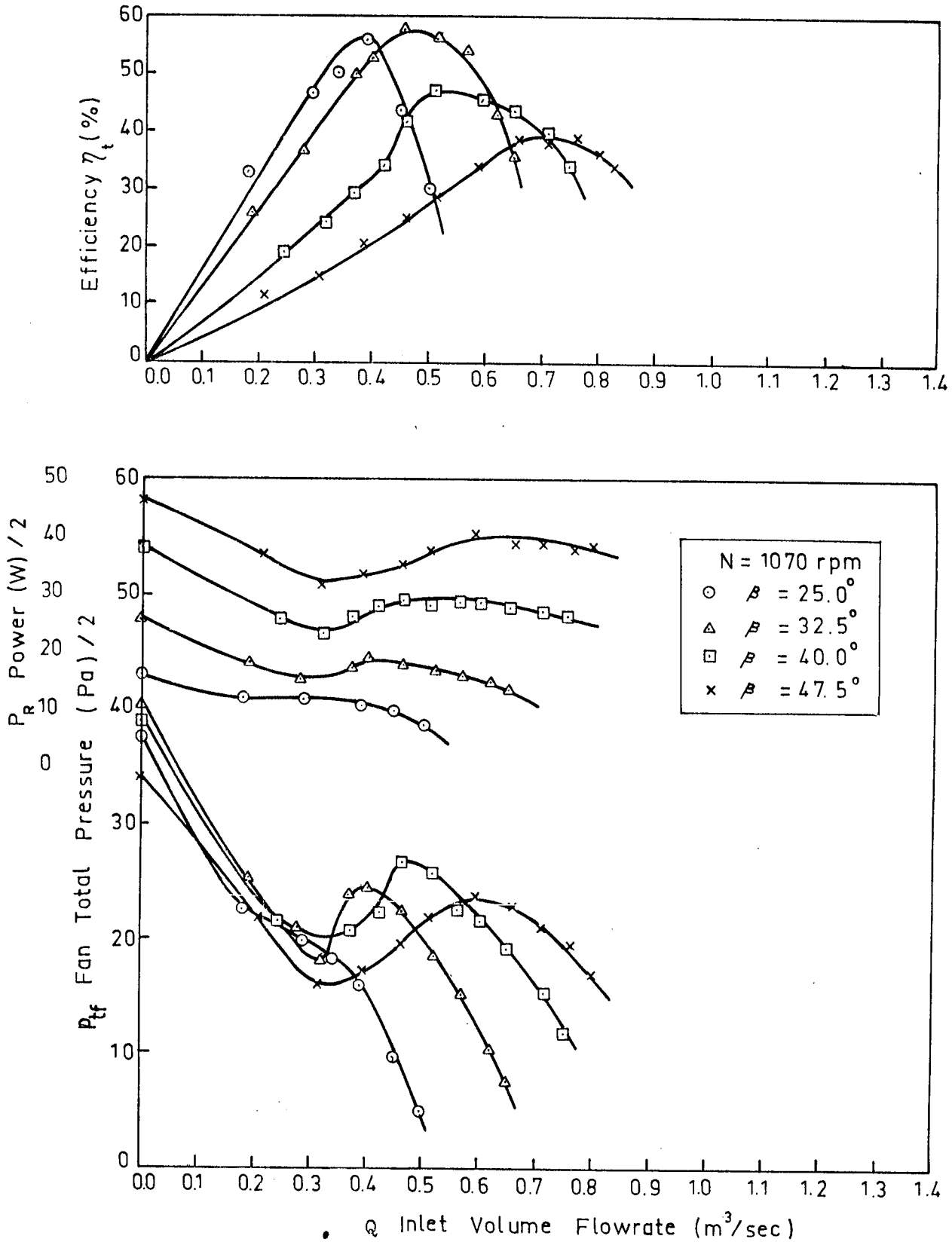

Fig.7.6 Fan Performance at 1070 rpm at Different Blade Root Angles

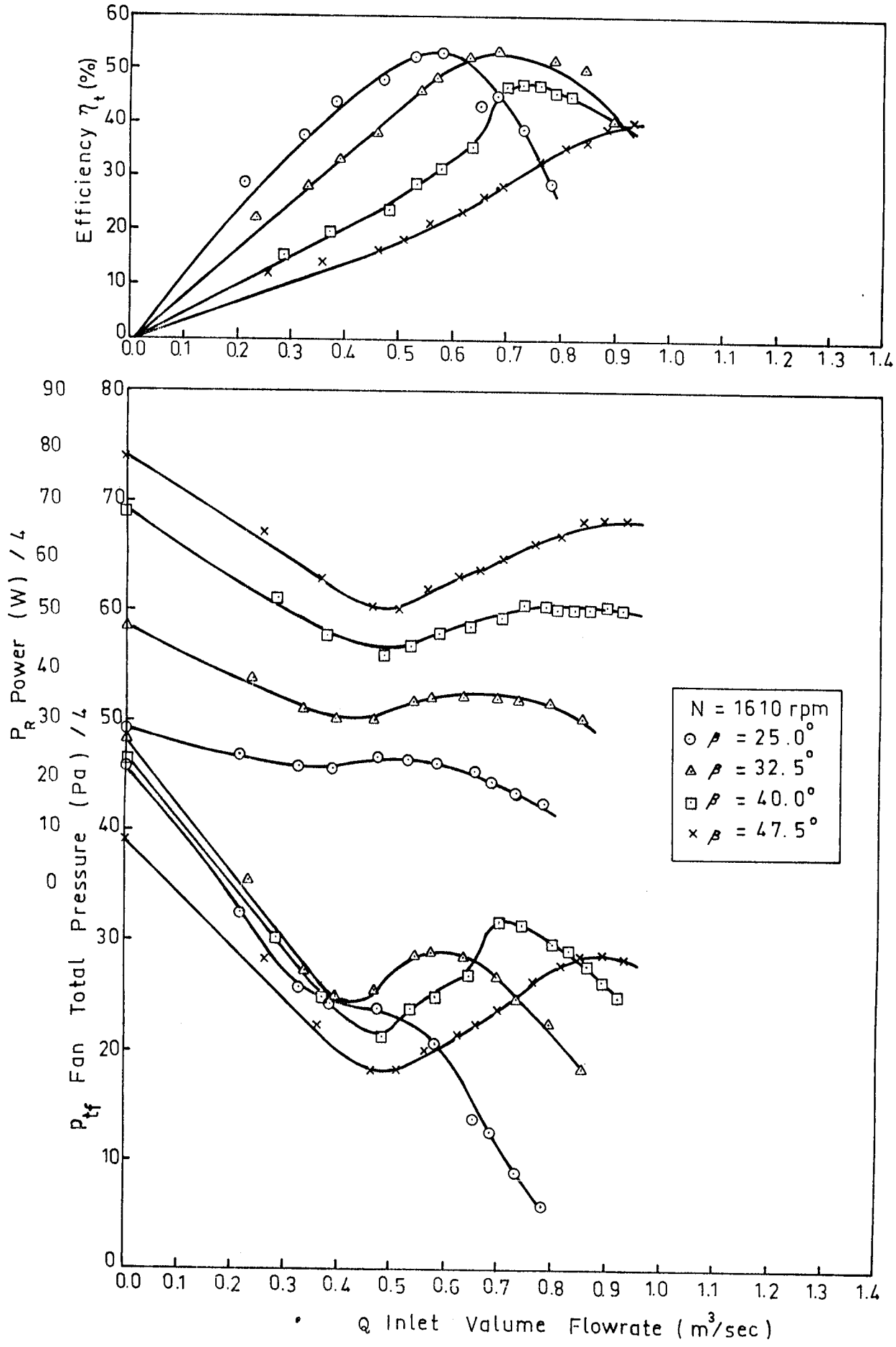

Fig.7.7 Fan Performance at 1610 rpm at Different Blade Root Angles

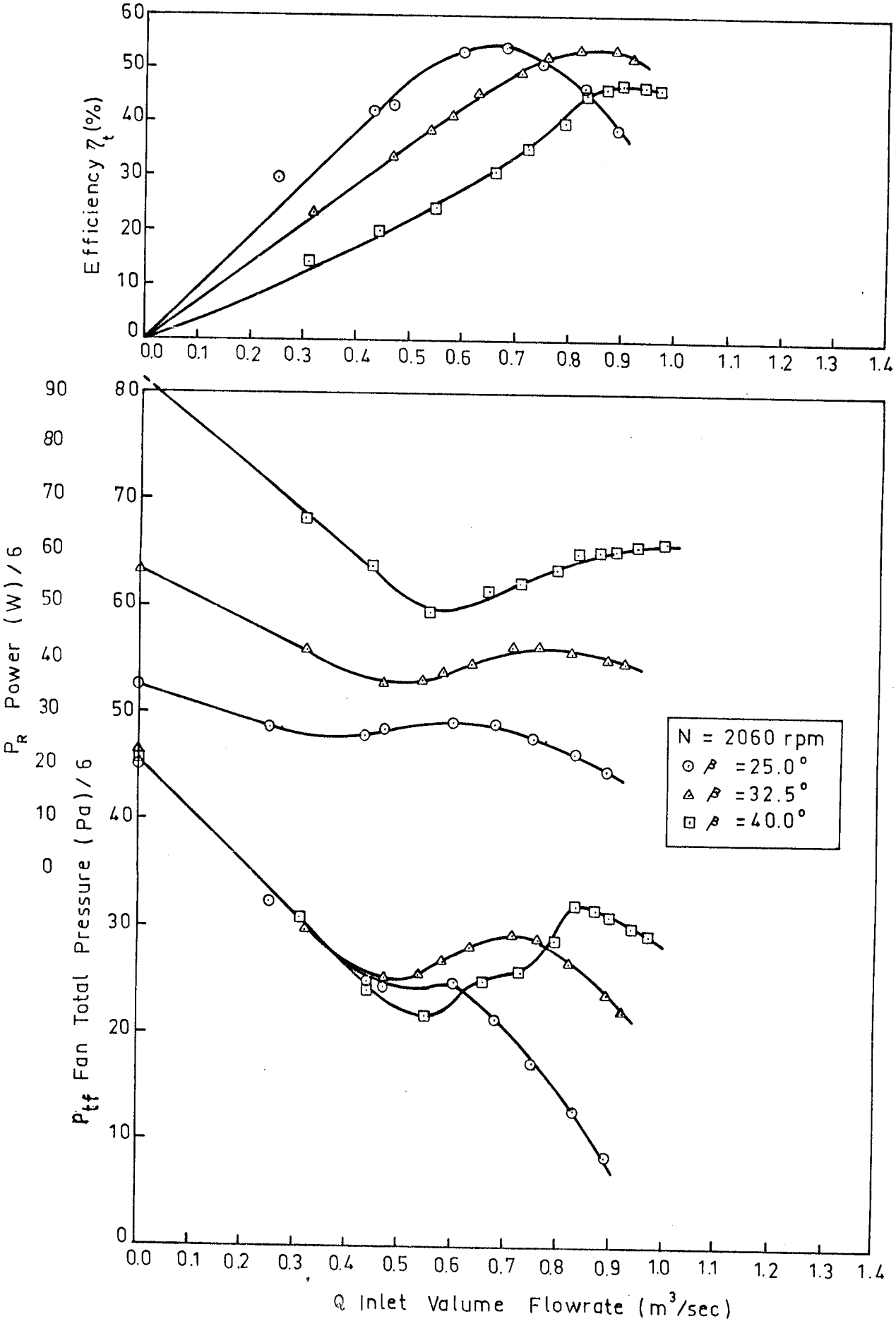

Fig.7.8 Fan Performance at 2060 rpm at Different Blade Root Angles

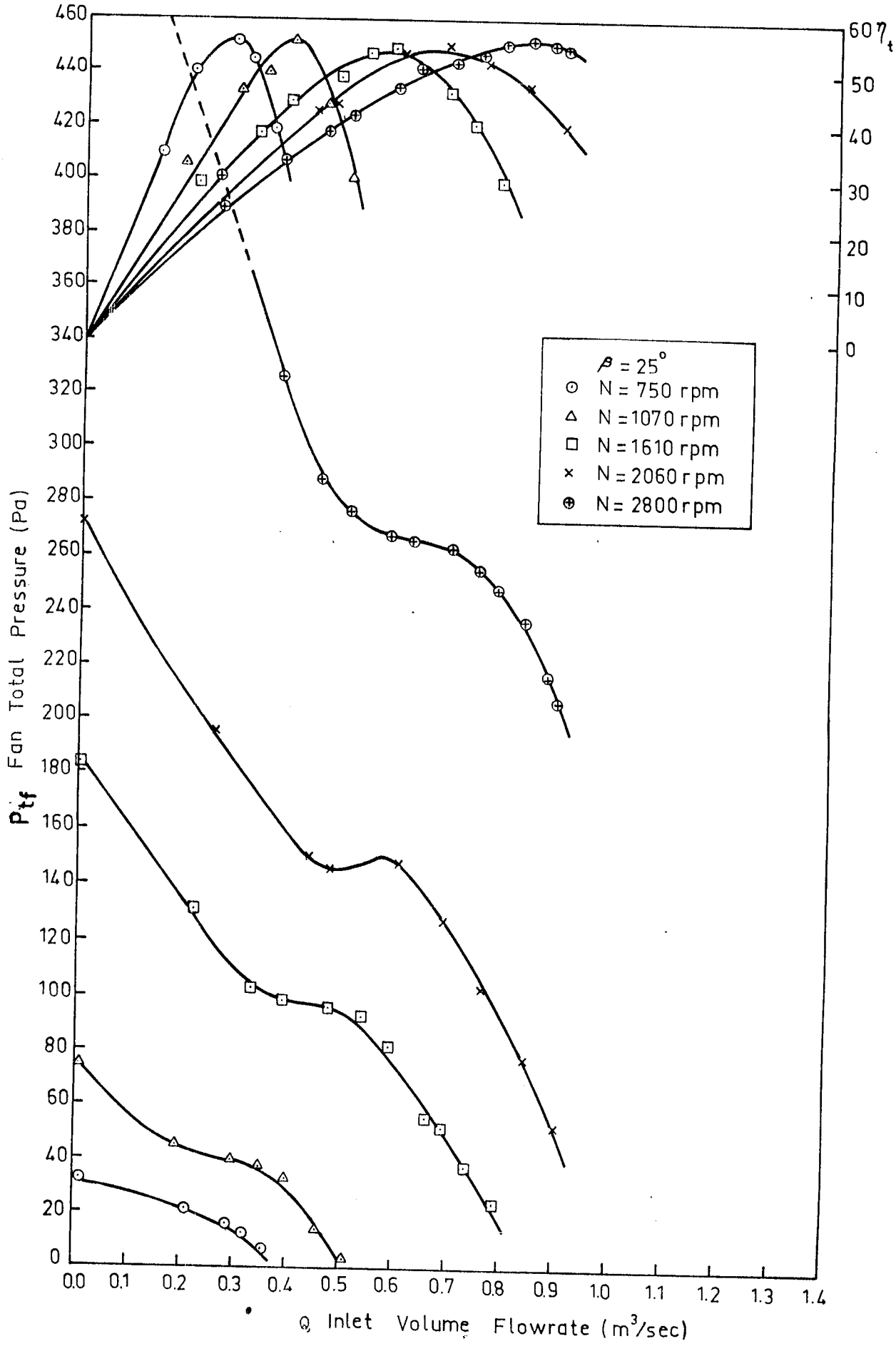

Fig.7.9 Fan Performance at Constant Blade Root Angle and at Different Speeds

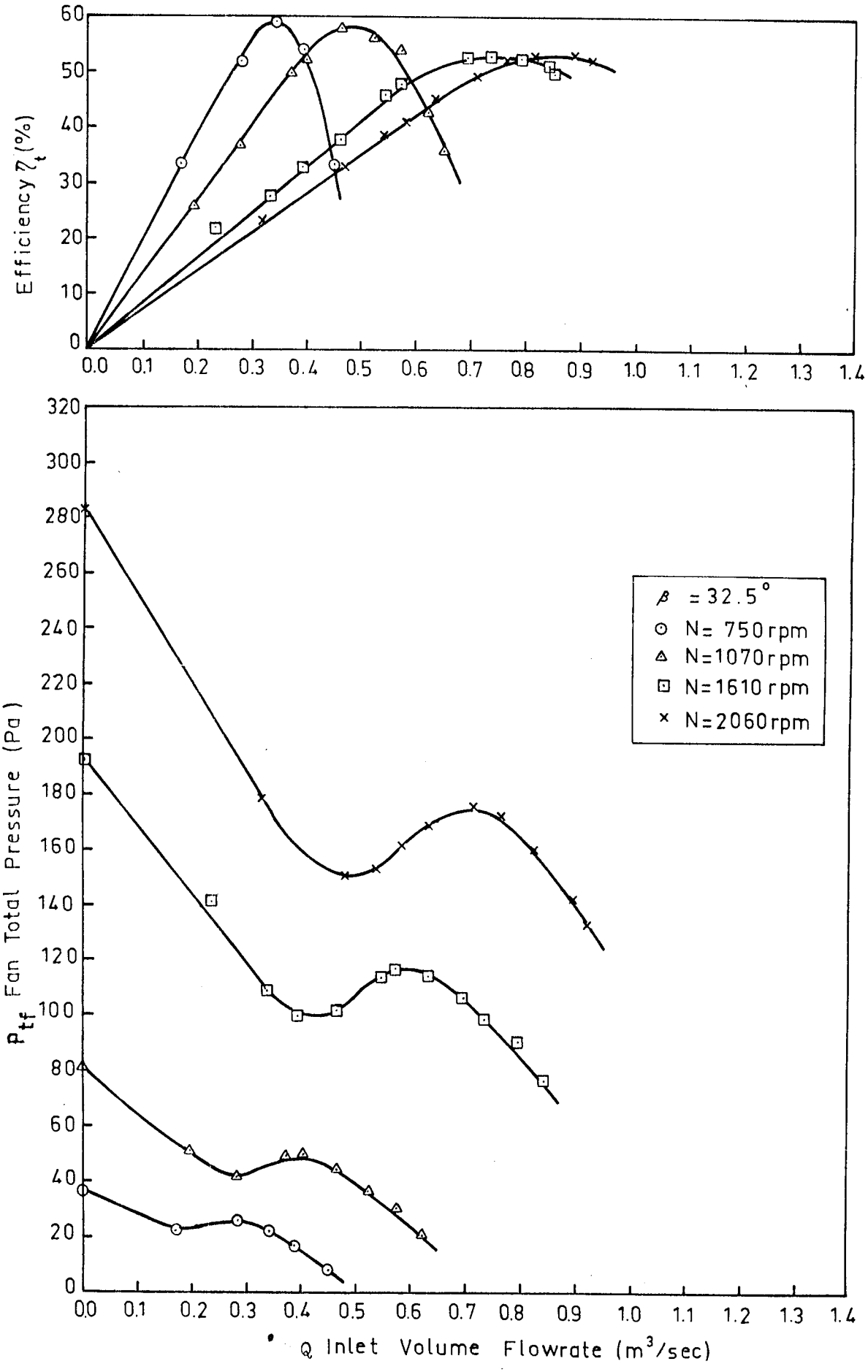

Fig.7.10 Fan Performance at Constant Blade Root Angle and at Different Speeds

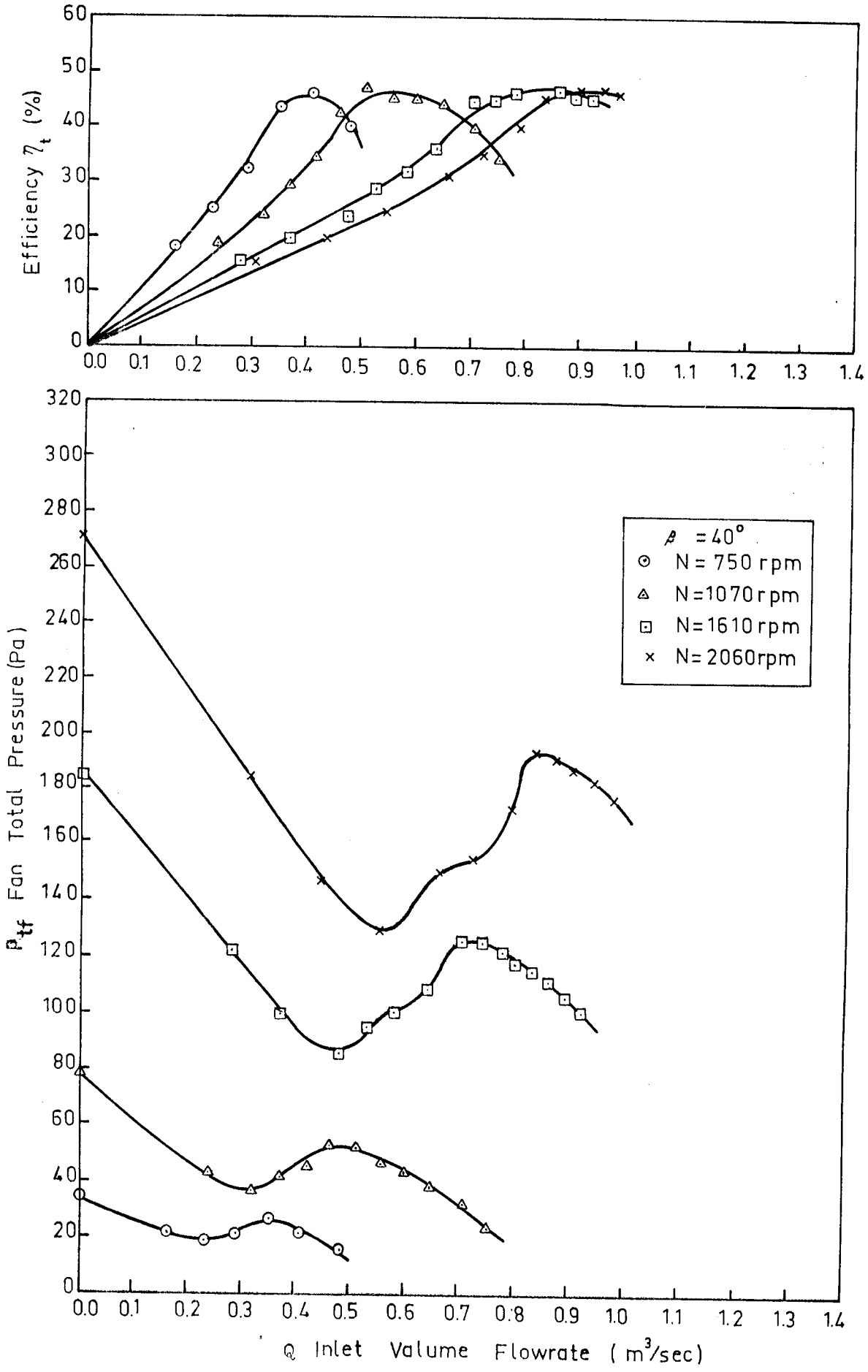

Fig.7.11 Fan Performance at Constant Blade Root Angle and at Different Speeds

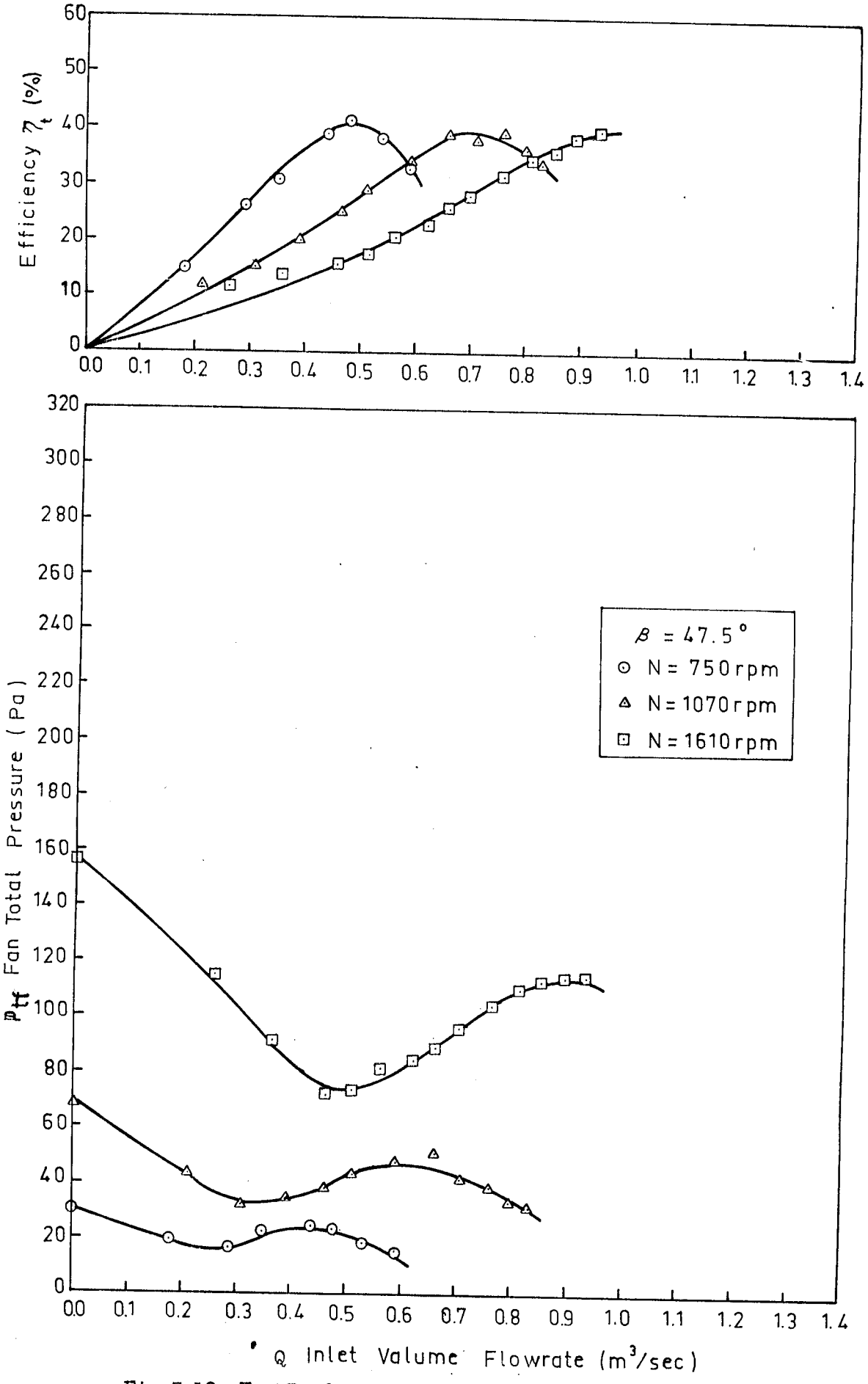

Fig.7.12 Fan Performance at Constant Blade Root Angle and at Different Speeds

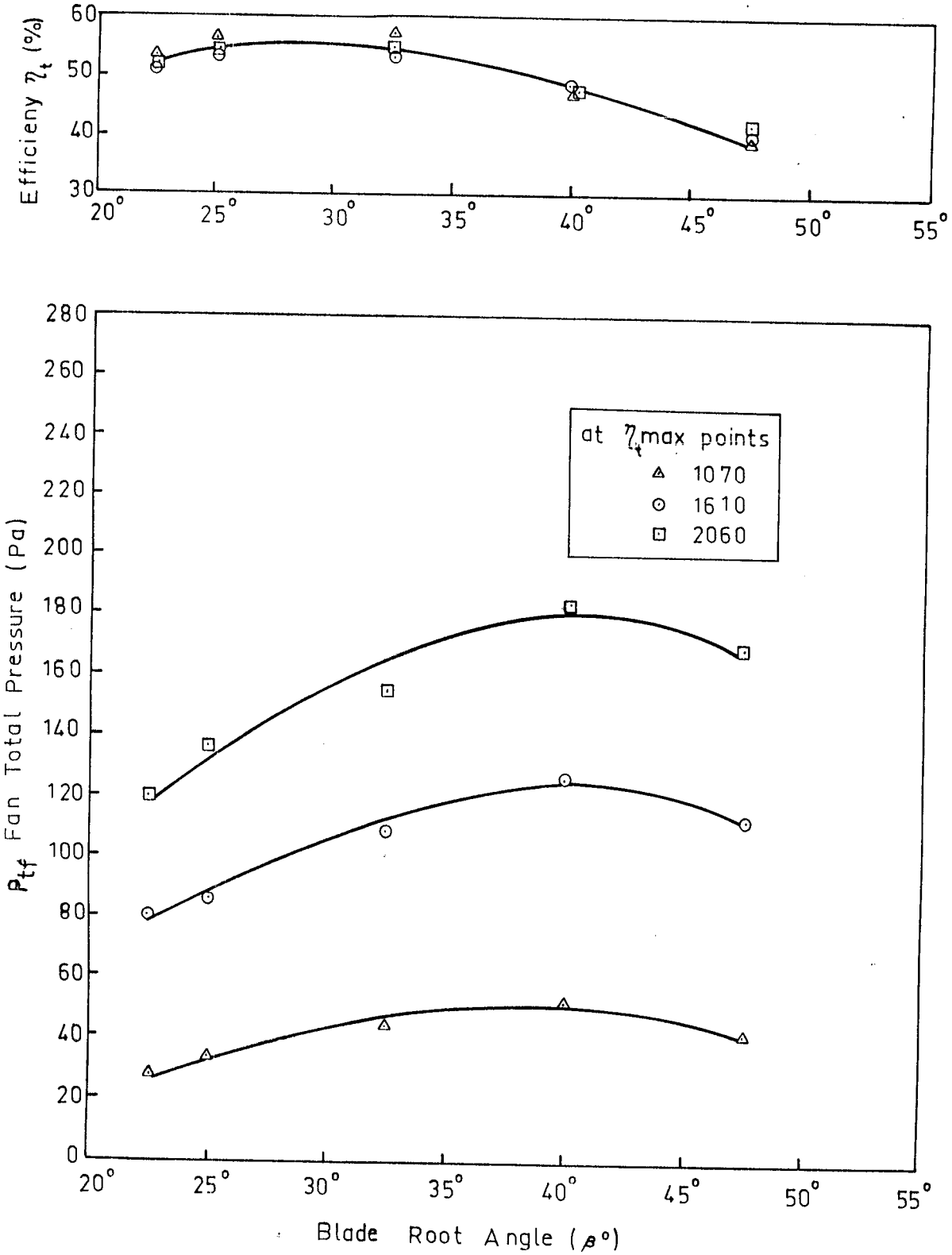

Fig.7.13 Blade Root Angle versus Fan Total Pressure and Efficiency at Maximum Efficiency Points

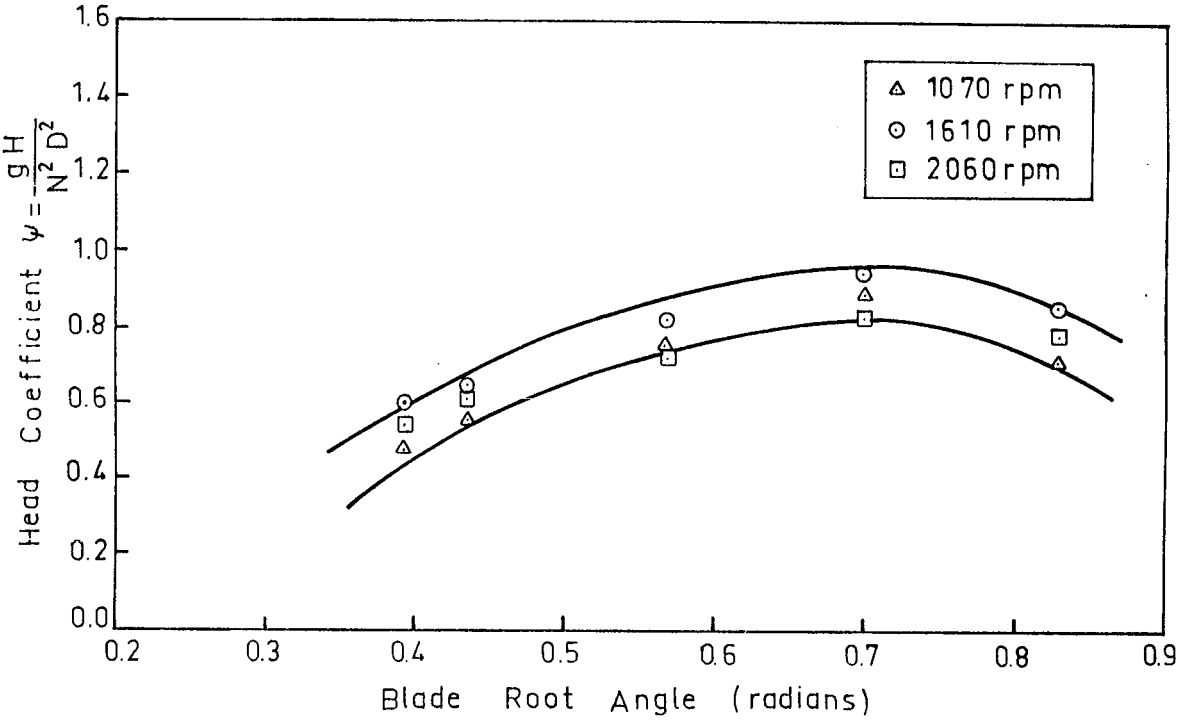

Fig.7.14 Head Coefficient versus Blade Root Angle at Maximum Efficiency Points

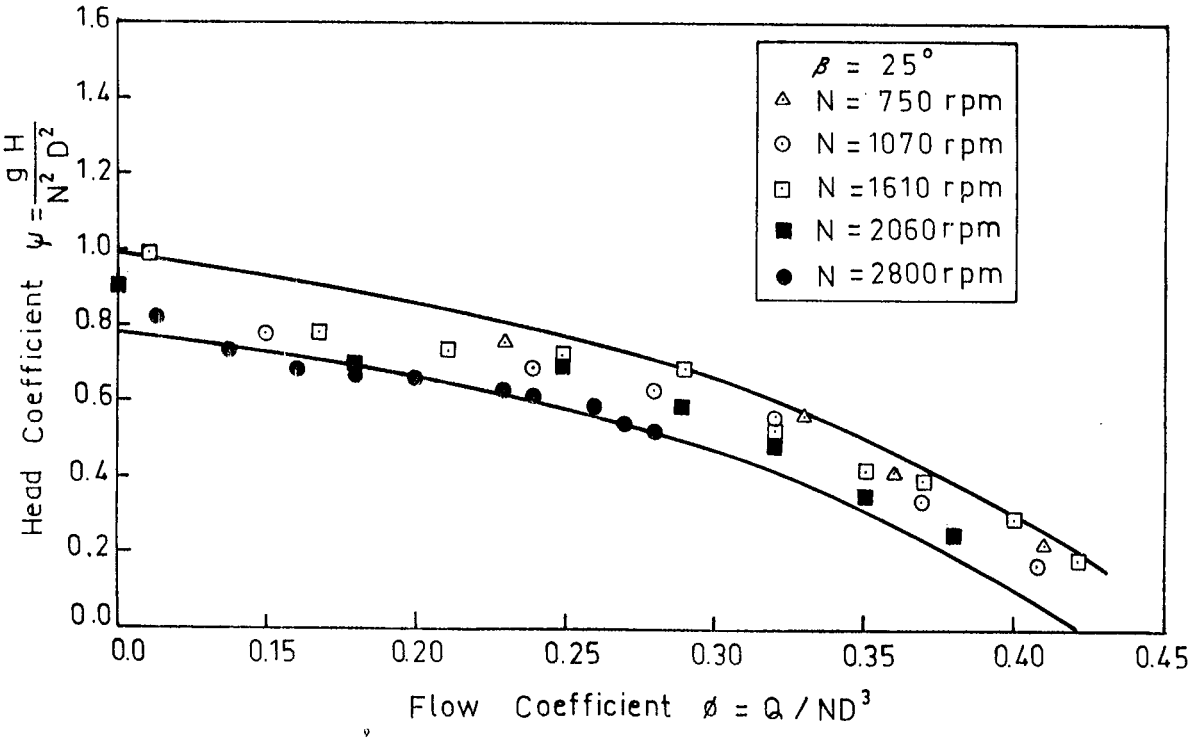

Fig.7.15 Dimensionless Fan Characteristic

7.2. DISCUSSION OF RESULTS

The present fan was designed to give a flowrate of approximately 1 m^3/sec at a total pressure p_{tf} = 270 Pa. Design calculations showed that the fan supplies the design flowrate if it is rotated at 2800 rpm and the blade root angle is set to 25^o. Also the static efficiency of the fan at this design point was found to be approximately 64 %.

The fan was tested at the design point i.e. at 2800 rpm and at the blade root angle of 25^o. As is shown in figure 7.1, the fan total pressure and the flowrate at the operating point were found to be 210 Pa and 0.88m^3/sec respectively. The fan total efficiency and the static efficiency at the same point were also found to be 54 % and 48 % respectively.

When the experimental results are compared with the design values, it is seen that the flowrate is 12 % smaller than the design value and the static efficiency is 16 % smaller than the theoretical calculated value. The difference between the calculated design values and the experimental results may be explained as follows :

In the design of the fan blade only the two dimensional losses called profile drag were considered. Two other losses known as secondary drag and annulus drag which are three dimensional losses were not taken into account because the two dimensional aerofoil data was used in the design.

Another reason for the difference between the design values and the experimental results, although the effect is small, may be the dimensional and angular errors made on the fan blade during the manufacturing and construction of the model and blade itself.

Furthermore the assumptions made for the blade interference, design constants and especially the assumption that the viscous drag forces may be neglected in comparison to the pressure drag forces could have had a cumulative effect which caused a significant difference between the experimental and the theoretical results.

It should be noted that near to the stalling point, drag forces increase sharply. This may be the major cause which increases the hydraulic losses and hence cause a drop in efficiency.

On the other hand, most of the design equations are emprical and do not consider the effect of viscous drag on the aerofoil. The present state of art of aerofoil design by using cascade or isolated aerofoil theory is not totally adequate; therefore the designed experimental fan rotor must be developed to achieve higher fan efficiencies.

To evaluate the general performance of the fan, it was tested at different speeds and different blade root angles. Since, at the design speed of 2800 rpm the auxiliary fan capacity was not sufficient to obtain the full range of $p_{tf} - Q$ characteristics at the blade root angles greater than 25°, it was tested at five different blade root angles of 5°, 10°, 15°, 20°, 25°. The performance characteristics at these angles together with the system characteristic are given in figure 7.2 . From this figure the operating points at the design speed for five different blade root angles were determined. The flowrates and efficiencies corresponding to these operating points were plotted against the blade root angle, and is shown in figure 7.3. If this figure is examined, it will be seen that as the blade angles are set more in axial direction, this causing an increase in the blade angle, the flowrate through the system (smoke tunnel) increases and also the efficiencies corresponding to these operation points increase untill the blade root angle 17.5° then they decrease with increasing blade angle. The flowrates at higher blade angles can be predicted by extrapolation of the results in figure 7.3 .

The flow velocity through the test section of the smoke tunnel versus blade root angle is plotted by using the results of figure 7.3 and is given in figure 7.4 .

The fan was also tested at rotor speeds of 750, 1070, 1610 and 2060 rpm. At each speed, the fan was tested at four different blade root angles, namely 25°, 32.5°, 40° and 47.5°. The performance

characteristics of the fan at the tested speeds are given in figures 7.5, 7.6, 7.7 and 7.8. As will be seen from these figures that at the blade root angles of 25°, 32.5°, 40° and 47.5° as the flowrate is reduced by throttling the inlet of the auxiliary fan, the pressure rise across the fan increases untill the fan "stalls" . At this point, the pressure rise suddenly decreases. This stalling occurs when the incidence of the flow onto the blade exceeds a certain critical value and the flow seperates from the blade. The effect of speed on stalling is clearly illustrated in figures 7.9 to 7.12 . As is shown in figures 7.9 for the blade angle of 25°, stalling does not seem to occur at 750 rpm. As the fan rotational speed is increased, tendency for stalling increases for blade angles greater than 25°. The lifting ability of the blade decreases just at the left of this stalling point . As is shown in figure 7.2, the stalling does not seem to occur at blade root angles less than 25°.

It is not proper to run axial flow machines in the stalled region because of poor efficiency and unstable operating conditions. An axial flow machine is always run to the right of stalled region where a dropping $p_{tf} - Q$ characteristic occurs. This region is called "stable working region". Another important point to be noted from these figures is that the efficiency has a maximum value at a flowrate corresponding to nearly the end of the stall region. When the stable working regions are examined in these figures, it is seen that as the blade root angle at constant speed increases, the fan total pressure increase untill the blade root angle of 40° is reached. Beyond this angle total fan pressures seem to decrease. As was explained previously, flowrates at the design speed but at blade angles greater than 25° can be predicted extrapolating the results plotted in figure 7.3 . However under the light of above explanation, this assumption will give correct results upto the blade angle of 40°.

To see the effect of speed on the fan performance paramaters, the fan performance characteristics at constant blade root angle but at different fan rotational speeds were plotted and are given in figures 7.9, 7.10, 7.11 and 7.12 . From these figures it is seen that at

constant blade angle, the flowrate and fan total pressure increase with increasing speed but maximum efficiencies remain approximately constant. As was also explained in previous paragraphes, the tendency for stalling increases with increasing speed.

Using figures 7.5, 7.6, 7.7 and 7.8 the blade root angle against fan total pressure and efficiency corresponding to the maximum efficiency points was plotted and is given in figures 7.13. As will be seen from this figure that as the blade angle increases, the fan total pressure at maximum efficiency points increases untill the blade root angle of 40° past this angle the fan total pressure decreases. In the case of efficiency, the efficiency increases with the blade angle upto 22.5° after which it decreases.

It is usually necessary to plot the performance characteristics in a non-dimensional form. Such a plot will show the performance characteristics of the similar machines. Using the data of figure 7.13, the pressure coefficient ψ was plotted against blade root angle β , in radians, and is given in figure 7.14. As will be seen from this figure, the points obtained at three different speeds all fall within an narrow band. Using this band, at any blade angle setting for the speed range of 1070 to 2060 rpm, the fan total pressure at maximum efficiency points can be approximately determined.

In figure 7.15, the head coefficient ψ is plotted against the flow coefficient ϕ at different speeds. The points obtained at five different speeds also fall on a narrow band. From this band it is also possible to predict the performance not only of this fan but also the performance of any geometrically similar fans. This is in general true as long as there are no large changes of blade Reynolds number.

7.3. CONCLUSIONS

The purpose of this study was to design an axial flow fan which could supply valume flowrate changing from zero to maximum flowrate of 1 m^3/sec through the smoke tunnel by only changing the blade angle of the fan. If figure 7.3 is examined, it is seen that the purpose is attained. When the blade root angle is changed from 4° to 30°, the flowrate through the smoke tunnel could be made to vary continuously from zero to 1 m^3/sec . Any flowrate between zero flowrate and maximum flowrate at the design speed can be obtained through the smoke tunnel by just adjusting the blade root angle to the corresponding value in figure 7.3 .

The conclusions reached on the general performance of the designed fan may be summarized as follows :

a) In order to have acceptable efficiencies at all speeds, the fan should be operated at the blade root angles between 10° and 40°.

b) The maximum efficiency at a given blade angle remains approximately constant with the change of speed.

c) As the blade angle increases from 5° to 40°, the fan total pressures at maximum efficiency points increase.

d) At constant blade angle, the flowrate and the fan total pressure increase with increasing speed.

e) For blade angles greater than 25°, the tendency for stalling increases with increasing speed.

7.4. RECOMENDATIONS FOR FURTHER WORK

During the testing of the experimental fan, pitch angles were adjusted by hand. When the fan is mounted onto the smoke tunnel, pitch angles must be adjusted by a suitable remote control manual mechanism while fan is in operation. Such a remote control mechanism should be

designed and manufactured. This mechanism should adjust the blade root angles between 5° and 40°. As is shown in this work, within this interval, the fan supplies the desired flowrates through the smoke tunnel.

LIST OF REFERENCES

1- Wallis, R.A., 1961. "Axial Flow Fans, Design and Practice", NewYork, Academic Press.

2- Eck, B., 1962. "Fans", Berlin, Stringer-Verlag.

3- Marcinowski, H., 1958. "Optimum Problems in Axial Flow Fans", Forschung U. Konstrution, No: 3.

4- Wallis, R.A., "Optimisation of Axial Flow Fan Design", Mech and Chem Engg Trans, I.E. Aust., Vol. MC 4, No : 1.

5- Wallis, R.A., 1968. "A Rationalized Approch to Blade Element Design, Axial Flow Fans", Third Australian Conference on Hydraulics an Fluid Mechanics, Sydney.

6- Collar, A.R.,1940. "Cascade Theory and the Design of Straighteners", R. and M. 1885. Aero. Res. Council.

7- Lighthill, M.J., "A Mathematical Method of Cascade Design, R.and M. 2104.

8- Osborn, W.C., 1966. "Fans", Pergamon Press.

9- Mairs, W.A. "The Design of Fans and Guide Vanes for High Speed Wind Tunnels", R. and M. 2435.

10- Pinkerton, R.M. and Greenberg., 1938. "Aerodynamic Characteristics of a Large Number of Aerofoils Tested in Variable Density Wind Tunnel", W.A.C.A. Tech. Rep 628.

11- Nelson.W.C. "Air Plane Propeller Principles", John Willey and Sons. Inc.

12- British Standards, BS 848. 1980., "Fans for General Purposes, Part 1 : Method of Testing Performance ".

13- "Operating and Service Manual for Tonque Sensor", BLH Electronic, Inc.

14- "Operating and Service Manual for 120 C Strain Indicator" BLH Electronic, Inc.

15- Shigley, J,E., "Mechanical Engineering Design", Second Ed., Mc Graw Hill.

16- Patterson, G.N., 1944. "Ducted Fans, Design for High Efficiency", Australian Council for Aeronautics. Report ACA. 7.

17- Albayrak. K, "Investigation of Boundary Layer Transition, Turbulent Boundary Layer Development and Recovery Length of the Turbulent Boundary Layer behind Three Dimensional Roughness elements ", Ph.D Thesis, M.E.T.U. Gaziantep Campus 1984 .

APPENDIX 1

DERIVATION OF DESIGN FORMULAS

a) Drivation of an expression for β_∞

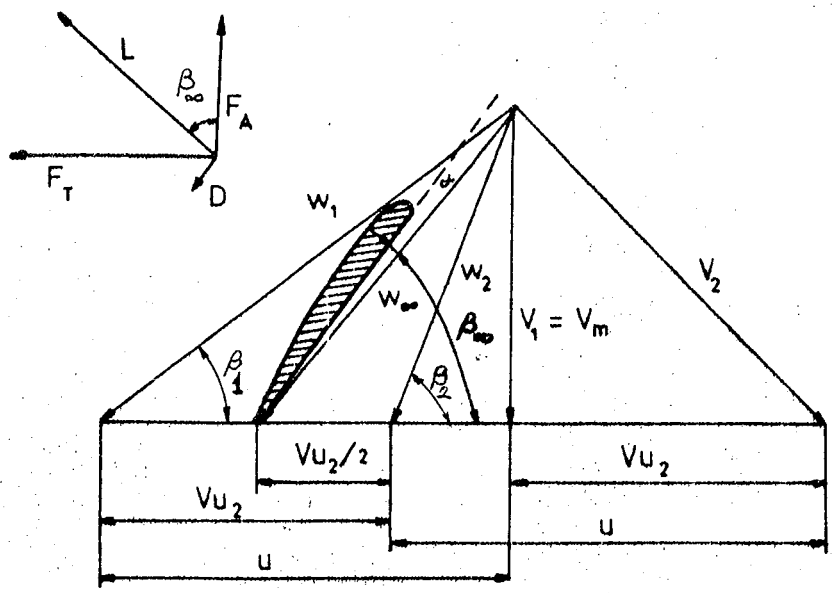

Fig.A1.1 Inlet and Outlet Velocity Triangles Relative to a Rotor Blade

The volume flowrate coefficient ϕ and the static pressure coefficient ψ_{st} are defined as follows :

$$\phi = \frac{v_a}{u} \tag{A1.1}$$

$$\psi_{st} = \frac{g H_{st}}{u^2} \tag{A1.2}$$

Since

$$H_i = \frac{u . v_{u_2}}{g} \tag{A1.3}$$

Where H_i is the ideal head developed by the fan.

Then, equation A1.3 may be written as

$$v_{u_2} = \frac{g H_i}{u} \cdot \frac{u}{u} = \psi_i \cdot u \tag{A1.4}$$

From figure A1.1, the following equalities may be written.

$$\mathrm{Cot}\beta_1 = \frac{u}{v_a} = \frac{1}{\phi} \tag{A1.5}$$

$$\mathrm{Cot}\beta_2 = \frac{u - v_{u_2}}{v_a} \tag{A1.6}$$

Substituting the equality of v_{u_2} from equation A1.4 into A1.6

$$\mathrm{Cos}\beta_2 = \frac{u - \psi_i . u}{v_a} = \frac{u(1 - \psi_i)}{v_a} = \frac{1 - \psi_i}{\phi} \tag{A1.7}$$

from figure A1.1, β_∞ may be expressed as

$$\mathrm{Cos}\beta_\infty = \frac{v_{u_2} + \mathrm{Cos}\beta_2 . v_a}{v_a} = \left(\frac{v_{u_2}}{v_a}\right) + (\mathrm{Cos}\beta_2) \tag{A1.8}$$

Substituting the equations A1.4 and A1.7 into equation A1.8

$$\mathrm{Cot} = \frac{\psi_i . u}{2v_a} + \frac{1 - \psi_i}{\phi} \tag{A1.9}$$

Equation A1.9 may be re-written in the following form.

$$\mathrm{Cot}\beta_\infty = \frac{\psi_i}{2\phi} + \frac{1}{\phi} - \frac{\psi_i}{\phi} = \frac{1}{\phi} - \frac{\psi_i}{2\phi} \tag{A1.10}$$

then

$$\mathrm{Cot}\beta_\infty = \frac{2 - \psi_i}{2\phi} \tag{A1.11}$$

or

$$\tan\beta_\infty = \frac{2\phi}{2 - \psi_i}$$

b) Derivation of an expression for solidity σ

If tangential force F_T due to the lift and drag forces shown in figure A1.1 is equated to the rate of change of momentum

$$F_T = \rho . v_a . v_{u_2} . 2\pi r . dr = L.\mathrm{Sin}\beta_\infty + D.\mathrm{Cos}\beta_\infty \tag{A1.12}$$

Substituting the expressions 3.15 and 3.16 for drag and lift forces into equation A1.12 and cancelling the same terms on both sides, the

following equality is obtained.

$$v_a . v_{u_2} . 2\pi r = z.c.\frac{1}{2} w_\infty^2 (C_L . \sin\beta_\infty + C_D . \cos\beta_\infty)$$

Substituting the equation $v_a = w_\infty . \sin\beta_\infty$ from figure A1.1 and the equation for $s = 2\pi r/z$ from Chapter 3 (Equation 3.13) into the above equality and simplifying

$$v_{u_2} . \sin\beta_\infty = \frac{1}{2} . \frac{c}{s} . w_\infty (C_L . \sin\beta_\infty + C_D . \cos\beta_\infty)$$

or

$$\frac{v_{u_2}}{w} = \frac{1}{2} . \frac{c}{s} (C_L + C_D . \frac{\cos\beta_\infty}{\sin\beta_\infty})$$

Since $\sigma = c/s$

and let $C_L' = (C_L + C_D . \cot\beta_\infty)$

then

$$\frac{v_{u_2}}{w} = \frac{1}{2} \sigma . C_L'$$

or

$$\sigma = \frac{2 v_{u_2}}{w} . \frac{1}{C_L'} \qquad (A1.13)$$

The expression for C_L' may be written as

$$C_L' = C_L (1 + \frac{C_D}{C_L} . \cot\beta_\infty)$$

or

$$C_L' = C_L (1 + \gamma \cot\beta_\infty) \qquad (A1.14)$$

Where $\gamma = \frac{C_D}{C_L}$

Substituting equation A1.14 into equation A1.13, equation A1.15 can be obtained.

$$\sigma = \frac{2 v_{u_2}}{w} . \frac{1}{C_L (1 + \gamma \cot\beta_\infty)} \qquad (A1.15)$$

Substituting equation A1.4 for v_{u_2} and the equation, $w_\infty = v_a/\mathrm{Sin}\beta_\infty$ from figure A1.1 into equation A1.15, following relation can be obtain

$$\sigma = \frac{2\psi_i \cdot \mathrm{Sin}\beta_\infty}{C_L(1 + \gamma C\mathrm{ot}\beta_\infty)} \cdot \frac{u}{v_a} \qquad (A1.16)$$

Since $\frac{u}{v_a} = \frac{1}{\phi}$

Equation A1.16 may oalso be written as

$$\sigma = \frac{2\psi_i \cdot \mathrm{Sin}\beta_\infty}{C_L \cdot \phi\,(1 + \gamma \mathrm{Cot}\beta_\infty)} \qquad (A1.17)$$

c) Derivation of an expression for hydraulic efficiency, η_h

Hydraulic efficiency η_h is defined as

$$\eta_h = \frac{H}{H_i} \qquad (A1.18)$$

Where H_i is the ideal head produced by the impeller and H is the useful head in fluid at the final discharge of the impeller.

Equation A1.18 may be written in the following form.

$$\eta_h = \frac{H_i - H_L}{H_i} = 1 - \frac{H_L}{H_i} \qquad (A1.19)$$

Where H_L is the loss through impeller.

H_L may also be written as

$$H_L = \frac{\Delta p}{\rho \cdot g} \qquad (A1.20)$$

Where Δp is the pressure loss through the impeller.

The pressure loss Δp is calculated as follows :

If in figure A1.1 the thrust force, F_A, which is due to the static pressure rise p_s less any pressure loss Δp, is equated to the axial force due to the lift and drag, equation A1.21 is obtained.

$$F_A = (p_s - \Delta p)\, 2\pi r.dr = L.\mathrm{Cos}\beta_\infty + D.\mathrm{Sin}\beta_\infty \qquad (A1.21)$$

Where p_s is the static pressure difference across the impeller.

p_s in equation A1.21 may be determined as follows :

$$p = \rho . v_{u_2} . u = p_{T_2} - p_{T_1} \qquad (A1.22)$$

Where p is the total head produced by the impeller and p_{T_1} and p_{T_2} are the total pressure at the inlet and outlet of the impeler respectively.

p_{T_1} and p_{T_2} may be written as

$$p_{T_1} = p_1 + \frac{1}{2} \rho . v_1^2 \qquad (A1.23)$$

$$p_{T_2} = p_2 + \frac{1}{2} \rho . v_2^2 \qquad (A1.24)$$

Where p_1 and p_2 are the static pressures at the inlet and outlet of the impeller respectively. v_1 and v_2 are the absolute velocities at inlet and outlet of the impeller respectively.

Substituting equations A1.23 and A1.24 into equation A1.22

$$\rho . v_{u_2} . u = (p_2 + \frac{1}{2} \rho . v_2^2) - (p_1 + \frac{1}{2} \rho . v_1^2) \qquad (A1.25)$$

If equation A1.25 is written as a function of pressure difference $p_s = p_2 - p_1$, equation A1.26 is obtained.

$$p_s = p_2 - p_1 = \rho . v_{u_2} - \frac{1}{2} \rho (v_2^2 - v_1^2) \qquad (A1.26)$$

and since $v_2^2 - v_1^2 = v_{u_2}$

then

$$p_s = p_2 - p_1 = \rho . v_{u_2} (u - \frac{1}{2} v_{u_2}) \qquad (A1.27)$$

Substituting equation A1.27 and expressions for lift and drag forces into equation A1.21

$$(\rho . v_{u_2} (u - \frac{1}{2} v_{u_2}) - \Delta p) \, 2\pi r . dr =$$

$$z . c . dr \, \frac{1}{2} \rho . w_\infty^2 \, (C_L . \mathrm{Cos}\beta_\infty - C_D . \mathrm{Sin}\beta_\infty) \qquad (A1.28)$$

and since $u - \frac{1}{2} v_{u_2} = w_\infty \cdot \cos\beta_\infty$

Thus, equation A1.28 may be written as

$$\Delta p = \rho \cdot v_{u_2} \cdot w_\infty \cdot \cos\beta_\infty - \frac{1}{2} \frac{c}{s} \cdot \rho \cdot w_\infty^2 (C_L - \cos\beta_\infty - C_D \cdot \sin\beta_\infty) \quad (A1.29)$$

Equation A1.13 may also be written as

$$\frac{v_{u_2}}{w_\infty} = \frac{1}{2} C_L' \cdot \sigma = \frac{1}{2} C_L' \cdot \frac{c}{s} \quad (A1.30)$$

Multiplying both sides of equation A1.30 by w_∞, equation A1.31 is obtained.

$$v_u \cdot w_\infty = \frac{1}{2} C_L' \cdot \frac{c}{s} \cdot w_\infty^2 \quad (A1.31)$$

and since $C_L' = C_L + C_D \cdot \cot\beta_\infty$

$$v_u \cdot w_\infty = \frac{1}{2} \cdot \frac{c}{s} \cdot w_\infty^2 (C_L + C_D \cdot \cot\beta_\infty) \quad (A1.32)$$

Substituting equation A1.32 into A1.29 and simplifing it, equation A1.33 is obtained.

$$\Delta p = \frac{1}{2} \rho \cdot \frac{c}{s} \cdot w_\infty^2 \cdot C_D \cdot \operatorname{cosec}\beta_\infty \quad (A1.33)$$

Since $H_L = \frac{\Delta p}{\rho \cdot g}$

Thus

$$H_L = \frac{\Delta p}{\rho \cdot g} = \frac{1}{2g} w_\infty^2 \cdot \sigma \cdot C_D \cdot \operatorname{cosec}\beta_\infty \quad (A1.34)$$

Where $\sigma = \frac{c}{s}$

Substituting equation A1.17 for σ into equation A1.34, equation A1.35 is obtained.

$$H_L = \frac{1}{2g} w_\infty^2 \cdot C_D \cdot \operatorname{cosec}\beta_\infty \left(\frac{2\psi_i}{C_L \cdot \phi} \cdot \frac{\sin\beta_\infty}{(1 + \gamma \cdot \cot\beta_\infty)} \right) \quad (A1.35)$$

and since $w_\infty = v_a / \sin\beta_\infty$

Then, equation A1.35 may be written as

$$H_L = \frac{v_a^2}{g.\mathrm{Sin}^2\beta_\infty} \cdot \frac{\psi_i}{\phi} \cdot \frac{C_D}{C_L} \cdot \frac{\mathrm{Sin}\,\beta_\infty}{(1 + \gamma\,\mathrm{Cot}\,\beta_\infty)} \cdot \mathrm{Cosec}\,\beta_\infty$$

and since $\gamma = \frac{C_D}{C_L}$, $\phi = \frac{v_a}{u}$ and $\mathrm{Cosec}\,\beta_\infty = \frac{1}{\mathrm{Sin}\,\beta_\infty}$

The above equation may be written as

$$H_L = \frac{v_a.u.\psi_i}{g} \cdot \frac{\gamma.\,\mathrm{Cosec}^2}{(1 + \gamma.\mathrm{Cot}\,\beta_\infty)} \qquad \text{(A1.36)}$$

and since $H_i = \frac{\psi_i.u^2}{g}$

Substituting equation A1.36 and the expression for H_i into equation A1.19 and simplifing it, equation A1.37 is obtained.

$$\eta_h = 1 - \phi\gamma \frac{\mathrm{Cosec}^2\beta_\infty}{(1 + \gamma\ \mathrm{Cot}\,\beta_\infty)} \qquad \text{(A1.37)}$$

d) Derivation of an expression for static efficiency, η_{st}

Static efficiency η_{st} is defined as

$$\eta_{st} = \frac{H_{st}}{H_i} \qquad \text{(A1.38)}$$

and the static pressure head H_{st} is also defined as

$$H_{st} = H - v_a^2/2g \qquad \text{(A1.39)}$$

Where $H = H_i - H_L$ and v_a is the discharge velocity at fan outlet.
Then equation A1.39 may be written as

$$\eta_{st} = \frac{H - v_a^2/2g}{H_i} \qquad \text{(A1.40)}$$

or

$$\eta_{st} = \frac{H}{H_i} + \frac{v_a^2/2g}{H_i} \qquad \text{(A1.41)}$$

and since $\eta_h = \frac{H}{H_i}$ and $H_i = \frac{\psi_i \cdot u^2}{g}$

Equation A1.41 may be written as

$$\eta_{st} = \eta_h - \frac{v_a^2/2g}{\psi_i \cdot u^2/g} \qquad \text{(A1.42)}$$

Simplifing equation A1.42, the following equation is obtained.

$$\eta_{st} = \eta_h - \phi^2/2\,\psi_i \qquad \text{(A1.43)}$$

APPENDIX 2

SECTION CO-ORDINATES OF NASCELLE % (i)

Distance From Nose / Total Length	Diameter at a Point / Maximum Diameter
0	0
1.25	24.8
2.5	34.8
5.0	48.4
10	66.2
20	86.6
30	96.8
40	100
50	97.7
60	90.5
70	78.2
80	60.0
90	34.7
95	18.7
100	0

APPENDIX 3

SPECIFICATIONS OF THE TORQUE TRANSDUCER AND STRAIN INDICATOR USED IN TEST SET UP

a. Torque Transducer

Trade Mark : BLP Electronics, INC. Torque Sensor

Type : A - 1

Capacity : 100 in - lb rpm (11.3 N - m)

Maximum Speed : 7000 rpm

Weight : 5.5 lb (2.5 kg)

Flexural Natural Frequency : 46600 rpm

Output at Rated Torque (R.T) : 1.5 mV/V

Calibration Accuracy : 0.25% R.T, clockwise or counter clockwise

Nonlinearity : 0.05% R.T

Repeatability : 0.05% R.T

Hysteresis : 0.05% R.T

Safe Temperature Range : - 50 to 140 F

Temperature Effect on Rated Output Torque : 0.005% reading per F°

Temperature Effect of Zero Balance : 0.0025% R.T per F°

Excitation : Recommended 12 V, AC or DC

Maximum 25 V, AC or DC

Zero Balance at 77 $\pm$ 3 F : 2.5% R.T.

Terminal Resistance : Input, 350 $\pm$ 1.5 ohm

Output, 350 $\pm$ 3 ohm

Termination : MS3102A - 18 - 85 - A105 connector with mating 15 ft cable assembly

Insulation Resistance : Bridge to Ground, 2000 megohms

Shield to Ground, 1000 megohms

Overload Ratings : Safe, 120%

Electrical failure, 300%

Allowable Axial Load Press Fit : 1000 lbs (454 kg)

b. Strain Indicator

Trade Mark : BLP Electronics, INC. Strain Indicator

Model : 120C

Total Reading Range : 60000 micro in/in

Readability : 1 micro in/in

Gage Factor Range : 1.5 to 4.5

Accuracy : $\pm$ 0.1% if gage factor is set to 2

Operating Temperature Range : 30 F to 130 F

Zero Drift : Not greater than $\pm$ 5 micro in per hour.

APPENDIX 4

COMPUTER PROGRAM WHICH WAS USED TO EVALUATE THE EXPERIMENTAL DATA AND A SAMPLE OUTPUT

a. Computer Program

```
      DIMENSION [illegible]
     1[illegible]
     1[illegible]
      READ(5,10) [illegible]
   10 FORMAT([illegible])
      DORF=0.1[illegible]
      AS=1.0009
      DRCORR=0.000[illegible]
      DOJCK=0.3
      VIS=0.00001[illegible]
      AZ=0.1[illegible]
      PI=3.14[illegible]
      READ(5,1)(DELP(I),[illegible](I),[illegible](I),[illegible](I),I=1,[illegible])
    1 FORMAT([illegible])
      DO 100 I=1,N
      ROA=(0.0[illegible])/([illegible])
      PO(I)=PATM+[illegible](I)
      ROO(I)=(ROA)*(PO(I)/[illegible])
      ROS(I)=(ROA)*([illegible](I))/([illegible])
      IF(DELP(I).LT.[illegible]) GO TO 11
      GAMA=1.4
      GO TO 22
   11 GAMA=1.
   22 EPS(I)=1.-(([illegible](I))/(GAMA*PO(I))))
      QM(I)=([illegible])/[illegible]
      QV(I)=QM(I)/ROS(I)
      VO(I)=[illegible]
      RE(I)=VO(I)*[illegible]
      VOST(I)=[illegible]
      RED(I)=[illegible]
      POS(I)=[illegible]
      PTT(I)=[illegible]
      PORK(I)=[illegible]
      POF(I)=[illegible]
      POF(I)=[illegible]
      PTF(I)=[illegible]
      ERFO(I)=[illegible]
      ERFI(I)=[illegible]
  100 CONTINUE
      WRITE(6,110)
  110 FORMAT([illegible]
     *[illegible]
     *[illegible])
      WRITE(6,111)([illegible],
     *ERFO(I),ERFI(I),I=1,N)
  111 FORMAT([illegible]
     *F0.4[illegible])
      STOP
      END
```

b. Sample Output

N = 2800 rpm = 25°

VO	[illegible]	[illegible]	[illegible]	PSF
0.00	0.00E+00	0.00E+00	0.00	561.0
3.92	0.71E+05	0.12E+06	0.25	590.9
5.24	0.10E+06	0.17E+06	0.37	574.6
6.55	0.13E+06	0.21E+06	0.46	593.6
7.84	0.14E+06	0.23E+06	0.50	569.5
8.15	0.15E+06	0.27E+06	0.58	598.5
8.84	0.17E+06	0.29E+06	0.62	595.7
9.71	0.19E+06	0.32E+06	0.68	590.1
10.99	0.21E+06	0.36E+06	0.74	603.9
11.10	0.21E+06	0.37E+06	0.76	630.6
11.73	0.23E+06	0.39E+06	0.83	617.0
12.33	0.25E+06	0.41E+06	0.87	605.4
12.86	0.25E+06	0.43E+06	0.89	594.6

PTF	POWR	EFFS	EFFT
504.0	492.6	0.00	0.00
400.7	395.9	0.25	0.25
383.6	394.0	0.34	0.34
359.2	337.2	0.38	0.39
376.8	331.3	0.40	0.42
208.2	326.4	0.45	0.47
307.1	326.4	0.49	0.51
284.9	351.9	0.49	0.52
256.6	357.7	0.50	0.53
348.9	357.7	0.51	0.55
337.2	351.9	0.51	0.56
217.4	346.0	0.49	0.55
207.5	343.1	0.48	0.54

APPENDIX 5

SHAFT DESIGN

The diameter of the fan shaft was calculated by using the Westinghouse code formula (13) which is given below.

$$d = \left(\frac{32.n}{\pi}\left(\left(\frac{T_a}{S_e} + \frac{T_m}{S_y}\right)^2 + \left(\frac{M_a}{S_e} + \frac{M_m}{S_y}\right)^2\right)^{1/2}\right)^{1/3} \qquad (A5.1)$$

Where d : minimum allowable shaft diameter

n : factor of safety

T_a : amplitude of torque variation, in-lb

T_m : mean value of torque variation, in-lb

M_a : amplitude of repeated bending moment

M_m : mean value of repeated bending moment, in-lb

S_e : endurence limit of shaft material, psi

S_y : yield strength of shaft material, psi

Endurence limit is equal to (13)

$$S_e = k_a \cdot k_b \cdot k_c \cdot k_d \cdot k_e \cdot k_f \cdot S'_e \qquad (A5.2)$$

Where S_e : endurence limit of mechanical element, psi

S'_e : endurence limit of rotating beam specimen, psi

k_e : surface factor

k_b : size factor

k_c : reliability factor

k_d : temperature factor

k_e : modifying factor for stress concentration

k_f : miscellaneous-effects factor

In the design, Ç1020 steel which has ultimate tensile strength of $S_{ut} = 42\ kg/mm^2$ (59740 psi) and yield strength of $S_y = 27\ kg/mm^2$ (38942 psi) was selected as shaft material.

According to reference 13, endurence limit for test specimen can be calculated by equation 5.3 .

$$S_e' = 0.5\, S_{ut} \qquad \text{if } S_{ut} < 200000 \text{ psi} \tag{A5.3}$$

Therefore

$S_e' = 21 \text{ kg/mm}^2$ (29870 psi)

The values of T_a, T_m, M_a and M_n are calculated as follows :

Maximum design torque can be calculated from the following equation (13)

$$T = \frac{60000\, P_{sh}}{2\pi N} \tag{A5.4}$$

Where P_{sh}:: shaft power, KW

N : rotational speed, rpm

T : torque, N-m

Shaft power, P_{sh}, may be calculated by using hydraulic power, P_{hyd}, at the design point of the fan. Hydraulic power is given as

$$P_{hyd} = p_{tf} \cdot Q \tag{A5.5}$$

Where p_{tf} : total fan pressure at the design point, Pa

Q : flowrate at the design point, m^3/sec

At the design point $p_{tf} = 250$ Pa , $Q = 1\ m^3/sec$

Since

$$P_{sh} = P_{hyd}/\eta \tag{A5.6}$$

Where η is the overall efficiency.

Shaft power at the design point is calculated by assuming $\eta = 0.5$ and is found as

$P_{sh} = 0.5$ KW

But, considering the losses in the coupling, torque transducer, V-belt pulley and bearings, the shaft power is increased by 20 %.

then

$P_{sh} = 0.6$ KW

Using the equation A5.4, the maximum torque transmitted by the shaft is calculated and is equal to

$T_{max} = 2.046$ N-m (18.11 in-lb)

To find the values of T_a and T_m, a torque variation shown in figure A5.1 is assumed. Because,the fan works under varing torque conditions and at the smallest speed, the torque on the fan shaft is very small, the minimum torque is assumed to be equal to zero.

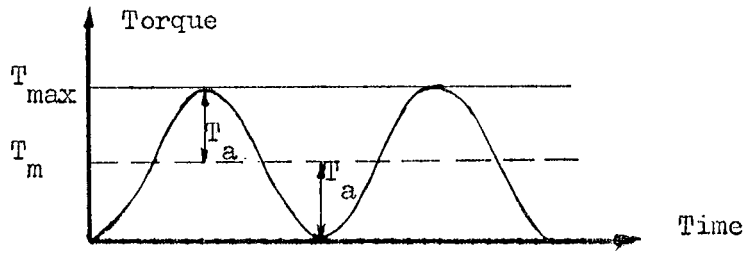

Fig.A5.1 Assumed Torque variation

According to this figure, the alternating and the mean components of torque become

$$T_a = T_m = \frac{T_{max}}{2} = 1.023 \text{ N-m} \quad (9.055 \text{ in-lb})$$

Free body diagram of the rotor shaft is shown in figure A5.2 . In this figure, W_R indicates the weight of the rotor connected to the shaft. Since it is an overhung rotor, bending moment must be maximum near support B and is equal to

$M_{max} = 7.842$ N-m (69.41 in-lb)

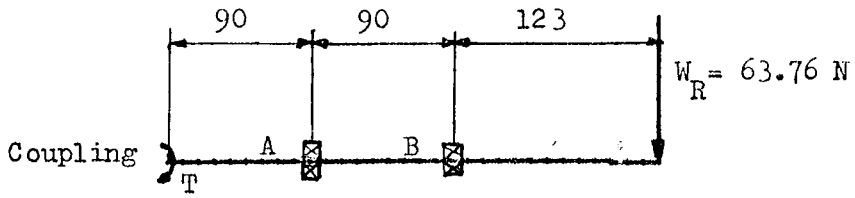

Fig.A5.2 Free Body Diagram of Rotor Shaft

The above calculated moment is the amplitude of an alternating moment as shown in figure A5.3

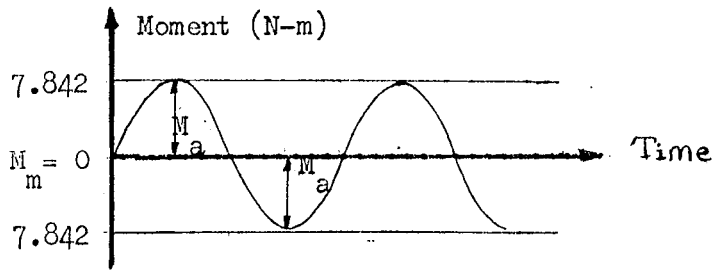

Fig.A5.3 Repeated Bending Moment

Therefore

$M_a = 7.842$ N-m (69.41 in-lb)

$M_m = 0$

In calculating the endurence limit of the shaft material, factors in equation A5.2 are specified as follows :

$k_a = 0.84$ (Machined)

$k_b = 0.85$ (0.3 inch $<$ d $<$ 2 inch)

$k_c = 0.814$ (for 99 % reliability)

$k_d = 1.0$ ($t < 70^{\circ}$)

$k_e = \frac{1}{K_f}$, $K_f = 1 + q(k_t - 1)$ Where k_t is the stress concentration factor and q is the notch sensitivity.

From reference (13) for D/d = 1.08 and r/d = 0.012, $k_t = 2.6$ and for r = 0.3 mm , q = 0.482. Hence $K_f = 1 + 0.48\ (2.6 - 1) = 1.768$ and

$k_e = 0.565$

$k_f = 1.0$

Substituting the above factors in equation A5.2,the endurence limit of the shaft material is calculated as

$S_e = 9808.6$ psi

Factor of safety, n, is taken to be as 3 and the minimum allowable shaft diameter is calculated as

d = 0.602 in = 15.4 mm

DRAWINGS

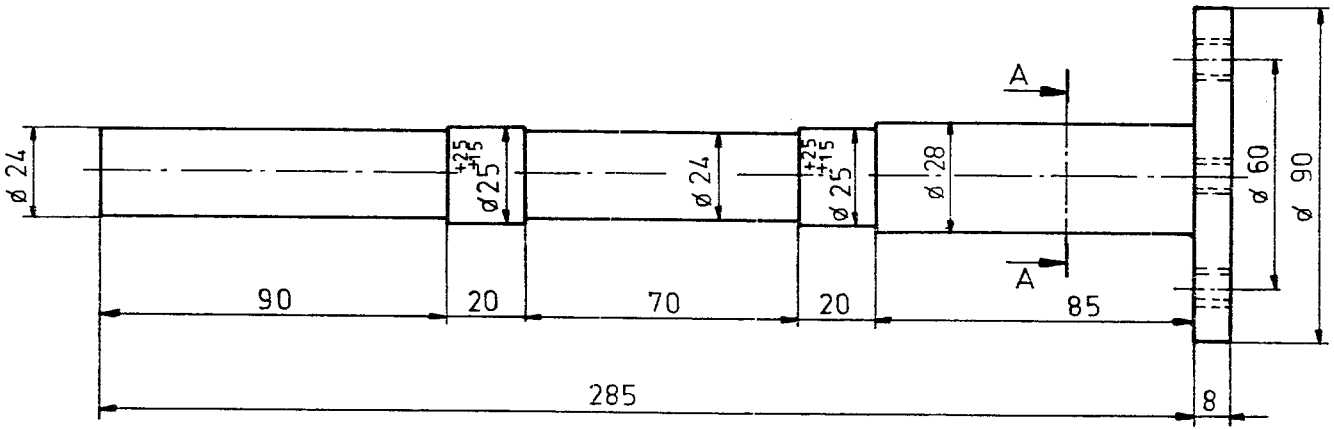

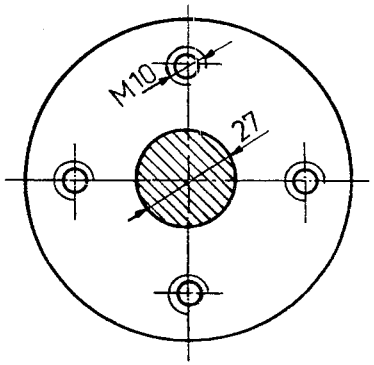

SECTION A-A

Quantity	Scale	Part Name	Material	Drawing No
1	1/2	Rotor Shaft	C 1020	1

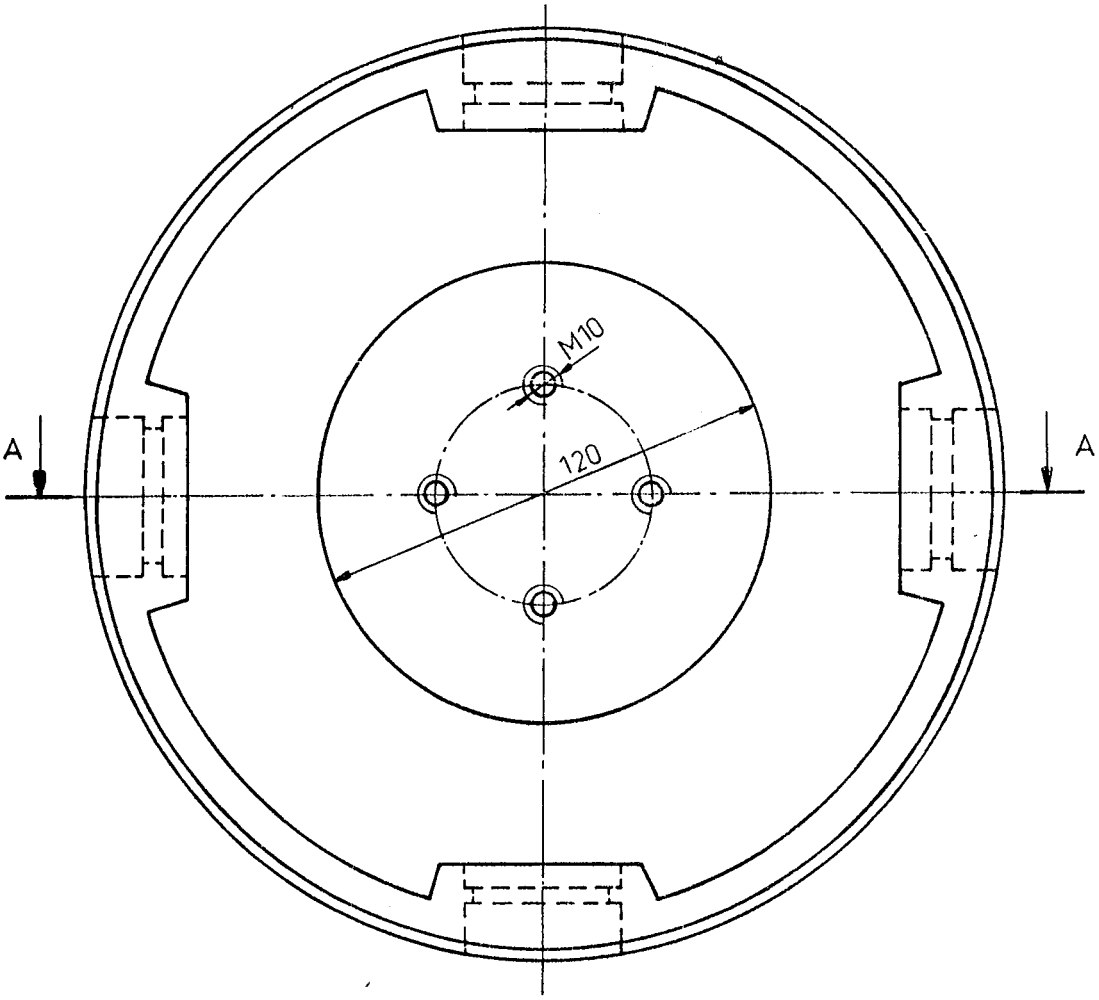

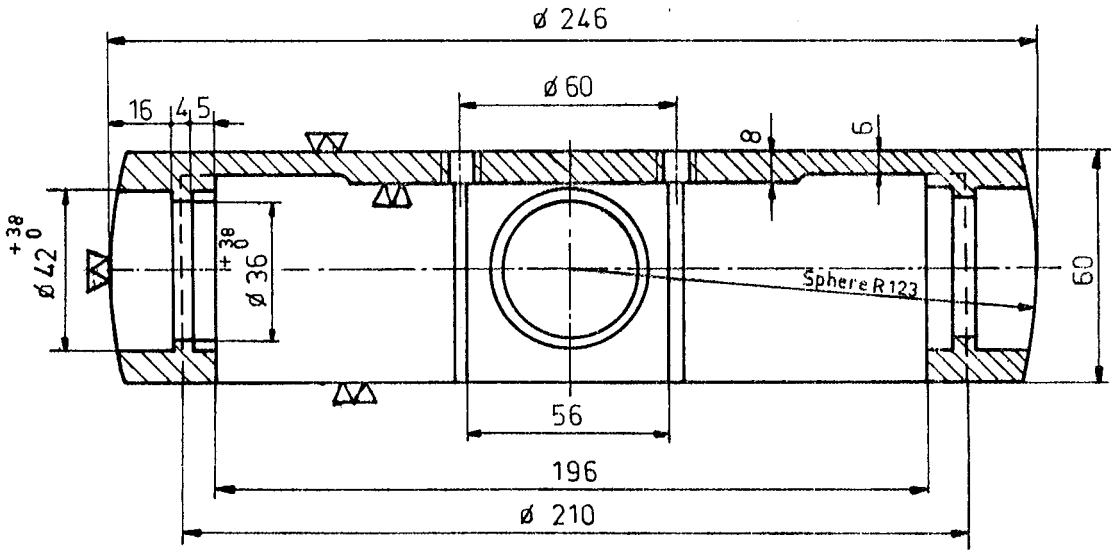

Section A-A

Drawn by	Quantity	Scale	Part Name	Material	Drawing No
A.Dalbudak	1	1/2	Fan bos	Aluminum	2

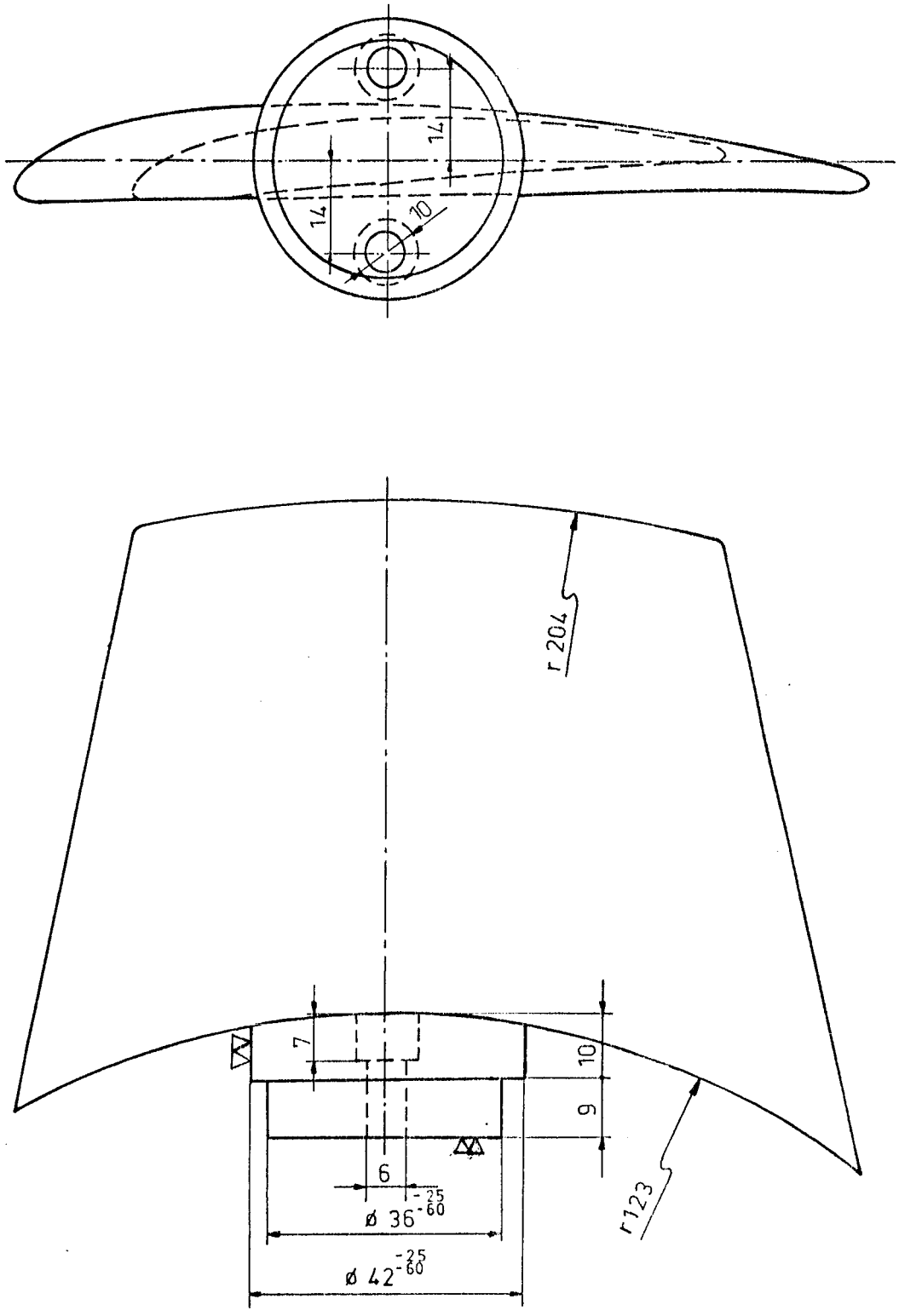

Drawn by	Quantity	Scale	Part Name	Material	Drawing No
A.Dalbudak	4	1/1	Fan blade	Aluminum alloy	3

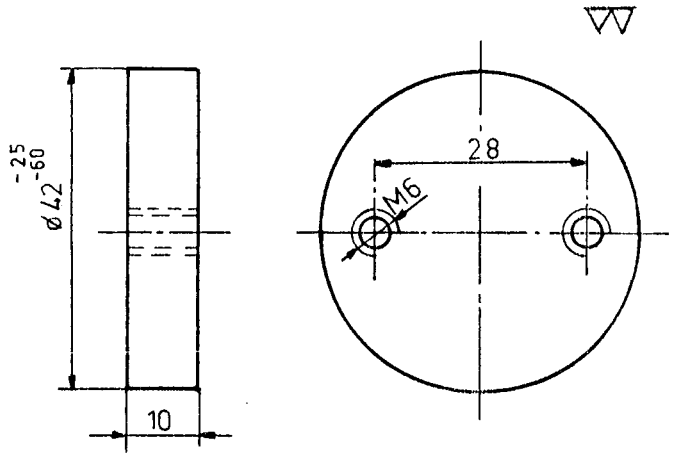

Quantity	Scale	Part Name	Material	Drawing No
4	1/1	Hold down plate	Aluminum	4

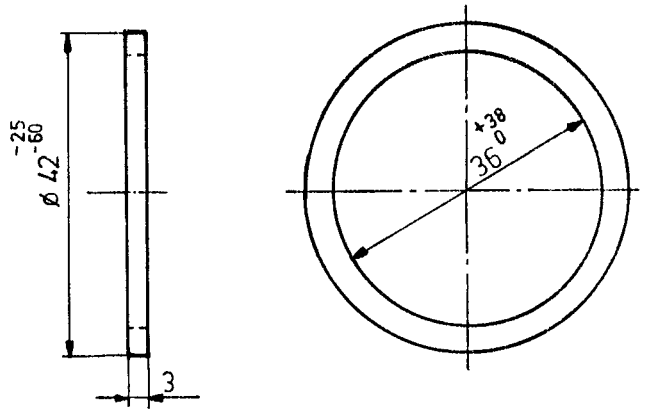

Drawn by	Quantity	Scale	Part Name	Material	Drawing No
A. Dalbudak	4	1/1	Steel ring	Steel	5

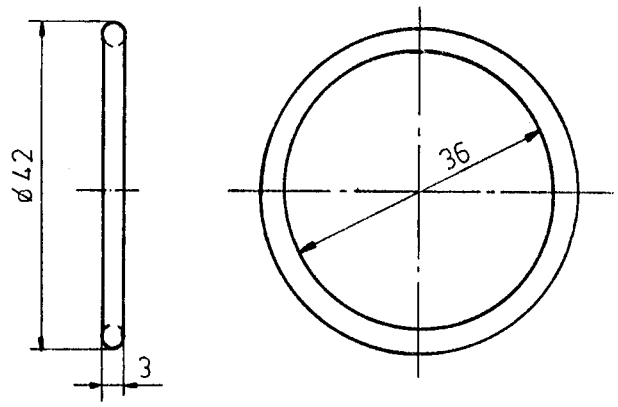

Quantity	Scale	Part Name	Material	Drawing No
4	1 1	O- Ring	Rubber	6

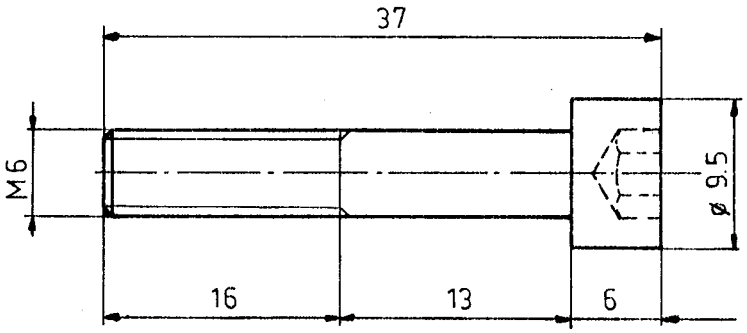

Drawn by	Quantity	Scale	Part Name	Material	Drawing No
A.Dalbudak	8	2/1	Socket head bolt	Steel	7